

What Controls Thermally Activated Delayed Fluorescence in Guest-Host Systems for Organic Light-Emitting Diodes?

Dissertation

Von der Universität Bayreuth
zur Erlangung des Grades eines
Doktors der Naturwissenschaften (Dr. rer. nat.)
genehmigte Abhandlung

von

Eimantas Duda

geboren am 11.05.1995 in Panevezys, Litauen

Bayreuth, 2021

Die vorliegende Arbeit wurde in dem Zeitraum von Oktober 2018 bis Juli 2021 am Lehrstuhl für Optoelektronik weicher Materie (Experimentalphysik II) der Universität Bayreuth unter der Betreuung von Prof. Dr. Anna Köhler angefertigt.

Dissertation eingereicht am: 05.07.2021

Datum des wissenschaftlichen Colloquiums: 15.10.2021

Prüfungsausschuss:

Erste Gutachterin: Prof. Dr. Anna Köhler

Zweiter Gutachter: Prof. Dr. Axel Enders

Drittprüfer: Prof. Dr. Holger Kress

Vorsitzender: Prof. Dr. Stephan Gekle

Table of Contents

Abstract	1
Kurzfassung	3
Extended summary	7
I. Introduction	
I.1 Motivation	11
I.2 Atomic and molecular orbitals	14
I.3 Singlet and triplet states	15
I.4 Electron spin	17
I.5 Spin-orbit coupling	19
I.6 Radiative transitions	20
I.7 Thermally activated delayed fluorescence (TADF)	22
I.8 Photophysical parameters to compare TADF systems	25
I.9 The role of the host molecule	28
I.10 The organic light-emitting diode (OLED)	30
I.11 State-of-the-art TADF and challenges	33
M. Methods	
M.1 Absorption	37
M.2 Steady-state photoluminescence and phosphorescence	37
M.3 Photoluminescence quantum yield (PLQY)	38
M.4 Time-resolved photoluminescence	39
1. Chapter 1	
1.a Fine-tuning the hole-electron overlap by donor extensions of different strength	47
1.b The optimal linkage position of the dendron donor group to the acceptor core	64
2. Chapter 2. How does TADF depend on the length of the oligomer chain?	75
3. Chapter 3. How does TADF depend on the nature of the host?	92
4. Chapter 4. TADF based on multi-resonant structures	110
5. Conclusions and outlook	124
APPENDIX 1. List of publications	127
APPENDIX 2. List of abbreviations	128
APPENDIX 3. Acknowledgements	129
APPENDIX 4. Erklärung und eidesstattliche Versicherung	131

Abstract

Thermally activated delayed fluorescence (TADF) enables the production of heavy-atom-free OLEDs that are of comparable or higher efficiency compared to currently commercialised phosphorescent emitters. My research work investigates the factors controlling TADF in guest-host systems for OLEDs. I explored four different aspects: the role of the donor group, including its linkage position to the acceptor core, the size of the oligomer length, the role of the host and, finally, a new type of TADF emitters that are based on the multi-resonant molecular structures. I evaluated the guest-host systems presented in this work using the absorption, steady-state photoluminescence (PL) emission and time-resolved PL emission techniques. First, I studied how TADF-related properties change based on the electron-hole wavefunction overlap that was controlled by the donor extension strength. The reference compound selected was based on the dicyanobenzene unit as the acceptor and carbazole units as donors. From the comparison of donor extensions consisting of carbazole, diphenylamine and phenoxazine-based units, I found that the optimal performance in terms of the singlet-triplet gap (ΔE_{ST}), TADF and photoluminescence quantum yield (PLQY) is reached for the molecule owning carbazole-based donor extensions. I then studied the molecules owning carbazole-based donor extensions in terms of their linkage position to the acceptor core via a phenylene bridge (*para*-, *meta*- and a synergistic *meta*- and *para*-connection). I discovered that while the *para*-connection owns the largest radiative decay rate, the *meta*-based connection shows the smallest ΔE_{ST} gap and largest TADF. Moreover, I revealed that the synergistic *meta*- and *para*-connection allows both a high radiative decay rate and a small ΔE_{ST} gap for efficient TADF. Furthermore, I found that the compound with the donor groups connected to the acceptor core synergistically in the *meta*- and *para*-positions possess almost no concentration quenching, allowing to use this emitter host-free in the emissive layer of the OLED. Second, I investigated the TADF-related parameters as a function of the oligomer length. Oligomers owning multiple donor-acceptor units were expected to create a larger number of quasi-degenerate states, enhancing the TADF-related properties. The oligomers investigated were based on the benzonitrile as acceptors and amines as donors. My photophysical study revealed that the intersystem

crossing and the reverse intersystem crossing rates are increasing with increasing oligomer size. I attributed this to the increasing number of intermediate triplet states along the series. Furthermore, I found that the enhancement of TADF-related properties can be achieved with no redshift of photoluminescence emission wavelength with the increasing oligomer size. Third, I explored the role of the host molecule on the TADF-related properties of the guest-host systems. Host materials of different ΔE_{ST} gaps were selected, including a small ΔE_{ST} gap (<200 meV) host showing TADF by itself. My photophysical study revealed that the guest-host systems with a host that demonstrates TADF by itself have a stronger TADF character as a whole, especially at lower emitter concentrations. My electroluminescence study of the organic light-emitting diodes (OLEDs) with different host materials in the emissive layer demonstrated that the highest external quantum efficiency (EQE) is present with the host showing TADF by itself, with the most significant difference at lower emitter concentrations. I ascribed this to both stronger TADF of the guest-host system and the bipolar nature of the host. Finally, I investigated a new type of TADF emitters that are based on multi-resonant structures. While such emitters possess very narrow emission spectra and high EQE, the major problem is a strong concentration quenching, induced by a rigid and planar molecular structure of such emitters. As a possible solution to a strong concentration quenching of TADF emitters based on multi-resonant structures, the bulky substituents can be introduced. To study how such modification reflects on the TADF performance of the compound, I compared the TADF-related properties for both compounds with and without bulky substituents. I found that TADF-related properties are comparable in both cases, yet the compound with bulky substituents shows a strong reduction in concentration quenching. This implies that concentration quenching in TADF emitters based on resonant structures can be successfully reduced without suppressing TADF. Overall, my photophysical study presented in this thesis successfully demonstrates several possible ways to enhance or preserve TADF for efficient emitters.

Kurzfassung

Thermisch aktivierte verzögerte Fluoreszenz (TADF) ermöglicht die Herstellung von schweratomfreien OLEDs, die eine vergleichbare oder höhere Effizienz im Vergleich zu den derzeit kommerzialisierten phosphoreszierenden Emittern aufweisen. Meine Forschungsarbeit untersucht die Faktoren, die TADF in Gast-Wirt-Systemen für OLEDs kontrollieren. Hierzu habe ich vier verschiedene Aspekte analysiert: die Rolle der Donorgruppe, einschließlich ihrer Bindungsposition zum Akzeptorkern, die Größe der Oligomerlänge, die Rolle des Wirts und eine neue Art von TADF-Emittern, die auf multiresonanten Molekülstrukturen basieren. Ich habe die in dieser Arbeit vorgestellten Gast-Wirt-Systeme mit Hilfe der Absorptions-, Steady-State-Photolumineszenz (PL)-Emissions- und zeitaufgelösten PL-Emissions-Techniken untersucht. Zunächst prüfte ich, wie sich TADF-bezogene Eigenschaften in Abhängigkeit von der Überlappung der Elektron-Loch-Wellenfunktion ändern, die durch die Donor-Ausdehnungsstärke gesteuert wurde. Die gewählte Referenzverbindung basierte auf der Dicyanobenzoleinheit als Akzeptor und Carbazoleinheiten als Donoren. Durch Vergleichen von Donor-Erweiterungen, die aus Carbazol-, Diphenylamin- und Phenoxazin-basierten Einheiten bestehen, fand ich heraus, dass die optimale Leistung, hinsichtlich der Singulett-Triplett-Lücke (ΔE_{ST}), der TADF und der Photolumineszenz-Quantenausbeute (PLQY), für das Molekül mit Carbazol-basierten Donor-Erweiterungen erzielt wird. Anschließend untersuchte ich die Moleküle, die Carbazol-basierte Donor-Erweiterungen besitzen, im Hinblick auf ihre Bindungsposition zum Akzeptorkern über eine Phenylenbrücke (*para*-, *meta*- und eine synergistische *meta*- und *para*-Verbindung). Ich entdeckte, dass, während die *para*-Verbindung die größte Fluoreszenzlebensdauer besitzt, die *meta*-basierte Verbindung die kleinste ΔE_{ST} -Lücke und die größte TADF aufweist. Darüber hinaus habe ich herausgefunden, dass die synergistische *meta*- und *para*-Verbindung sowohl eine hohe Fluoreszenzlebensdauer als auch eine kleine ΔE_{ST} -Lücke für eine effiziente TADF ermöglicht. Zudem beobachtete ich, dass die Verbindung mit den Donorgruppen, die in der *meta*- und *para*-Position synergistisch mit dem Akzeptorkern verbunden sind, fast kein Konzentrationsquenching besitzt, was es erlaubt, diesen Emitter wirtsfrei in der emittierenden Schicht der OLED zu verwenden. Zweitens habe ich die TADF-bezogenen Parameter als Funktion der

Oligomerlänge untersucht. Es wurde erwartet, dass Oligomere, die mehrere Donor-Akzeptor-Einheiten besitzen, eine größere Anzahl von quasi-entarteten Zuständen erzeugen, wodurch die TADF-bezogenen Eigenschaften verbessert werden. Die untersuchten Oligomere basierten auf dem Benzonitril als Akzeptor und Aminen als Donor. Meine photophysikalische Studie ergab, dass die Intersystem-Kreuzungsraten und die umgekehrten Intersystem-Kreuzungsraten mit zunehmender Oligomergröße ansteigen. Ich führte dies auf die zunehmende Anzahl von Triplett-Zwischenzuständen entlang der Reihe zurück. Des Weiteren fand ich heraus, dass eine Verbesserung der TADF-bezogenen Eigenschaften ohne Rotverschiebung der Photolumineszenz-Emissionswellenlänge mit zunehmender Oligomergröße erreicht werden kann. Drittens habe ich die Rolle des Wirtsmoleküls auf die TADF-bezogenen Eigenschaften der Gast-Wirt-Systeme untersucht. Es wurden Wirtsmaterialien mit unterschiedlichen ΔE_{ST} -Lücken ausgewählt, einschließlich eines Wirts mit kleiner ΔE_{ST} -Lücke (<200 meV), der selbst TADF-bezogen ist. Meine photophysikalische Studie ergab, dass die Gast-Wirt-Systeme mit einem TADF-bezogenen Wirt insgesamt einen stärkeren TADF-Charakter haben, insbesondere bei niedrigeren Emitterkonzentrationen. Meine Elektrolumineszenzstudie der organischen Leuchtdioden (OLEDs) mit verschiedenen Wirtsmaterialien in der emissiven Schicht zeigte, dass die höchste externe Quanteneffizienz (EQE) mit dem Wirt, der selbst TADF aufweist, vorhanden ist, mit dem signifikantesten Unterschied bei niedrigeren Emitterkonzentrationen. Ich schrieb dies sowohl der stärkeren TADF des Gast-Wirt-Systems als auch einer bipolaren Natur des Wirts zu. Schließlich untersuchte ich einen neuen Typ von TADF-Emittern, die auf multiresonanten Strukturen beruhen. Während solche Emitter ein sehr schmales Emissionsspektrum und eine hohe EQE besitzen, ist das Hauptproblem ein starkes Konzentrationsquenching, das durch die starre und planare Molekülstruktur solcher Emitter induziert wird. Als mögliche Lösung für ein starkes Konzentrationsquenching von TADF-Emittern, die auf multiresonanten Strukturen basieren, können sperrige Substituenten eingeführt werden. Um zu untersuchen, wie sich eine solche Modifikation auf die TADF-Leistung der Verbindung auswirkt, habe ich die TADF-bezogenen Eigenschaften für beide Verbindungen mit und ohne sperrige Substituenten verglichen. Ich fand heraus, dass die TADF-bezogenen Eigenschaften in beiden Fällen vergleichbar sind, jedoch zeigt die Verbindung mit sperrigen

Substituenten eine starke Reduzierung des Konzentrationsquenchings. Damit präsentiere ich abschließend, dass das Konzentrationsquenching in TADF-Emittern, die auf resonanten Strukturen basieren, erfolgreich reduziert werden kann, ohne TADF zu unterdrücken. Insgesamt zeigt meine in dieser Arbeit vorgestellte photophysikalische Studie erfolgreich mehrere Möglichkeiten auf, wie TADF für effiziente Emmitter verbessert oder erhalten werden kann.

Extended summary

Organic light-emitting diodes (OLEDs) based on thermally activated delayed fluorescence (TADF) can achieve similar or even higher efficiencies without the need for expensive heavy-metals as in currently commercialized phosphorescent emitters. The main question of the thesis is which material-related parameters can be optimised to enhance TADF. Obtaining an efficient TADF emitter is not straightforward, as the molecule has to possess a small gap between the singlet and triplet state, ΔE_{ST} , and a high radiative decay rate. Unfortunately, a small ΔE_{ST} gap requires a small hole-electron wavefunction overlap which prevents a high radiative decay rate. Therefore, balancing the hole-electron overlap just right to get a sufficiently small ΔE_{ST} gap while preserving a fast radiative decay rate is a complex issue. The thesis aims to further address the question of obtaining efficient TADF in guest-host systems by considering the role of the donor group of the guest, the length of the oligomer chain of the guest, the role of the host and a new type of TADF emitters that are based on multi-resonant structures. To address the main question of the thesis, I divided my work into the following four chapters as presented in Figure 1.

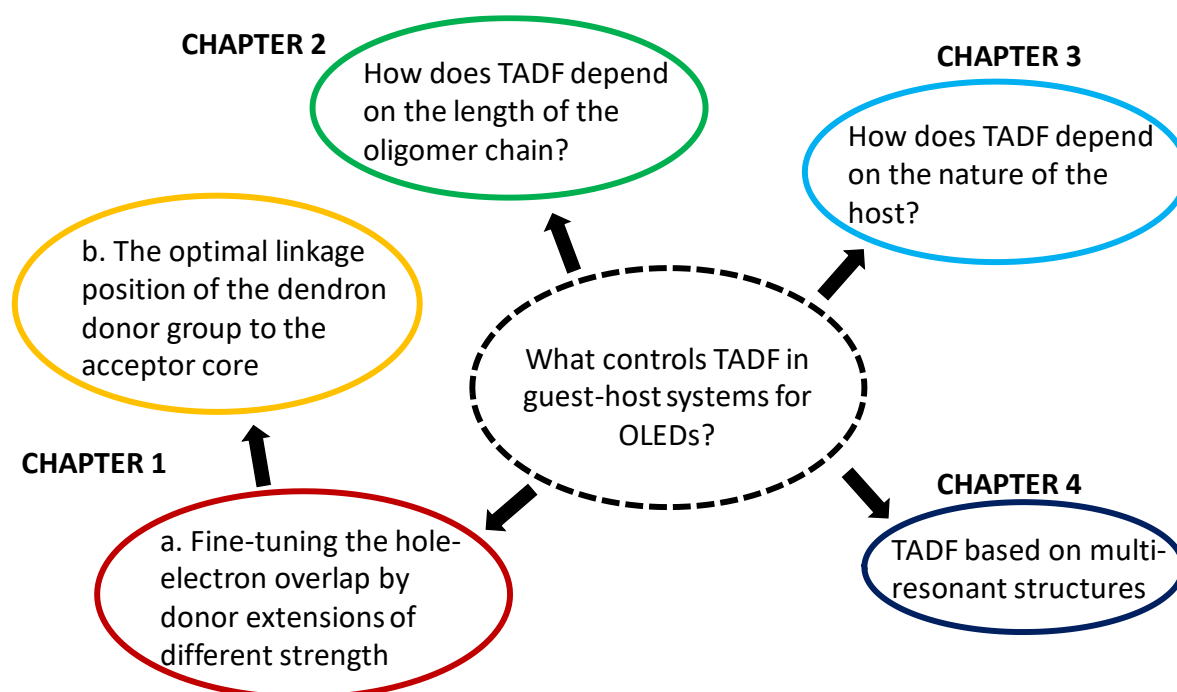


Figure 1. Summary of the chapters presented in this work.

Extended summary

In Chapter 1a, I first investigate whether the effects of extending the donor group with molecular units of increasing strength can help to enhance TADF. Carbazole, diphenylamine and phenoxazine-based structures were selected as donor extensions for the carbazolyl-phthalonitrile-based donor-acceptor core, 2CzPN. My photophysical study shows that extending the core structure 2CzPN with carbazole, diphenylamine or phenoxazine-based units successfully decreases the singlet-triplet gap, yet I also demonstrate why a small ΔE_{ST} gap alone is not enough. In the case of diphenylamine-based extension, I find a significantly larger non-radiative decay rate compared to 2CzPN which hinders high PLQY and a strong TADF contribution. In the case of phenoxazine-based extension, I find the hole-electron wavefunction overlap to be insufficient for a reasonably high radiative decay rate. While diphenylamine and phenoxazine-based extensions can be ruled out from further implementation, the carbazole-based extension shows enhanced TADF and a higher PLQY value in toluene than in 2CzPN alone. Based on these promising results, I investigate the carbazole-based donor extensions further in Chapter 1b.

In Chapter 1b, I focus on understanding the optimal linkage position of the dendron donor unit to the acceptor core. To account for quenching channels via guest to guest interactions, *tert*-butyl groups are introduced on the outer carbazole units. I study TADF-related properties on the carbazole-based dendrimer-type donor units linked to the triazine acceptor unit via *meta*- and *para*-connections using a phenylene bridge. I find that donor and acceptor units connected via a *para*-connection own a stronger radiative decay rate but the ΔE_{ST} gap is also larger which is not beneficial for TADF. At the same time, donor and acceptor units connected via a *meta*-connection show a smaller ΔE_{ST} gap which is beneficial for TADF but the radiative decay rate is not as high as using a *para*-connection. When the donor units are connected to the acceptor synergistically via a *para* and *meta*-connection, both a small ΔE_{ST} gap and a high radiative decay rate are found. I also find almost no concentration quenching (the PLQY only drops from 90 to 86% when comparing a 1 wt% PMMA film and the neat film, respectively). High efficiency combined with a small concentration quenching enables to use such extended carbazole-based molecules without the host matrix in the emissive layer of the OLED.

In Chapter 2, I investigate how TADF changes depending on the oligomer length. A series of donor-acceptor type TADF emitters that have benzonitrile (BN) as the acceptor units that are connected via the amine donors, acting as bridges to adjacent BN acceptors, are selected. I show that the intersystem crossing and the reverse intersystem crossing rates increase along the series. I ascribe the increase in these TADF-related properties to the increase in the number of intermediate triplet states, as also supported by the DFT calculation. A larger number of intermediate triplet states increases the transition probability for the intersystem crossing (ISC) process (Fermi's golden rule) and also reduces the effective gap between the singlet and triplet state, enhancing the reverse intersystem crossing (RISC) process. Furthermore, I demonstrate that increasing the oligomer length suppresses aggregation. Overall, in Chapter 2, I present a way to enhance TADF-related properties while still preserving the blue monomolecular emission wavelength.

In Chapter 3, I investigate how the host material itself affects the TADF-related properties of the guest-host system. In addition to widely used high ΔE_{ST} gap (TADF-inactive) host materials, mCP and DPEPO, a host owning a sufficiently small ΔE_{ST} gap for TADF, ATRZ, was also selected for the investigation. To study the effects of the host, a sky-blue TADF emitter, mPTC, was used. I prepare a series of films and OLEDs at 5, 10 and 15% doping concentrations by weight ("doping" refers to the emitter concentration in the guest-host system). From the photophysical study, I discover that guest-host systems with ATRZ as a host show a two times higher RISC rate at lower emitter concentrations. I explain this by a strong ISC in the host itself and a poor singlet-singlet energy transfer from host to guest leading to a significant amount of energy stored in the triplet state of the host. Significant involvement of the triplet state in the energy transfer from host to guest leads to a stronger contribution of TADF of the guest-host system as a whole. Combining photophysical measurements with electroluminescence measurements, I demonstrate that opposite to lower PLQY values in films, a TADF-active host ATRZ shows higher EQE values in devices with lower emitter concentrations. I attribute this to the enhanced TADF of the guest-host system and also a better charge balance due to the bipolar nature of ATRZ. Due to better photophysical and electroluminescent properties at lower emitter concentrations when TADF-active

Extended summary

ATRZ is used as a host, ATRZ could be of particular interest for devices where only low emitter concentration are possible due to a strong concentration quenching of the guest, for example, TADF emitters based on multi-resonant structures as introduced in Chapter 4.

Finally, in Chapter 4, I focus on TADF emitters that are based on multi-resonant structures (“resonance TADF”). These types of emitters enable narrow emission spectra (<40 nm) and high efficiency even in the blue range, making them one of the most attractive selections for OLEDs in the TADF field. However, there are still some problems to solve. One of these problems that I investigate in this work is a strong concentration quenching due to the rigid and planar structure of the molecules. In this chapter, my photophysical study demonstrates a possible way to reduce concentration quenching when the bulky side groups are attached to the emitter to limit guest to guest interaction. To better understand the effects of bulky side groups on aggregation, TADF and PLQY, I study the two resonance TADF emitters in solution and film. The difference between the two emitters (DiKTa and Mes₃DiKTa) are the outer mesityl groups (Mes) that are expected to suppress guest to guest interactions. My photophysical study shows that for both emitters the ΔE_{ST} gaps are in the range of 200 meV, sufficiently low for TADF. For both emitters, the photophysical rate constants are largely the same, yet I observe severe differences in terms of aggregation. I find that the introduction of mesityl groups in the molecule prevents the formation of low energy emission band, associated with aggregation, even in neat films. In addition to this, Mes₃DiKTa demonstrates a strongly reduced concentration quenching. Mesityl groups in Mes₃DiKTa show a possible way to reduce guest to guest interactions in rigid and planar systems such as resonance TADF emitters while still preserving TADF and PLQY.

Overall, in this work I demonstrate how TADF can be enhanced or preserved in the guest-host systems for OLEDs.

I. Introduction

I.1 Motivation

Most of the current televisions or mobile phone displays are based either on a liquid-crystal display (LCD) technology or its new organic counterpart – organic light-emitting diode (OLED) technology. While the LCDs are robust and long-lived, the OLED displays often own more flexibility, sharper colours and smaller energy consumption.¹⁻³ Thanks to OLEDs, not only foldable televisions or computer monitors are possible to produce,⁴ but also electronic band-aids to treat skin-related diseases⁵ are emerging.

In recent years, OLEDs have exceeded external quantum efficiencies (EQE) higher than 20%.^{1, 6-7} To achieve such efficiencies in the device, nearly 100% of internal quantum efficiency (IQE) is required in the emitter followed by an excellent light outcoupling from the device (see Section I.10). Under electrical excitation, 25% of singlets and 75% of triplet excitons are generated. Thus, IQE of 100% in the emitter is only possible when triplet states are employed. There are three generations of OLEDs that are based on fluorescence, phosphorescence and thermally activated delayed fluorescence (TADF),⁸ with only the latter two generations able to employ triplet states and possess an IQE of 100% in the device (see Sections I.5 and I.7).⁸⁻⁹ Since the devices based on phosphorescence involve heavy metals, making the OLED fabrication process more expensive, a new type of emitter was desired which would not contain heavy atoms but could still employ triplet states. A possible solution is TADF where the energy required for the triplet exciton transition to the singlet state is low and can be obtained from the ambient energy present at room temperature.¹⁰⁻¹³ The first observation of TADF was announced in 1961 by Parker *et al.* using the compound called eosin.¹⁴ The detected emission was called “E-type” emission and the mechanism for such emission was not well understood. Between 2009 and 2012, Adachi *et al.* published several articles reminding the display community about the possibility to upconvert triplet excitons into singlet excitons given a sufficiently small gap between the singlet and triplet state (ΔE_{ST}) leading to efficient OLEDs.^{10, 15-16}

Introduction

The molecular design for TADF often involves spatially separated donor and acceptor moieties thus allowing for a minimal electron exchange interaction and a small ΔE_{ST} , often in the range of tens of millielectronvolts.¹⁷⁻¹⁸ However, a small ΔE_{ST} gap can also lead to an insufficient radiative decay rate which is also known as a trade-off between a small ΔE_{ST} and a large radiative decay rate in the molecule.¹⁹⁻²⁰ To approach this problem, a new molecular design of the so-called “resonance TADF” emitters was reported by Hatakeyama *et al.* in 2016,²¹ proposing a way to obtain both a small ΔE_{ST} and a large radiative decay rate in the molecule.²¹ The molecules showing “resonance TADF” involve a rigid conjugated molecular structure allowing for a short-range separation of hole and electron densities that ensures both a small ΔE_{ST} and a sufficient radiative decay rate (see also Section I.11).²²⁻²³ Compared to conventional donor-acceptor type TADF emitters owning broad emission spectra (70-100 nm), resonance TADF emitters show very narrow emission spectra (<40 nm).²⁴⁻²⁶ Furthermore, remarkable OLED efficiencies exceeding 30% were recently reported.²⁷⁻²⁸

Other challenges in the field include a lack of efficient and stable blue emitters and suitable host materials for them.²⁹⁻³⁰ Blue emitters are an important part of the colour scheme for displays and could decrease the total energy consumption if efficient and stable blue OLEDs were produced.³¹ Furthermore, as most emitters need to be dispersed in a matrix (host) to prevent concentration quenching, the other struggle is the development of stable host materials that possess a sufficiently high triplet energy for blue-emitting guests (see also Section I.9).³²

To assess the potential of the TADF emitter in a specific environment (the so-called “guest-host” system), photoluminescence quantum yield (PLQY), lifetimes of photoluminescence emission, singlet and triplet state-related rate constants as well as TADF contribution in the molecule can be estimated with the help of spectroscopic methods such as absorption measurements, steady-state and time-resolved spectroscopy (see also Methods). Some of the most important parameters quantifying TADF systems are the contribution of TADF to the total emission, the rate at which singlet excitons are transferred to the triplet state (intersystem crossing rate or ISC) and the rate at which triplet excitons are converted to singlet excitons (the reverse intersystem crossing rate or RISC) as well as the non-

radiative decay rates. In this work, I study TADF-defining parameters in different guest-host systems to better understand what makes a molecule a good TADF emitter and how to enhance TADF in the molecule. First, I investigate the effects of the donor group extensions on TADF-related properties in the same matrix environment. Second, I explore the role of the oligomer chain length on TADF properties. Third, I study the effects of different matrix environments (hosts) on TADF of the guest-host systems. Finally, I explore TADF of a new group of TADF emitters based on multi-resonant structures.

The following sections introduce the scientific background required for the understanding of the origin of TADF. The atomic and molecular orbitals, the origin of singlet and triplet states, radiative transitions and, finally, TADF are introduced next. The later sections also provide a mathematical background to evaluate and compare TADF in guest-host systems. The introductory sections (I.2-I.6), providing the key aspects for understanding the formation of singlet and triplet states and the energetic separation between them which is relevant for TADF, are based on textbooks *Electronic Processes in Organic Semiconductors* by Köhler and Bässler,³³ *Molecular Spectroscopy of the Triplet State* by McGlynn,³⁴ and *Principles of Fluorescence Spectroscopy* by Lakowicz.³⁵

I.2 Atomic and molecular orbitals

An atomic orbital defines the probability to find an electron in space around the atom. Four quantum numbers define the atomic orbitals: the principal quantum number n describes the distance between the electron cloud to the nucleus, the angular momentum quantum number ℓ describes the shape of the orbital, the magnetic quantum number m_ℓ describes the specific orbital within the subshell while the magnetic quantum number m_s describes the spin of the molecule (described in more detail later). There are four types of atomic orbitals: s, p, d and f, corresponding to the angular momentum quantum number ℓ of 0, 1, 2 and 3. The s-type orbital has 1 subshell, the p-type has three subshells, the d-type orbital has 5 subshells while the f-type orbital has 7 subshells, each addressable by the magnetic quantum number m_ℓ from $-\ell$ to ℓ , where ℓ is an integer number (for example, for p-type orbitals one has 3 subshells thus $m_\ell = -1, 0, 1$). The maximum number of electrons in each orbital is defined as $2(2\ell+1)$. The standard notation to describe the orbital is in the format of nX^y , where n is the principal quantum number, X is the type of atomic orbital (s, p, d or f) and y is the number of electrons in the subshell. For example, $2s^2$ describes the s type orbital with a principal quantum number of 2 with 2 electrons in the subshell. The atomic orbitals can form bonds as illustrated in Figure I.1.

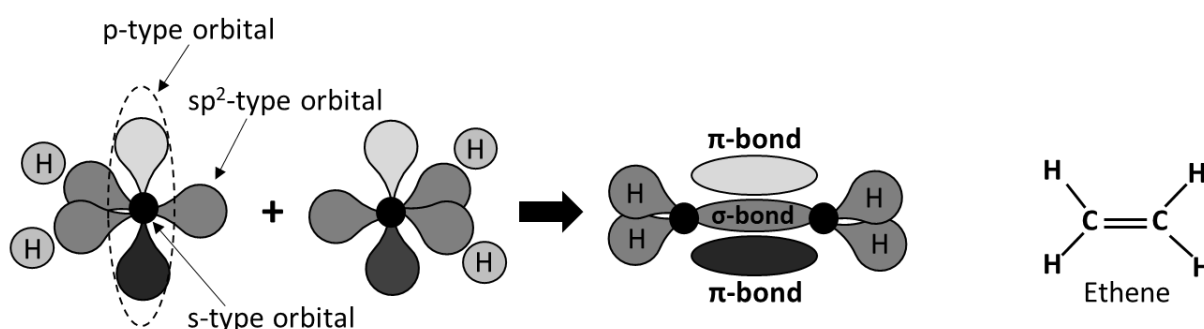


Figure I.1. The combination of two sp^2 hybrid orbitals leading to ethene owning a π -bond and a σ -bond. After Köhler and Bässler.³³

To understand how atomic orbitals on two different atoms can form bonds, one needs to consider the number of electrons an atom has. For example, a carbon atom has six electrons in its electronic cloud allowing 1s and 2s orbitals to be fully occupied. The two remaining electrons are placed in two out of three p-type subshells, leaving one p-type subshell unoccupied. One electron from the 2s orbital can

be excited to the empty p-type subshell to create three sp^2 hybrid states with one p-type orbital unchanged which is named as p_z -type. On the left side of Figure I.1, two molecular units each owning one s, three sp^2 and one p-type orbital are shown. Due to the presence of an sp^2 -type orbital with an unpaired electron, two such molecular units can connect through a σ -bond, forming ethene. The remaining p-type orbitals form a π -bond. The formed σ and π -bonds can be illustrated in an energy level diagram as in Figure I.2.

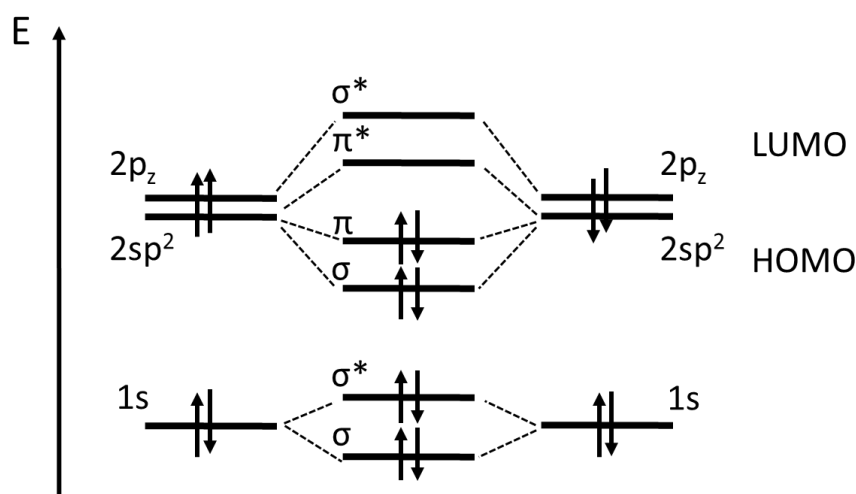


Figure I.2. An energy level diagram demonstrating the formation of σ and π bonds from atomic orbitals for ethene. After Atkins.³⁶

When two atomic units with s, sp^2 and p_z type orbitals connect, not only σ -type and π -type orbitals are formed but also the anti-bonding (σ^* and π^*) orbitals are formed, as illustrated in Figure I.2. The nature of bonding and anti-bonding orbitals are essentially the two solutions to Schrödinger's equation, representing the constructive and destructive interference of two interacting wavefunctions.³⁶

I.3 Singlet and triplet states

To understand the origin of singlet and triplet states, a two-electron system needs to be considered as outlined in Ref³⁴. The energy of a single electron confined in a box can be defined as

Introduction

$$E_n = \frac{h^2}{8mL^2} n^2 \quad (1)$$

where n is a quantum number that can only have integer values, m is the electron mass and L is the size of the box the electron is in. The corresponding wavefunction for an electron can be written as follows.

$$\varphi_n(x_1) = \left(\frac{2}{L}\right)^{\frac{1}{2}} \sin\left(\frac{n\pi x_1}{L}\right) \quad (2)$$

Given that there is no interaction with the first electron in the box, the energy and wavefunction for the second electron in the box can be described in a similar manner as

$$E_k = \frac{h^2}{8mL^2} k^2 \quad \text{and} \quad (3)$$

$$\varphi_k(x_2) = \left(\frac{2}{L}\right)^{\frac{1}{2}} \sin\left(\frac{k\pi x_2}{L}\right) \quad (4)$$

Then the combined wavefunction for two electrons and their corresponding energy can be described as

$$\varphi_n(x_1)\varphi_k(x_2) \quad \text{and} \quad (5)$$

$$E_{nk} = \frac{h^2}{8mL^2} (n^2 + k^2) \quad (6)$$

Since two electrons are not distinguishable, the combined wavefunction for the two electrons can be written as follows.

$$\Psi_{\pm} = \left(\frac{1}{2}\right)^{\frac{1}{2}} \left[\varphi_n(x_1)\varphi_k(x_2) \pm \varphi_n(x_2)\varphi_k(x_1) \right] \quad (7)$$

where the factor $(1/2)^{(1/2)}$ is a normalization factor and the sign “ \pm ” represents wavefunctions that are symmetric (+) and anti-symmetric (-) to the electron coordinate interchange. In the absence of inter-electronic forces, the energies for the wavefunctions described by Equation 7 are similar. However,

once repulsive energy between two electrons is introduced (for example, Coulomb repulsion), the energies for the symmetric and anti-symmetric wavefunction combinations become different and can be described as follows.

$$E_{\pm} = E_{nk} + J_{nk} \pm K_{nk} \quad (8)$$

where J_{nk} and K_{nk} are both positive and can be called coulomb and exchange energy between two electrons, respectively. The difference between the two solutions for the energy yields the following.

$$E_{+} - E_{-} = 2K_{nk} \quad (9)$$

The two solutions for the equation describe a symmetric E_{+} and an anti-symmetric E_{-} wavefunction. The energy difference between the symmetric and anti-symmetric wavefunction is the exchange energy which can be described as follows.

$$K_{nk} = \iint \varphi_n^*(x_1)\varphi_k(x_1)\varphi_n^*(x_2)\varphi_k(x_2) \left(\frac{e^2}{|\mathbf{x}_1 - \mathbf{x}_2|} \right) dx_1 dx_2 \quad (10)$$

The exchange energy depends on the box size, *i.e.*, the separation between two electrons, $|\mathbf{x}_1 - \mathbf{x}_2|$. This implies that for conjugated molecular systems where electrons have plenty of space to move the exchange integral is minimal while for non-conjugated molecular systems the exchange energy is large.

1.4 Electron spin

For a complete description of the molecule's state, the magnetic spin quantum number m_s needs to be considered. The magnetic spin quantum number is either $+1/2$ or $-1/2$ and the corresponding wavefunctions describing a two-electron system can be denoted as α and β . These spin states can also be referred to as spin-up and spin-down, respectively. The interaction between two electrons can be defined with four different wavefunction combinations as follows.

$$\alpha(\omega_1)\alpha(\omega_2) \quad (11)$$

$$\left(\frac{1}{2}\right)^{\frac{1}{2}} [\alpha(\omega_1)\beta(\omega_2) + \alpha(\omega_2)\beta(\omega_1)] \quad (12)$$

$$\beta(\omega_1)\beta(\omega_2) \quad (13)$$

$$\left(\frac{1}{2}\right)^{\frac{1}{2}} [\alpha(\omega_1)\beta(\omega_2) - \alpha(\omega_2)\beta(\omega_1)] \quad (14)$$

Three of these wavefunction combinations are antisymmetric and one is symmetric. The pictorial representation of two interacting spin states is presented in Figure I.3.

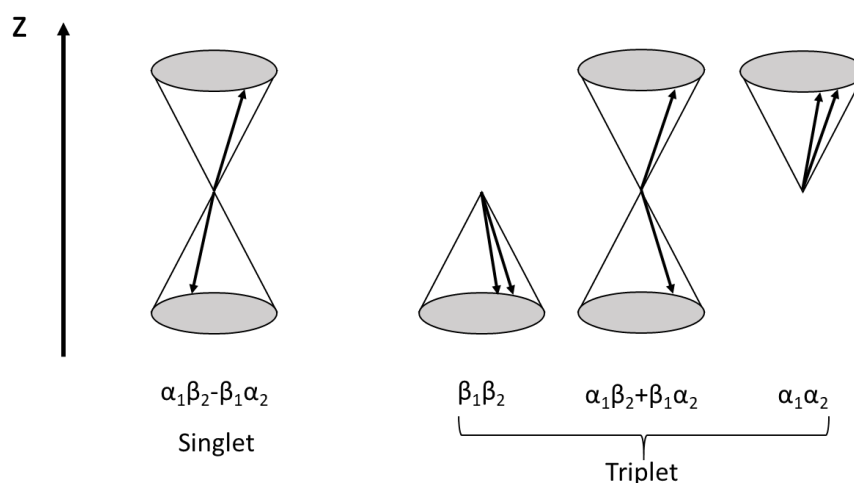


Figure I.3. Two electron spins as vector diagrams corresponding to the formation of singlet and triplet states. After Köhler and Bäessler.³³

The symmetric and anti-symmetric wavefunctions have different energies and are the origin for the singlet and triplet states. The symmetric wavefunction is also referred to as a singlet state while the three antisymmetric wavefunctions are referred to as a triplet state. Equation 9 can also be rewritten as

$$E(S_i) - E(T_i) = 2K_i \quad (15)$$

The energy difference between the singlet and triplet states is equal to two times the exchange integral. As the exchange integral cannot be negative, Equation 15 also implies that the triplet state

must be lower in energy than the singlet state. This can be more clearly visualized by considering two interacting electrons. When two electrons are in an antisymmetric combination, the interaction between electrons is smaller as there is more space for two electrons to keep out of one another's way. Whereas for the symmetric combination, the electron-electron interaction is larger due to the possibility for electrons to be in closer proximity with each other that increases the repulsion energy between them. This explains why the triplet state is lower in energy compared to the singlet state.

I.5 Spin-orbit coupling

Spin-orbit coupling (SOC) is a phenomenon occurring due to the interaction of a particle's spin with the motion of the orbital the particle is in. For example, let's consider a system consisting of an electron and a nucleus from two frames of reference. First, if one considers a nucleus as a point of reference (stationary object), then the electron spins on its own axis and orbits the nucleus. However, if one transforms the coordinates onto the electron frame of reference, it is now the nucleus that is orbiting the electron. Since a moving charge creates a magnetic field around it, the electron-nucleus system owns two distinct magnetic fields that interact with each other. The magnitude of the spin-orbit coupling depends on such parameters as the charge of the nucleus (*i.e.*, the molecular weight of an atom) and distance from the electron to the nucleus. A large charge of the nucleus and a short distance from the electron to the nucleus gives the largest amount of spin-orbit coupling. Due to the strong spin-orbit coupling, compounds involving heavy atoms can emit from the non-emissive triplet state allowing for efficient phosphorescent emitters.³⁷ The spin-orbit interaction in such molecules essentially allows the triplet state to borrow some of the singlet state character, increasing the probability of radiative transition from the T_1 to S_0 state. Even in the absence of heavy atoms, SOC is an important factor in the TADF process when triplet excitons are upconverted to the singlet state.³⁸⁻

³⁹ The importance of SOC in TADF is discussed further in the TADF section (I.7).

I.6 Radiative transitions

Solving Schrödinger's equation for a two-electron system at different distances from the nucleus gives the potential energy surface for the ground S_0 as well as excited states $S_{1,2,3,\dots}$, consisting of several vibrational energy levels (Figure I.4).

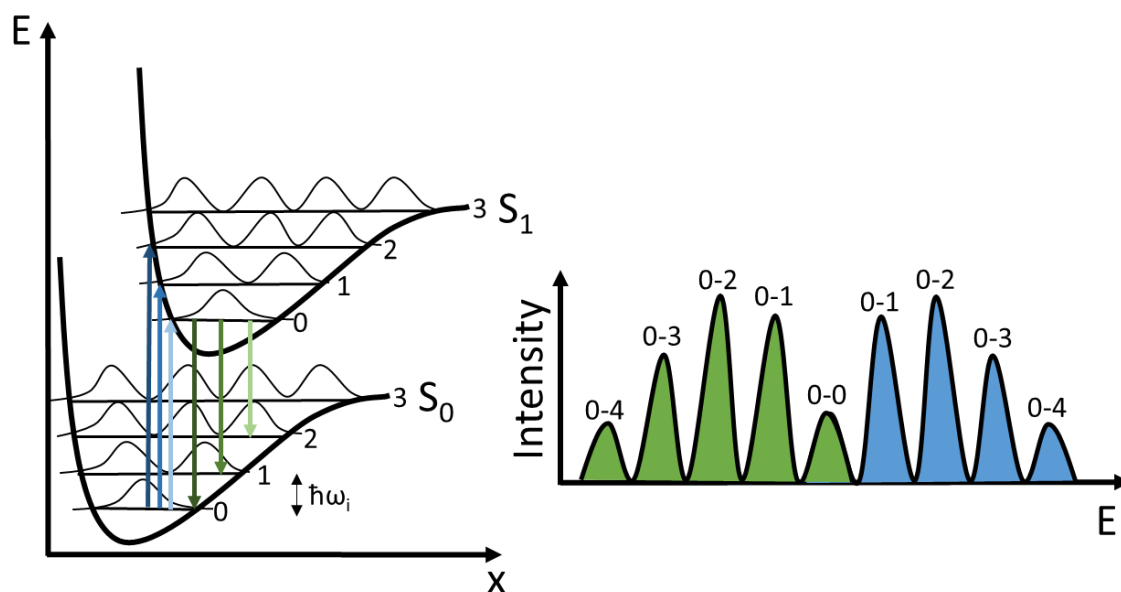


Figure I.4. Potential energy curves for the singlet and triplet states and corresponding transition intensities for absorption (blue) and emission (green). After Kearwell and Wilkinson.⁴⁰

Depending on the excitation energy, transitions between vibrational levels in the ground S_0 and excited states can occur. The transition from the ground S_0 to any of the excited states is called absorption while the reverse process is called emission. Noteworthy is that the emission always occurs from the lowest excited state which is also known as *Kasha's rule*. In Figure I.4, the absorption-related transitions from S_0 to S_1 are marked in blue while the emission processes are marked in green. The probability of the transition from the 0th vibrational level to the m^{th} vibration level depends on the wavefunction overlap between the initial and final state and is described by *Frack-Condon-factor*.³³ The illustration of absorption and emission profile based on transition probabilities between different states is shown in Figure I.4. The same principle applies to triplet states. While *Frack-Condon-factor*

describes the shape and intensity of the absorption and emission spectrum, the probability of a radiative decay to the ground state is defined via the oscillator strength.³⁴

$$f = 4.31 \times 10^{-9} \int \epsilon d\nu \quad (16)$$

where ϵ is a decadic extinction coefficient and ν is energy in wavenumbers. The oscillator strength being proportional to the extinction coefficient, one can estimate the likelihood of the radiative decay in the molecule by evaluating the extinction coefficient from the absorption data. Since the extinction coefficient in the molecule depends on the overlap integral between donor and acceptor orbitals, different types of transitions can be identified based on the value of the extinction coefficient. For example, a π - π^* transition (Figure I.2) has a typical value of the extinction coefficient higher than $10^4 \text{ M}^{-1} \text{ cm}^{-1}$ while for the n - π^* transition (where n is a non-bonding electron pair) the extinction coefficient is usually smaller ($<10^4 \text{ M}^{-1} \text{ cm}^{-1}$).³⁴ Both π - π^* and n - π^* transitions are also known as locally-excited (LE) transitions and can be recognised by the structured absorption/emission spectra. In case when the overlap integral between donor and acceptor orbitals is minimal, the so-called charge-transfer states (CT) can be formed, usually accompanied by broad and unstructured emission spectra, with extinction coefficients of normally below $10^4 \text{ M}^{-1} \text{ cm}^{-1}$.³³⁻³⁴

Normally, the energy of the absorbed light is higher than the energy of the emitted light. The energy difference between the band maxima of the absorption and emission spectra of the same electronic transition is called the Stokes shift. There are two types of Stokes shift, internal and external. The internal Stokes shift occurs when the molecules reorganize themselves after excitation leading to the emission from the lowest vibrational level (see Figure I.4). The external Stokes shift arises when the excited molecule is stabilised through the interactions with the environment. For example, the solvent can stabilise the excited molecule via dipole interactions. The amount of stabilization through solvent dipoles and thus the redshift of the emitted light from the molecule with respect to the absorbed energy mostly depends on the polarity of the solvent, with more polar solvents showing more redshift in the emitted light with respect to the absorbed light.³⁵ The redshift of the emission with respect to

Introduction

the absorbed light can also occur due to other effects such as stabilisation of excited molecule via hydrogen bonding or formation of internal charge transfer (ICT) states.³⁵

I.7 Thermally activated delayed fluorescence (TADF)

A simplified three-level energy diagram demonstrating forward and reverse processes between the singlet and triplet states is presented in Figure I.5.

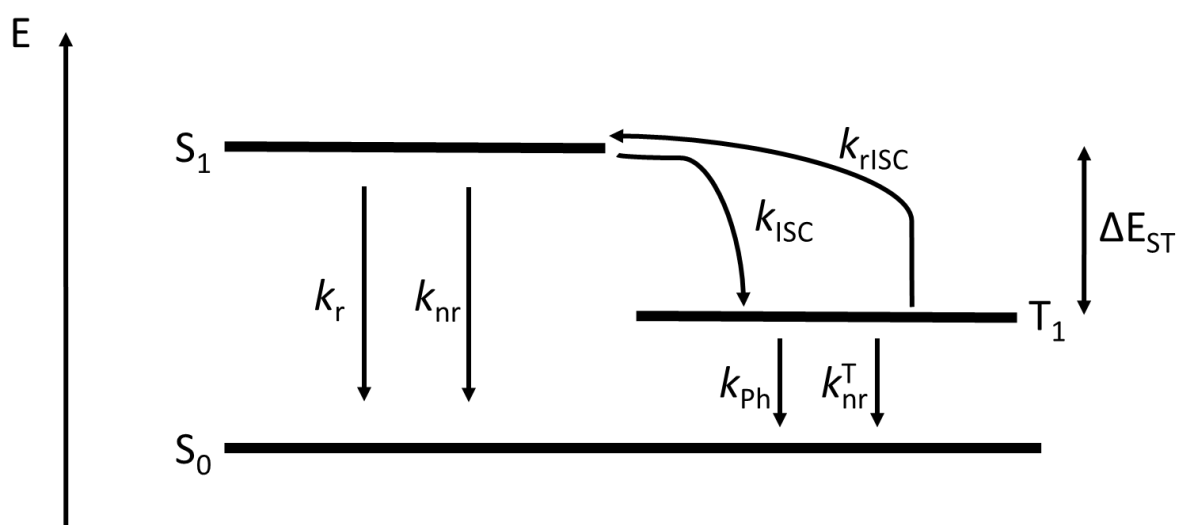


Figure I.5. A three-level diagram demonstrating transitions from and between singlet and triplet states. The singlet state conversion to the triplet state and the reverse process are denoted as k_{ISC} and k_{rISC} , respectively. The energy gap between the singlet and triplet state is ΔE_{ST} .

Since radiative transitions from the triplet state to the ground state are generally not efficient at room temperature, a possible way to prevent the energy loss through the non-radiative decay from the triplet state is to upconvert the triplet exciton to the singlet state non-coherently using the ambient energy. Triplet exciton upconversion to the singlet state usually requires the energy gap between the singlet and triplet state, ΔE_{ST} , to be smaller than 0.2 eV. Given a sufficiently low ΔE_{ST} , triplet excitons can be upconverted to the singlet state at a rate which is defined as the reverse intersystem crossing (RISC) rate, k_{rISC} . The RISC rate depends on the ΔE_{ST} value and is defined as follows,

$$k_{rISC} = A \exp\left(-\frac{\Delta E_{ST}}{k_B T}\right) \quad (17)$$

where A is the pre-exponential factor, k_B is Boltzmann's constant and T is the temperature.

Once the triplet exciton is upconverted to the singlet state, it can then be either back-converted to the triplet state using the intersystem crossing (ISC) or decay from the singlet state at a radiative decay rate, k_r .

Although it has been recently demonstrated that, in the presence of a flexible angle between the donor and acceptor unit, a spin-flip can also happen between the triplet and singlet charge-transfer states (^3CT and ^1CT),⁴¹⁻⁴² normally, the energy transfer between the states of the same electronic character is forbidden (El Sayed's rule).⁴³⁻⁴⁴ It has been reported that for the efficient RISC process between ^3CT and ^1CT states, a higher-lying triplet state of a different electronic character (for example, a locally-excited triplet state ^3LE) should be present.^{38, 45-46} Having a higher-lying triplet state of a different nature allows for a stronger spin-orbit coupling (SOC) between the triplet and singlet manifolds, making the triplet exciton conversion to the singlet state more probable.^{38-39, 47} To increase the probability of having higher-lying triplet states of a SOC-suitable nature, molecular designs leading to a higher density of intermediate triplet states have been developed.⁴⁸⁻⁴⁹ It is noteworthy that in cases when higher triplet states are involved in the RISC process, a spectroscopic determination of the lowest triplet state is not always a good estimation for the ΔE_{ST} gap. In such cases, the activation energy E_{act} for the RISC process can be lower than the ΔE_{ST} gap, resulting in E_{act} being a better approximation for the energy barrier for the TADF process.

To study TADF, the temperature-dependent transient photoluminescence (PL) decay measurements are performed and analysed. Figure I.6 shows an example of a transient PL decay measurement at a temperature range when TADF is active.

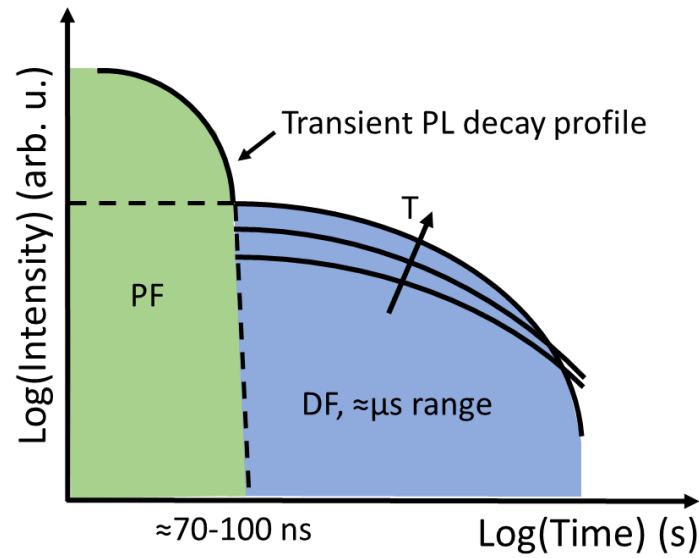


Figure I.6. An example of a transient photoluminescence decay profile at a few different temperatures.

TADF can be identified experimentally from a transient PL decay profile. The transient photoluminescence decay profile for a TADF material typically consists of a prompt part lasting until around 70-100 ns and a delayed part usually occurring in the microsecond range (Figure I.6). With increasing temperature, the intensity of delayed emission increases which is an indication of TADF. Both prompt and delayed parts can be fitted with exponentials. While a single exponential fit is sufficient for transient PL measurements in solution for both prompt and delayed part, fitting of the transient PL decay profile for films is usually more complicated. Due to a distribution of molecular conformations in films owning different ΔE_{ST} gaps,^{47, 50} a multi-exponential fit is usually necessary to fit the delayed part of the decay. The sum of two or three exponentials can be used to describe the delayed part of the transient PL decay profile in films.

$$y = Ae^{-t/\tau_1} + Be^{-t/\tau_2} + \dots \quad (18)$$

In case when multi-exponentials are employed, the average lifetime can be calculated as follows.

$$\langle \tau \rangle = \frac{A \cdot \tau_1^2 + B \cdot \tau_2^2 + \dots}{A \cdot \tau_1 + B \cdot \tau_2 + \dots} \quad (19)$$

The total area of prompt or delayed emission (I_{PF} and I_{DF}) can then be evaluated as follows.

$$I_{PF} = A_{PF} \cdot \tau_{PF} \quad (20)$$

$$I_{DF} = A_{DF_1} \cdot \tau_{DF_1} + A_{DF_2} \cdot \tau_{DF_2} + \dots \quad (21)$$

Another way to estimate the average lifetime in the molecule without the need for a multi-exponential fit is to directly integrate the experimental data consisting of transient photoluminescence intensity and time as follows.

$$\tau_{avg} = \frac{\int I(t)tdt}{\int I(t)dt} \quad (22)$$

where $I(t)$ is the intensity and t is the delay time. When the delayed lifetime is evaluated using Equation 22, the total emission of the delayed part can be evaluated by integrating the transient PL decay profile. While the integration of the transient PL decay profile to get the total area of the emission is suitable for the delayed part, the prompt part of the emission should still be fitted using an exponential fit (Equation 18) and the total area of the prompt emission should be evaluated using Equation 20. The areas of prompt or delayed emission are useful for the estimation of relative quantum yields of the prompt and delayed emission.

1.8 Photophysical parameters to compare TADF systems

To evaluate the efficiency of the emitter, the photoluminescence quantum yield (PLQY) measurements are done in solution and film. PLQY is measured under the nitrogen atmosphere to prevent quenching of singlet and triplet states with oxygen.⁵¹ The total PLQY is defined as follows.

$$\Phi_{PL} = \Phi_{PF} + \Phi_{DF} \quad (23)$$

where Φ_{PF} and Φ_{DF} are the prompt and delayed photoluminescence quantum yields. To estimate the prompt and delayed emission contributions to the total emission as well as other TADF-related properties, the total areas under the prompt and delayed emission curves of the transient PL decay data are evaluated (Figure I.6). The TADF-related parameter (Φ_{DF}/Φ_{PF} , k_{ISC} , k_{rISC} , k_{nr}^T) calculations are based on the works of Baleizao and Dias (a diagram illustrating TADF-related parameters is presented

Introduction

in Figure I.5).⁵²⁻⁵³ The ratio between the total intensity for the delayed and prompt emission represents the ratio between the quantum yields of the delayed and prompt emission.

$$\frac{I_{DF}}{I_{PF}} = \frac{\Phi_{DF}}{\Phi_{PF}} \quad (24)$$

Given that the total PLQY and the ratio between Φ_{DF} and Φ_{PF} are known, the quantum yields of prompt Φ_{PF} and delayed emission Φ_{DF} can be evaluated separately. Knowing the prompt emission yield and lifetime allows for the calculation of the radiative decay rate constant.

$$k_r^s = \frac{\Phi_{PF}}{\tau_{PF}} \quad (25)$$

where k_r^s is the radiative decay rate constant of the singlet state, Φ_{PF} is the prompt emission quantum yield and τ_{PF} is the prompt emission lifetime. The non-radiative decay rate constant of the singlet state can then be evaluated from the following equation.

$$k_{nr}^s = \frac{1}{\tau_{PF}} - k_r^s \quad (26)$$

where k_{nr}^s is the non-radiative decay rate constant from the singlet state. The non-radiative decay of the excited singlet state consists of the internal conversion (IC) of the excited singlet state to the ground state and the intersystem crossing (ISC) to the triplet state. The evaluation of the RISC-related parameters depends on the ratio between Φ_{DF} and Φ_{PF} .

In the case when the ratio of delayed and prompt emission quantum yield is more than four, $\Phi_{DF}/\Phi_{PF} > 4$, the evaluation of the RISC-related properties is simplified and can be obtained from the data available from the transient photoluminescence decay measurements at room temperature, *i.e.*, τ_{DF} and Φ_{DF}/Φ_{PF} . As demonstrated by Dias *et al.*, when $\Phi_{DF}/\Phi_{PF} > 4$, the reverse intersystem crossing yield can be approximated to unity ($\Phi_{RISC} \approx 1$) so that the intersystem crossing yield can be evaluated in a simplified way to a high accuracy as follows.⁴⁷

$$\Phi_{ISC} = \frac{\Phi_{DF}}{\Phi_{PF} + \Phi_{DF}} \quad (27)$$

where Φ_{ISC} is the yield of intersystem crossing. Once Φ_{ISC} is known, the intersystem crossing rate constant can be evaluated using the following equation.

$$k_{ISC} = \frac{\Phi_{ISC}}{\tau_{PF}} \quad (28)$$

where k_{ISC} is the intersystem crossing rate constant. The reverse process, named after a reverse intersystem crossing rate (RISC), k_{rISC} , defines how fast triplet excitons are converted to the singlet state. The RISC rate can be evaluated as follows.

$$k_{rISC} = \frac{1}{\tau_{DF}} \left(1 + \frac{\Phi_{DF}}{\Phi_{PF}} \right) \quad (29)$$

where k_{rISC} is the reverse intersystem rate constant.

If the TADF contribution is small, *i.e.*, $\Phi_{DF}/\Phi_{PF} < 4$, there are two ways to evaluate the RISC-related properties. First, if the molecule is rigid, it can be assumed that the non-radiative decay rate via the internal conversion of the single state is negligible. In such cases, the intersystem crossing yield can be simplified as follows.⁵⁴

$$\Phi_{ISC} = 1 - \Phi_{PF} \quad (30)$$

Second, if the non-radiative rate via internal conversion cannot be approximated to zero, the simplification presented in Equation 30 is not suitable and thus Φ_{ISC} should be estimated in a non-simplified approach using Equation 31.

$$\tau_{DF} = \tau_{ph}^0 - \left(\frac{1}{\Phi_{ISC}} - 1 \right) \tau_{ph}^0 \frac{\Phi_{DF}}{\Phi_{PF}} \quad (31)$$

where τ_{ph}^0 is the phosphorescence lifetime. To calculate Φ_{ISC} from Equation 31, a linear fit of τ_{DF} versus Φ_{DF}/Φ_{PF} is needed and thus requires calculating τ_{DF} and Φ_{DF}/Φ_{PF} at several temperatures. Once Φ_{ISC} is known, the RISC rate can be calculated as follows.

Introduction

$$k_{rISC} = \frac{1}{\tau_{DF} \Phi_{ISC}} \left(\frac{\Phi_{DF}}{\Phi_{PF}} \right) \quad (32)$$

To evaluate the non-radiative decay of the triplet state, the yield of the reverse intersystem crossing is needed and can be obtained from the following expression.

$$\Phi_{rISC} = \frac{\Phi_{DF}}{\Phi_{ISC} \Phi_{PL}} \quad (33)$$

where Φ_{rISC} is the yield of the reverse intersystem crossing. Finally, the non-radiative decay constant of the triplet state can be calculated as follows.

$$k_{nr}^T = \frac{k_{rISC}}{\Phi_{rISC}} - k_{rISC} \quad (34)$$

where k_{nr}^T is the non-radiative decay rate constant of the triplet state.

1.9 The role of the host molecule

The purpose of the host molecule is to disperse the guest molecules and to reduce the interactions between them that could lead to concentration quenching, resulting in the decrease of PLQY with increasing emitter concentration in the guest-host system. The amount of concentration quenching is related to the trapping of diffusive exciton either by an aggregate of the molecule itself or by traps of different nature (impurity, interface between microcrystals, interaction with substrate). Quenching by aggregate formation largely depends on the ability of the molecule to form aggregates that is related to the planarity and rigidity of the molecule, essentially defining how closely the molecules can be situated in a solid film. Figure 1.7 presents an example of a strong concentration quenching in TADF emitters based on multi-resonance (see Section 1.11 and Chapter 4 for more details, including molecular structures).

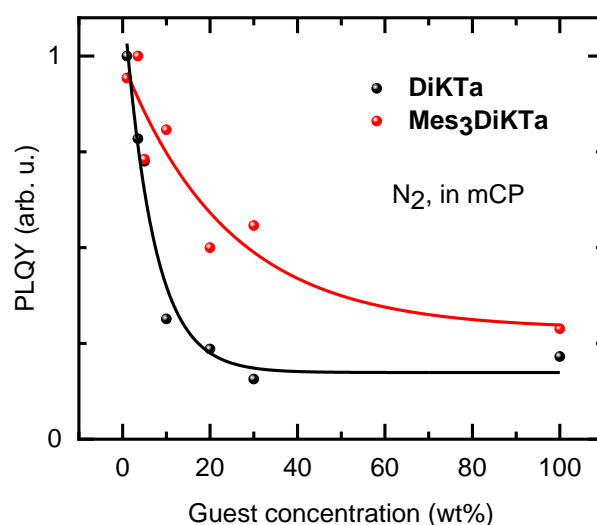


Figure I.7. PLQY dependence on the guest concentration of **DiKTA** and **Mes₃DiKTA** in mCP. Discussed further in Chapter 4.

For **DiKTA**, PLQY in film drops by around three times when increasing the doping concentration (emitter concentration in the guest-host system) from 1% to 10% by weight. For **Mes₃DiKTA**, the drop in PLQY is less severe yet still significant. Therefore, for TADF emitters based on multi-resonant structures, the doping concentration is usually kept low (<4 wt%)^{23, 27} compared to standard donor-acceptor type emitters where doping concentrations can even exceed 15 wt% in some cases.⁵⁵ Interestingly, given a dendrimer-type molecular structure or structures with bulky side groups, the usage of host materials can sometimes be prevented (see also Chapter 1b).⁵⁶

To select a suitable host material for the guest, one needs to consider a few aspects. First, the singlet and triplet energy levels of the host should be higher in energy than the corresponding levels of the guest (Figure I.8).

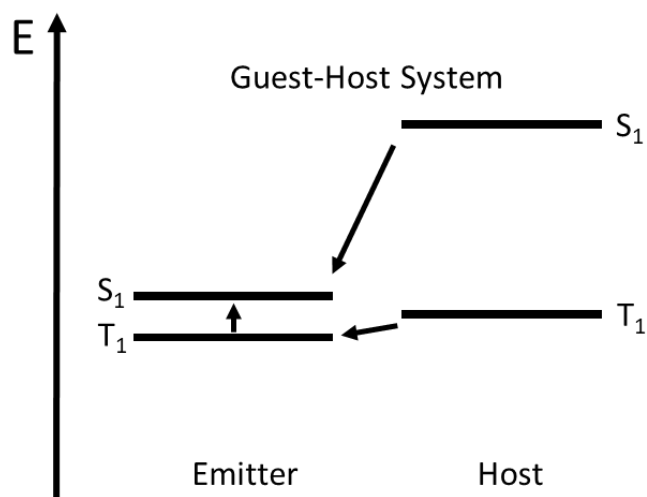


Figure I.8. Singlet and triplet energy level diagram for a guest-host system.

Furthermore, not only the singlet and triplet energy levels of the host should be energetically higher compared to the corresponding energy levels of the guest, but also the absorption of the guest should overlap with the emission of the host.⁵⁵ A host material for long-lasting and efficient OLEDs should also possess a good thermal and chemical stability as well as a suitable HOMO level for OLED applications.⁵⁵

I.10 The organic light-emitting diode (OLED)

To assess the guest-host systems in a device, OLEDs are fabricated. Figure I.9 presents a layout of a basic OLED.

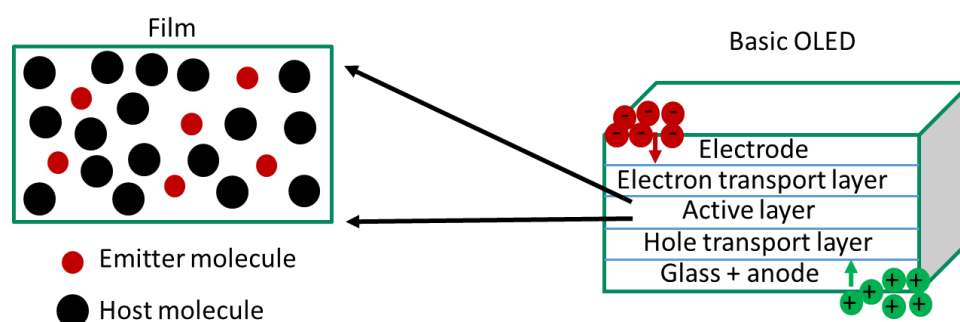


Figure I.9. A basic structure for an OLED. The active layer is a combination of emitter molecules dispersed in a host.

The active layer in an OLED is essentially the guest-host system sandwiched between electron and hole transport layers and electrodes for charge injection. For an efficient charge accumulation in the active layer, HOMO and LUMO levels of electron and hole transporting layers should be selected in such a way so that the injected charges do not face energetic barriers to travel towards the emissive layer. For an efficient charge transfer from host to guest, the HOMO and LUMO levels of the emitter should be between the HOMO and LUMO levels of the host. OLEDs can be made either by evaporation or solution processing, with the latter technique usually showing poorer efficiencies.⁵⁶ The external quantum efficiency (EQE) of an OLED is defined as the ratio of the number of emitted photons divided by the number of injected charges and can be expressed as follows.⁵⁷

$$\eta_{\phi}(ext) = \gamma \eta_r \Phi_f \eta_{ext} \quad (35)$$

where γ is the charge balance factor, η_r is the internal quantum efficiency (IQE), Φ_f is the photoluminescence quantum efficiency or PLQY and η_{ext} is the external quantum efficiency. After the hole and electron are injected into the OLED, they can meet and form an exciton which can then decay via a radiative decay and generate light. Unfortunately, for injected holes and electrons, there are also several possible loss channels that decrease the total efficiency of the device (Figure I.10).

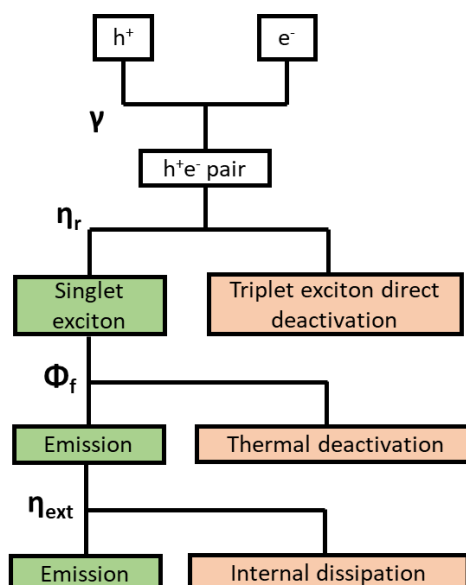


Figure I.10. A schematic representation of the processes defining the external quantum efficiency (EQE) in an OLED. After Tsutsui.⁵⁷

Introduction

When the hole and electron meet, there is a 25% chance of singlet and a 75% chance of triplet exciton generation. This implies that if the triplet exciton cannot be transferred to the singlet state (for example, via TADF or TTA), then 75% of energy is lost (η_r is strongly reduced). Furthermore, singlet excitons are not guaranteed to emit light, as they can also be lost via a non-radiative decay (reducing Φ_r). Even if the singlet exciton happens to decay in a radiative way, there is still a chance that the generated light does not find its way out of the OLED (η_{ext}). The external efficiency η_{ext} describes how easily the light generated in the active layer can escape the device. The external efficiency η_{ext} can be approximated using the refractive index of the emissive medium n .⁵⁷

$$\eta_{\text{ext}} = \frac{1}{2n^2} \quad (36)$$

Assuming the balanced charge injection ($\gamma = 1$) and the internal quantum yield (IQE) as unity (for example, due to TADF), the external quantum efficiency in the OLED is then governed by the outcoupling efficiency. Given that the refractive index of the materials used in OLEDs ranges between 1.5 and 2.1,⁵⁸ the maximum η_{ext} is only around 20% (using Equation 36 with a refractive index of 1.5), meaning that the maximum external quantum efficiency (EQE) in an OLED is normally in the range of around 20%. To acknowledge the currently existing approaches to obtain TADF emitters allowing for such efficient OLEDs, the next section is dedicated to the state-of-the-art TADF and challenges.

I.11 State-of-the-art TADF and challenges

This section presents a brief overview of the currently existing approaches to obtain efficient TADF emitters. Since TADF requires a small ΔE_{ST} gap (usually, less than 0.2 eV) for the triplet excitons to be upconverted non-coherently to the singlet state using the ambient energy, the main question is how to obtain such molecules owning small ΔE_{ST} gaps. The energy gap between the lowest singlet and triplet states, ΔE_{ST} , that governs the magnitude of the TADF process largely depends on the hole-electron wavefunction overlap.^{19, 59} This implies that the singlet-triplet gap can be reduced by localizing hole and electron wavefunctions onto different parts of the molecule, and this is commonly achieved by employing spatially separated donor and acceptor moieties. Nevertheless, the spatially separated donor and acceptor moieties should still have enough hole-electron overlap for a good radiative decay rate.^{19, 59} The balance of these two factors is required to obtain a high-performance TADF emitter. There are a few techniques to limit the spatial separation of the donor and acceptor moieties.

The simplest strategy to adjust the wavefunction overlap is by fine-tuning the torsion between the donor and the acceptor moieties, which controls the extent of the conjugation between these two fragments.^{11, 18, 60-61} A more sensitive approach to control the electron-hole separation is to increase the delocalization of the hole density over the donor unit alone.⁸ This has been implemented in molecules owning larger donor structures, often consisting of a few generations of donor units of the same or different functionality (dendrimers).^{59, 62-65} Comparing to standard donor-acceptor emitters, consisting of single generation donor units, even more moderate donor-acceptor torsions in the dendrimers can ensure sufficient overlap between hole and electron densities to achieve the paradox of a small ΔE_{ST} and a large radiative decay rate.⁶⁰ Unfortunately, only a few variants have been explored and thus a deeper understanding of the effect of structure modulation on the TADF-related properties is currently missing in the field.

The ΔE_{ST} gap is not the only prerequisite for efficient TADF. The rate of the reverse intersystem crossing also depends on the magnitude of the spin-orbit coupling (SOC) between the singlet and triplet manifolds.^{38, 66} A pronounced SOC requires that the singlet and triplet states are of a different nature,

Introduction

for example, the lowest singlet state of a charge-transfer (CT) nature can have an effective SOC with a triplet state having a stronger locally-excited nature.^{39, 67-68} Usually, compounds with more intermediate triplet state have an increased chance of more effective TADF as there are more states that can potentially be a good match for the SOC between singlet and triplet manifolds.^{39, 67-68} There are a few strategies to achieve compounds owning a higher number of intermediate triplet states.^{10, 48-49, 69-70} A possible solution is to employ molecular designs with repetitive donor and/or acceptor unit, resulting in a larger number of quasi-degenerate states.⁴⁸ For example, one existing strategy is based on a multi-donor to a single acceptor systems where a higher number of carbazole units in the molecule successfully enhanced TADF.⁷¹ Another possible way to ensure a larger number of intermediate triplet states is to increase the number of repetitive donor-acceptor units within the main chain polymer.⁴⁹ Unfortunately, the attempts to enhance TADF-related properties in such systems resulted in a strong redshift of photoluminescence.⁴⁹ Therefore, an approach to gradually fine-tune TADF-related properties without the redshift of photoluminescence is currently not available.

The state-of-the-art approaches to obtain efficient TADF emitters mentioned so far were mainly focused on donor-acceptor units. There is, however, also a new approach to obtain both a small ΔE_{ST} gap and a fast radiative decay rate. This approach is based on TADF emitters with multi-resonant molecular structures. In 2015, the molecular design showing resonance effects of electron-donating oxygen and electron-withdrawing boron moieties was presented by Hatakeyama and co-workers.⁷² Later it was demonstrated that a small ΔE_{ST} and a fast radiative decay rate in selected TADF molecules based on multi-resonant structures is achieved via a short-range separation between hole and electron densities, providing a small exchange interaction yet still ensuring a high radiative decay rate.²² To illustrate the short-range charge separation of hole and electron densities, the DFT calculation was performed by David Hall (University of St Andrews) (Figure I.11).

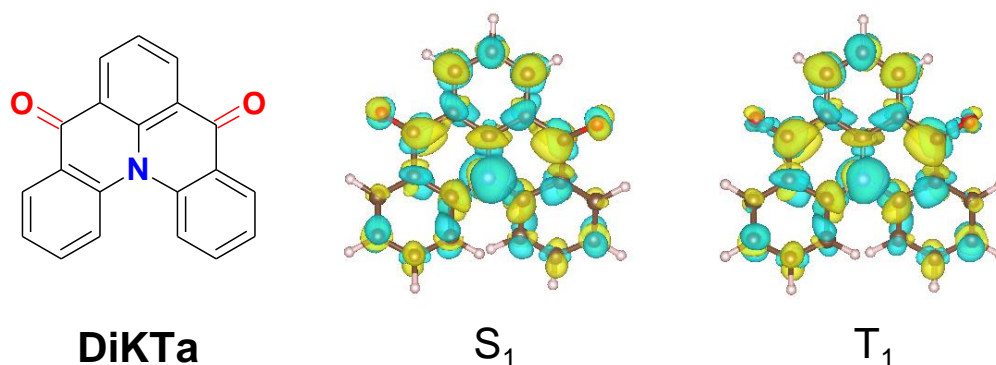


*Figure I.11. Difference density plots of lowest singlet and triplet excited states for **DiKTa** calculated in the gas phase using SCS-CC2.²³ Blue indicates an area of decreased electron density while yellow indicates increased electronic density between the ground and excited states.²³ This figure is presented with the permission of David Hall (University of St Andrews). **DiKTa** was first mentioned in Section I.9 and it is further discussed in Chapter 4.*

The DFT calculation presented in Figure I.11 reveals a short-range separation between hole and electron densities for both the lowest singlet and triplet states of the TADF emitter based on a multi-resonant structure. As investigated later in Chapter 4, such molecular design enables both a small ΔE_{ST} gap and a fast radiative decay rate. Furthermore, opposite to conventional donor-acceptor type emitters, usually possessing a full width at half maximum (FWHM) of up to 100 nm, the TADF emitters based on multi-resonant structures have much narrower FWHM, often below 40 nm.^{22-23, 27} Unfortunately, all these benefits come at a cost. Due to the rigid and planar structure of such emitters, the major challenge is a strong concentration quenching (Figure I.7).²³ To address this problem, bulkier substituents can be attached to prevent strong guest to guest interactions, yet it is not clear if this would preserve the photoluminescence emission colour and TADF-related properties.

To complement the current state-of-the-art knowledge in the TADF field, I approach the challenges presented in this section in the following chapters of my work. I demonstrate that ΔE_{ST} and TADF can be successfully optimised either by controlling the hole delocalization on the dendron donor unit or by carefully selecting the linkage position of the dendron donor unit to the acceptor core via a phenylene bridge. I also find that TADF-related properties can be enhanced without the redshift of the photoluminescence emission in oligomers of gradually increasing size. Finally, I demonstrate that

Introduction

bulkier substituents employed in TADF emitters based on multi-resonant structures can successfully decrease the concentration quenching of the molecules without disturbing TADF-related properties.

M. Methods

M.1 Absorption

Absorption measurements were carried out using the Cary 5000 UV-Vis-NIR spectrophotometer. The working principle of the absorption measurement is based on Beer-Lambert's law.

$$I(\lambda) = I_0 \cdot 10^{-OD(\lambda)} \quad (37)$$

where OD is the optical density. For solution measurements, the optical density can be expressed as follows.

$$OD(\lambda) = \varepsilon(\lambda) \cdot c \cdot d \quad (38)$$

where ε is the decadic extinction coefficient, c is the molarity of the solution and d is the thickness of the cuvette. The decadic extinction coefficient ε can be expressed as follows.

$$\varepsilon(\lambda) = \frac{OD(\lambda)}{c \cdot d} \quad (39)$$

The standard cuvette size used in the experiments is 1 mm.

M.2 Steady-state photoluminescence and phosphorescence

Steady-state spectra at room temperature (RT) and 77 K and the photoluminescence emission in the millisecond range at 77 K were obtained using the Jasco FP-8600 spectrofluorometer. For steady-state and phosphorescence measurements at 77 K using the Jasco FP-8600 spectrofluorometer, the film or cuvette for solution measurements was immersed in the liquid nitrogen as there is no cryostat integrated into the device to gradually change the temperature. If other temperatures than 300 K or 77 K were required, the photoluminescence measurements were conducted in the time-resolved setup with the integrated helium cryostat as outlined in Figure **M.2**. Noteworthy is that 77 K can sometimes be not sufficiently low for the phosphorescence measurements as the contribution from delayed fluorescence is still significant. This can occur for molecules owning a small ΔE_{ST} gap and having a fast RISC rate. In such cases, the sample was cooled down to 5 K using the helium cryostat integrated into the setup outlined in Figure **M.2**.

M.3 Photoluminescence quantum yield (PLQY)

The photoluminescence quantum yield can be measured both for solution and film in an integrating sphere using the excitation light source and the detector. The PLQY measurements at room temperature were obtained using the integrating sphere integrated into the Jasco FP-8600 spectrofluorometer. To prevent oxygen interaction with the samples, the thin film PLQY was measured in N₂ filled sphere whereas PLQY in solution was measured using oxygen-free solvents. The PLQY measurements are done in three steps as shown in Figure M.1.

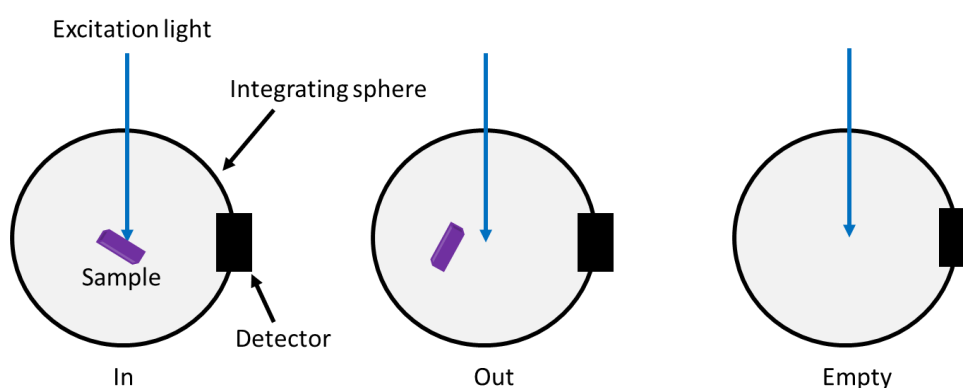


Figure M.1. Three steps for the PLQY measurements.

First, the steady-state emission of the sample is measured in the integrating sphere (“in”). Second, the measurement is repeated with the sample moved away from the excitation light (“out”). Third, the sample is removed from the integrating sphere and the measurement is performed on an empty sphere to account for the background of the integrating sphere (“empty”). The detected light output is then integrated for both the excitation light L and the photoluminescence signal from the sample P . The PLQY value is then calculated according to the following equations adapted from de Mello.⁷³

$$A = \left(1 - \frac{L_{in}}{L_{empty}} \right) \quad (40)$$

and

$$\Phi = \frac{(P_{in} - P_{empty}) - (1 - A)(P_{out} - P_{empty})}{L_{empty} A} \quad (41)$$

where A is the absorption of the sample and Φ is the total quantum yield of the sample.

M.4 Time-resolved photoluminescence

The experimental setup for the time-resolved photoluminescence measurements at different temperatures is presented in Figure M.2.

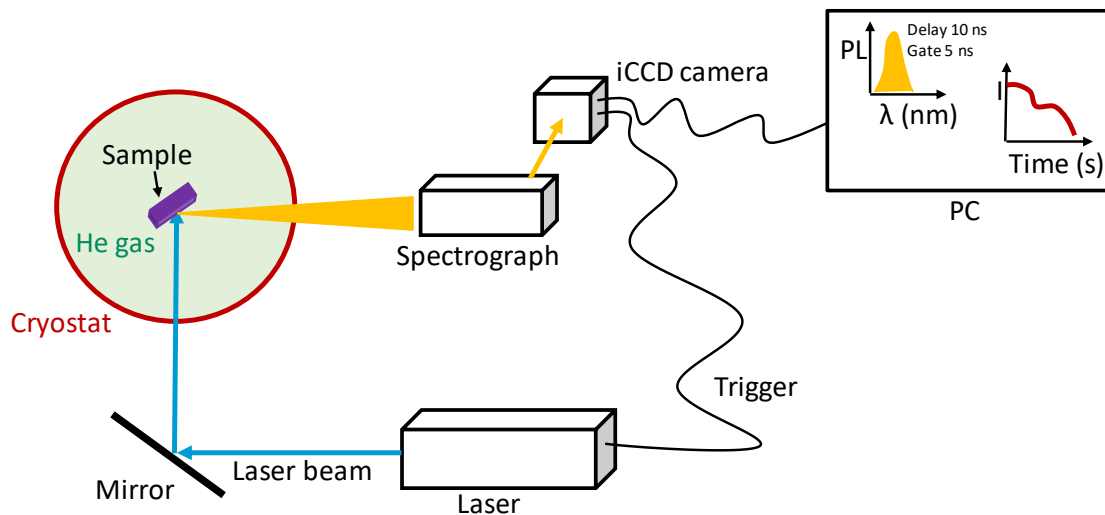


Figure M.2. The experimental setup for transient PL decay measurements.

The time-resolved photoluminescence setup consists of a nanosecond laser with a 355 nm emission output (QS Lasers MPL15100-DP). The laser beam is directed onto the sample. The sample is excited and the excitation light is collected by a spectrograph (Oriel MS257) which is connected to the iCCD camera (iStar A-DH334T-18F-03). The sample is placed in a helium cryostat which allows changing the temperature from 5 K until 345 K. The sample is kept in a helium atmosphere unless stated otherwise. The emitted light from the sample is then analysed with respect to time yielding a photoluminescence spectrum at a specific delay (d) and gating time (g) as well as the transient photoluminescence decay profile from a few nanoseconds until the millisecond range. The gating time for transient photoluminescence decay measurements is kept 10 times lower compared to the delay time according to Ref⁵³. As an example, the exponential functions to generate delay and gating times are as follows.

$$t_d(x) = 250 \exp(0.4x) + t_{d_0} \quad (42)$$

$$t_g(x) = 25 \exp(0.4x) + t_{g_0} \quad (43)$$

Methods

where t_d is the delay time in picoseconds and t_g is the gating time in picoseconds. x is the step number. t_{d0} and t_{g0} are the initial delay and gating times, respectively.

In the analysis of the transient photoluminescence decay data, the delay time is corrected for the time of arrival of the laser pulse with respect to the iCCD camera (Figure **M.3**). Furthermore, the recorded emission output at a specific delay time is divided by the corresponding gating time, to normalize the emission at every delay time to the same amount of collected photons.

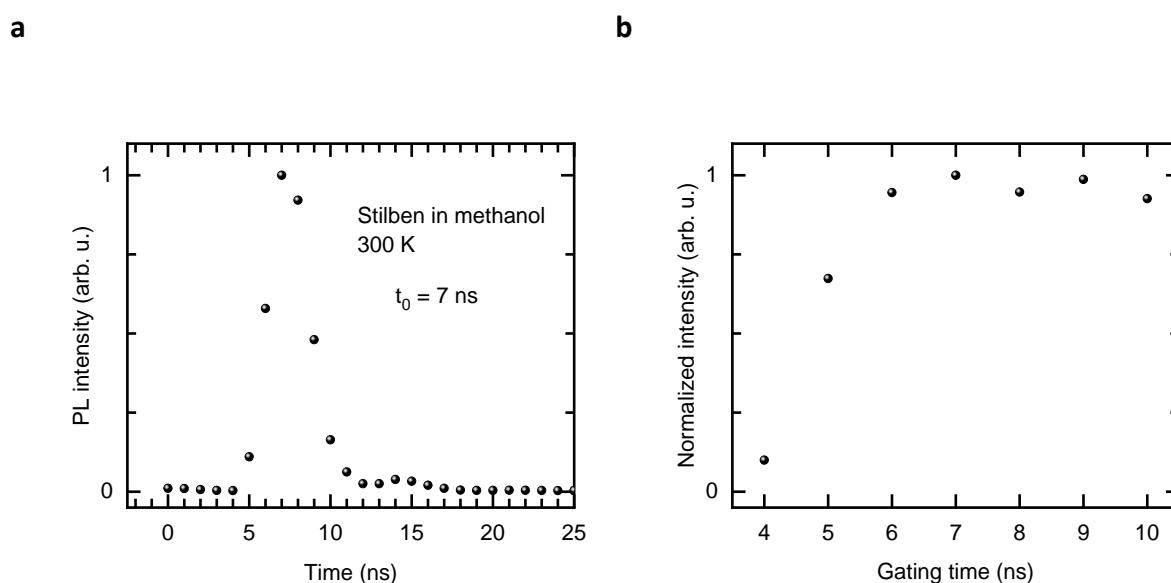


Figure **M.3**. (a) The laser pulse profile as seen by the iCCD camera measured using *trans*-stilbene in methanol. (b) The normalized light emission as seen by the iCCD camera for different gating times (the delay time is 10 ns). 300 K, $\lambda_{exc} = 355$ nm.

Figure **M.3a** shows the arrival of the laser pulse as seen by the iCCD camera. The detection of the laser pulse by the iCCD camera once the camera is triggered is not exactly at the delay time of zero and depends also on the optical beam path (the laser pulse must travel a specific distance before it reaches the sample which emits light detected by the iCCD camera). For example, for the experimental setup shown in Figure **M.2**, the laser pulse is detected at a delay time of 7 ns (Figure **M.3**), meaning that to get a real delay time after excitation of the sample, 7 ns must be subtracted from the set delay time.

Figure **M.3b** shows the normalized light emission against the gating time as detected by the iCCD camera. The data presented in Figure **M.3b** was divided by the corresponding gating time so that the

detected light intensity at a specific delay time, for example, 10 ns, is independent of the duration of the signal collection, *i.e.*, the number of photons. Once the collected signal at a specific delay time is normalized by the gating time, the signal should be independent of the gating time. However, as can be seen from Figure **M.3b**, until the gating time of around 6 ns, the response of the iCCD camera to the incoming number of photons is still not linear, meaning that to normalize the amount of photons for a specific delay time, a simple division by the gating time is not suitable. Therefore, for standard measurements using an exponential delay and gating time distribution, a starting gating time of 7 ns is selected so that the collected light at every delay time could be easily corrected for the number of incoming photons.

To assess the fastest lifetime which can be resolved using the transient PL decay setup outlined in Figure **M.2**, the *trans*-stilbene,⁷⁴ which is known to have the fluorescence decay lifetime of fewer than 1 ns, was measured in methanol (Figure **M.4**).

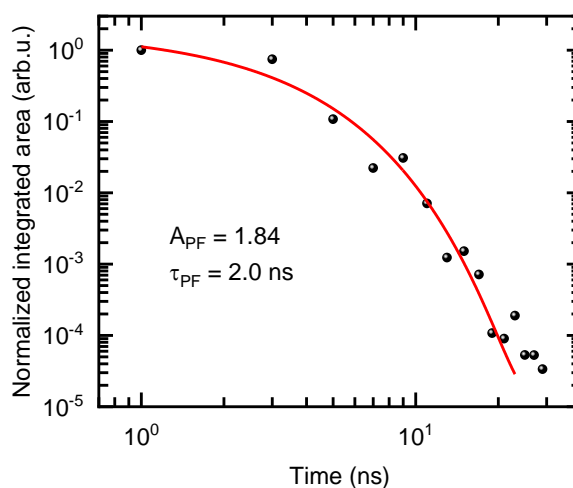


Figure **M.4**. The transient photoluminescence decay of *trans*-stilbene in methanol at 300 K. $\lambda_{exc} = 355$ nm.

Figure **M.4** presents the transient photoluminescence decay of *trans*-stilbene in methanol. The transient PL decay can be fitted with a mono-exponential with a lifetime of 2.0 ns. Given that the actual fluorescence lifetime of *trans*-stilbene is in the picosecond range,⁷⁴ it can be assumed that the transient

Methods

PL decay setup cannot resolve faster than 2.0 ns PL decays. Therefore, using the setup outlined in Figure **M.2**, only transient PL decays of slower than 2.0 ns can be investigated.

References

1. Zou, S.-J.; Shen, Y.; Xie, F.-M.; Chen, J.-D.; Li, Y.-Q.; Tang, J.-X., Recent advances in organic light-emitting diodes: toward smart lighting and displays. *Materials Chemistry Frontiers* **2020**, *4*, 788-820.
2. Forrest, S. R., The path to ubiquitous and low-cost organic electronic appliances on plastic. *Nature* **2004**, *428*, 911-918.
3. Kim, J.-J.; Han, M.-K.; Noh, Y.-Y., Flexible OLEDs and organic electronics. *Semiconductor Science and Technology* **2011**, *26*, 030301.
4. Lee, W.; Souk, J., Flexible OLED Manufacturing. **2018**, 173-191.
5. Lee, G.-H.; Moon, H.; Kim, H.; Lee, G. H.; Kwon, W.; Yoo, S.; Myung, D.; Yun, S. H.; Bao, Z.; Hahn, S. K., Multifunctional materials for implantable and wearable photonic healthcare devices. *Nature Reviews Materials* **2020**, *5*, 149-165.
6. Zhang, Q.; Li, B.; Huang, S.; Nomura, H.; Tanaka, H.; Adachi, C., Efficient blue organic light-emitting diodes employing thermally activated delayed fluorescence. *Nature Photonics* **2014**, *8*, 326-332.
7. Wong, M. Y.; Zysman-Colman, E., Purely Organic Thermally Activated Delayed Fluorescence Materials for Organic Light-Emitting Diodes. *Advanced Materials* **2017**, *29*, 1605444.
8. Yang, Z.; Mao, Z.; Xie, Z.; Zhang, Y.; Liu, S.; Zhao, J.; Xu, J.; Chi, Z.; Aldred, M. P., Recent advances in organic thermally activated delayed fluorescence materials. *Chemical Society Reviews* **2017**, *46*, 915-1016.
9. Xu, H.; Chen, R.; Sun, Q.; Lai, W.; Su, Q.; Huang, W.; Liu, X., Recent progress in metal-organic complexes for optoelectronic applications. *Chem. Soc. Rev.* **2014**, *43*, 3259-3302.
10. Uoyama, H.; Goushi, K.; Shizu, K.; Nomura, H.; Adachi, C., Highly efficient organic light-emitting diodes from delayed fluorescence. *Nature* **2012**, *492*, 234-238.
11. Kaji, H.; Suzuki, H.; Fukushima, T.; Shizu, K.; Suzuki, K.; Kubo, S.; Komino, T.; Oiwa, H.; Suzuki, F.; Wakamiya, A.; Murata, Y.; Adachi, C., Purely organic electroluminescent material realizing 100% conversion from electricity to light. *Nature Communications* **2015**, *6*, 8476.
12. Lin, T.-A.; Chatterjee, T.; Tsai, W.-L.; Lee, W.-K.; Wu, M.-J.; Jiao, M.; Pan, K.-C.; Yi, C.-L.; Chung, C.-L.; Wong, K.-T.; Wu, C.-C., Sky-Blue Organic Light Emitting Diode with 37% External Quantum Efficiency Using Thermally Activated Delayed Fluorescence from Spiroacridine-Triazine Hybrid. *Advanced Materials* **2016**, *28*, 6976-6983.
13. Dias, F. B.; Bourdakos, K. N.; Jankus, V.; Moss, K. C.; Kamtekar, K. T.; Bhalla, V.; Santos, J.; Bryce, M. R.; Monkman, A. P., Triplet Harvesting with 100% Efficiency by Way of Thermally Activated Delayed Fluorescence in Charge Transfer OLED Emitters. *Advanced Materials* **2013**, *25*, 3707-3714.
14. Parker, C. A.; Hatchard, C. G., Triplet-singlet emission in fluid solutions. Phosphorescence of eosin. *Transactions of the Faraday Society* **1961**, *57*, 1894.
15. Endo, A.; Ogasawara, M.; Takahashi, A.; Yokoyama, D.; Kato, Y.; Adachi, C., Thermally Activated Delayed Fluorescence from Sn⁴⁺-Porphyrin Complexes and Their Application to Organic Light Emitting Diodes - A Novel Mechanism for Electroluminescence. *Advanced Materials* **2009**, *21*, 4802-4806.
16. Endo, A.; Sato, K.; Yoshimura, K.; Kai, T.; Kawada, A.; Miyazaki, H.; Adachi, C., Efficient up-conversion of triplet excitons into a singlet state and its application for organic light emitting diodes. *Applied Physics Letters* **2011**, *98*, 083302.
17. Im, Y.; Kim, M.; Cho, Y. J.; Seo, J.-A.; Yook, K. S.; Lee, J. Y., Molecular Design Strategy of Organic Thermally Activated Delayed Fluorescence Emitters. *Chemistry of Materials* **2017**, *29*, 1946-1963.
18. Stachelek, P.; Ward, J. S.; dos Santos, P. L.; Danos, A.; Colella, M.; Haase, N.; Raynes, S. J.; Batsanov, A. S.; Bryce, M. R.; Monkman, A. P., Molecular Design Strategies for Color Tuning of Blue TADF Emitters. *ACS Applied Materials & Interfaces* **2019**, *11*, 27125-27133.
19. Gibson, J.; Penfold, T. J., Nonadiabatic coupling reduces the activation energy in thermally activated delayed fluorescence. *Physical Chemistry Chemical Physics* **2017**, *19*, 8428-8434.
20. Miwa, T.; Kubo, S.; Shizu, K.; Komino, T.; Adachi, C.; Kaji, H., Blue organic light-emitting diodes realizing external quantum efficiency over 25% using thermally activated delayed fluorescence emitters. *Scientific Reports* **2017**, *7*.

21. Hatakeyama, T.; Shiren, K.; Nakajima, K.; Nomura, S.; Nakatsuka, S.; Kinoshita, K.; Ni, J.; Ono, Y.; Ikuta, T., Ultrapure Blue Thermally Activated Delayed Fluorescence Molecules: Efficient HOMO-LUMO Separation by the Multiple Resonance Effect. *Advanced Materials* **2016**, *28*, 2777-2781.
22. Pershin, A.; Hall, D.; Lemaire, V.; Sancho-Garcia, J.-C.; Muccioli, L.; Zysman-Colman, E.; Beljonne, D.; Olivier, Y., Highly emissive excitons with reduced exchange energy in thermally activated delayed fluorescent molecules. *Nature Communications* **2019**, *10*, 597.
23. Hall, D.; Suresh, S. M.; dos Santos, P. L.; Duda, E.; Bagnich, S.; Pershin, A.; Rajamalli, P.; Cordes, D. B.; Slawin, A. M. Z.; Beljonne, D.; Köhler, A.; Samuel, I. D. W.; Olivier, Y.; Zysman-Colman, E., Improving Processability and Efficiency of Resonant TADF Emitters: A Design Strategy. *Advanced Optical Materials* **2019**, *8*, 1901627.
24. Zhang, Y.; Zhang, D.; Wei, J.; Hong, X.; Lu, Y.; Hu, D.; Li, G.; Liu, Z.; Chen, Y.; Duan, L., Achieving Pure Green Electroluminescence with CIEy of 0.69 and EQE of 28.2% from an Aza-Fused Multi-Resonance Emitter. *Angewandte Chemie International Edition* **2020**, *59*, 17499-17503.
25. Zhang, Y.; Zhang, D.; Wei, J.; Liu, Z.; Lu, Y.; Duan, L., Multi-Resonance Induced Thermally Activated Delayed Fluorophores for Narrowband Green OLEDs. *Angewandte Chemie International Edition* **2019**, *58*, 16912-16917.
26. Liang, X.; Yan, Z.-P.; Han, H.-B.; Wu, Z.-G.; Zheng, Y.-X.; Meng, H.; Zuo, J.-L.; Huang, W., Peripheral Amplification of Multi-Resonance Induced Thermally Activated Delayed Fluorescence for Highly Efficient OLEDs. *Angewandte Chemie International Edition* **2018**, *57*, 11316-11320.
27. Kondo, Y.; Yoshiura, K.; Kitera, S.; Nishi, H.; Oda, S.; Gotoh, H.; Sasada, Y.; Yanai, M.; Hatakeyama, T., Narrowband deep-blue organic light-emitting diode featuring an organoboron-based emitter. *Nature Photonics* **2019**, *13*, 678-682.
28. Yang, M.; Park, I. S.; Yasuda, T., Full-Color, Narrowband, and High-Efficiency Electroluminescence from Boron and Carbazole Embedded Polycyclic Heteroaromatics. *Journal of the American Chemical Society* **2020**, *142*, 19468-19472.
29. Cai, X.; Su, S.-J., Marching Toward Highly Efficient, Pure-Blue, and Stable Thermally Activated Delayed Fluorescent Organic Light-Emitting Diodes. *Advanced Functional Materials* **2018**, *28*, 1802558.
30. Bui, T.-T.; Goubard, F.; Ibrahim-Ouali, M.; Gimes, D.; Dumur, F., Thermally Activated Delayed Fluorescence Emitters for Deep Blue Organic Light Emitting Diodes: A Review of Recent Advances. *Applied Sciences* **2018**, *8*, 494.
31. Xu, Z.; Tang, B. Z.; Wang, Y.; Ma, D., Recent advances in high performance blue organic light-emitting diodes based on fluorescence emitters. *Journal of Materials Chemistry C* **2020**, *8*, 2614-2642.
32. Rodella, F.; Bagnich, S.; Duda, E.; Meier, T.; Kahle, J.; Athanasopoulos, S.; Köhler, A.; Strohriegel, P., High Triplet Energy Host Materials for Blue TADF OLEDs—A Tool Box Approach. *Frontiers in Chemistry* **2020**, *8*, 657.
33. Köhler, A.; Bässler, H., *Electronic Processes in Organic Semiconductors: An Introduction*. 2015.
34. S. P. McGlynn, S. M. G., T. Azumi, M. Kinoshita, *Molecular Spectroscopy of the Triplet State*. 1969.
35. Lakowicz, J. R., *Principles of Fluorescence Spectroscopy*. 2006.
36. Atkins, P. W., *Molecular Quantum Mechanics*. **1983**.
37. Adachi, C.; Baldo, M. A.; Thompson, M. E.; Forrest, S. R., Nearly 100% internal phosphorescence efficiency in an organic light-emitting device. *Journal of Applied Physics* **2001**, *90*, 5048-5051.
38. Hosokai, T.; Matsuzaki, H.; Nakanotani, H.; Tokumaru, K.; Tsutsui, T.; Furube, A.; Nasu, K.; Nomura, H.; Yahiro, M.; Adachi, C., Evidence and mechanism of efficient thermally activated delayed fluorescence promoted by delocalized excited states. *Science Advances* **2017**, *3*, e1603282.
39. Wang, M.; Chatterjee, T.; Foster, C. J.; Wu, T.; Yi, C.-L.; Yu, H.; Wong, K.-T.; Hu, B., Exploring mechanisms for generating spin-orbital coupling through donor-acceptor design to realize spin flipping in thermally activated delayed fluorescence. *Journal of Materials Chemistry C* **2020**, *8*, 3395-3401.
40. Kearwell, A. W., F., *Transfer and Storage of Energy by Molecules*. 1969.

41. Wada, Y.; Wakisaka, Y.; Kaji, H., Efficient Direct Reverse Intersystem Crossing between Charge Transfer-Type Singlet and Triplet States in a Purely Organic Molecule. *ChemPhysChem* **2021**, *22*, 625-632.
42. Serdiuk, I. E.; Mońka, M.; Kozakiewicz, K.; Liberek, B.; Bojarski, P.; Park, S. Y., Vibrationally Assisted Direct Intersystem Crossing between the Same Charge-Transfer States for Thermally Activated Delayed Fluorescence: Analysis by Marcus–Hush Theory Including Reorganization Energy. *The Journal of Physical Chemistry B* **2021**, *125*, 2696–2706.
43. El-Sayed, M. A., Spin–Orbit Coupling and the Radiationless Processes in Nitrogen Heterocyclics. *The Journal of Chemical Physics* **1963**, *38*, 2834-2838.
44. El-Sayed, M. A., Triplet state. Its radiative and nonradiative properties. *Accounts of Chemical Research* **2002**, *1*, 8-16.
45. Noda, H.; Chen, X.-K.; Nakanotani, H.; Hosokai, T.; Miyajima, M.; Notsuka, N.; Kashima, Y.; Brédas, J.-L.; Adachi, C., Critical role of intermediate electronic states for spin-flip processes in charge-transfer-type organic molecules with multiple donors and acceptors. *Nature Materials* **2019**, *18*, 1084-1090.
46. Samanta, P. K.; Kim, D.; Coropceanu, V.; Brédas, J.-L., Up-Conversion Intersystem Crossing Rates in Organic Emitters for Thermally Activated Delayed Fluorescence: Impact of the Nature of Singlet vs Triplet Excited States. *Journal of the American Chemical Society* **2017**, *139*, 4042-4051.
47. Dias, F. B.; Santos, J.; Graves, D. R.; Data, P.; Nobuyasu, R. S.; Fox, M. A.; Batsanov, A. S.; Palmeira, T.; Berberan-Santos, M. N.; Bryce, M. R.; Monkman, A. P., The Role of Local Triplet Excited States and D-A Relative Orientation in Thermally Activated Delayed Fluorescence: Photophysics and Devices. *Advanced Science* **2016**, *3*, 1600080.
48. Yin, C.; Zhang, D.; Duan, L., A perspective on blue TADF materials based on carbazole-benzonitrile derivatives for efficient and stable OLEDs. *Applied Physics Letters* **2020**, *116*, 120503.
49. Lee, S. Y.; Yasuda, T.; Komiyama, H.; Lee, J.; Adachi, C., Thermally Activated Delayed Fluorescence Polymers for Efficient Solution-Processed Organic Light-Emitting Diodes. *Advanced Materials* **2016**, *28*, 4019-4024.
50. Woo, S.-J.; Kim, J.-J., TD-DFT and Experimental Methods for Unraveling the Energy Distribution of Charge-Transfer Triplet/Singlet States of a TADF Molecule in a Frozen Matrix. *The Journal of Physical Chemistry A* **2021**, *125*, 1234-1242.
51. Notsuka, N.; Nakanotani, H.; Noda, H.; Goushi, K.; Adachi, C., Observation of Nonradiative Deactivation Behavior from Singlet and Triplet States of Thermally Activated Delayed Fluorescence Emitters in Solution. *The Journal of Physical Chemistry Letters* **2019**, *11*, 562-566.
52. Baleizão, C.; Berberan-Santos, M. N., Thermally activated delayed fluorescence as a cycling process between excited singlet and triplet states: Application to the fullerenes. *The Journal of Chemical Physics* **2007**, *126*, 204510.
53. Dias, F. B.; Penfold, T. J.; Monkman, A. P., Photophysics of thermally activated delayed fluorescence molecules. *Methods and Applications in Fluorescence* **2017**, *5*, 012001.
54. Kreiza, G.; Banevičius, D.; Jovaišaitė, J.; Maleckaitė, K.; Gudeika, D.; Volyniuk, D.; Gražulevičius, J. V.; Juršėnas, S.; Kazlauskas, K., Suppression of benzophenone-induced triplet quenching for enhanced TADF performance. *Journal of Materials Chemistry C* **2019**, *7*, 11522-11531.
55. Chatterjee, T.; Wong, K.-T., Perspective on Host Materials for Thermally Activated Delayed Fluorescence Organic Light Emitting Diodes. *Advanced Optical Materials* **2019**, *7*, 1800565.
56. Godumala, M.; Choi, S.; Cho, M. J.; Choi, D. H., Recent breakthroughs in thermally activated delayed fluorescence organic light emitting diodes containing non-doped emitting layers. *Journal of Materials Chemistry C* **2019**, *7*, 2172-2198.
57. Tsutsui, T.; Bradley, D. D. C.; Friend, R. H.; Holmes, A. B.; Aminaka, E.; Lin, C. P.; Kim, D. U., Extended molecular design concept of molecular materials for electroluminescence: sublimed–dye films, molecularly doped polymers and polymers with chromophores. *Philosophical Transactions of the Royal Society of London. Series A: Mathematical, Physical and Engineering Sciences* **1997**, *355*, 801-814.
58. Salehi, A.; Chen, Y.; Fu, X.; Peng, C.; So, F., Manipulating Refractive Index in Organic Light-Emitting Diodes. *ACS Applied Materials & Interfaces* **2018**, *10*, 9595-9601.

59. Miwa, T.; Kubo, S.; Shizu, K.; Komino, T.; Adachi, C.; Kaji, H., Blue organic light-emitting diodes realizing external quantum efficiency over 25% using thermally activated delayed fluorescence emitters. *Scientific Reports* **2017**, *7*, 284.
60. Shizu, K.; Tanaka, H.; Uejima, M.; Sato, T.; Tanaka, K.; Kaji, H.; Adachi, C., Strategy for Designing Electron Donors for Thermally Activated Delayed Fluorescence Emitters. *The Journal of Physical Chemistry C* **2015**, *119*, 1291-1297.
61. Rajamalli, P.; Chen, D.; Li, W.; Samuel, I. D. W.; Cordes, D. B.; Slawin, A. M. Z.; Zysman-Colman, E., Enhanced thermally activated delayed fluorescence through bridge modification in sulfone-based emitters employed in deep blue organic light-emitting diodes. *Journal of Materials Chemistry C* **2019**, *7*, 6664-6671.
62. Matsuoka, K.; Albrecht, K.; Yamamoto, K.; Fujita, K., Multifunctional Dendritic Emitter: Aggregation-Induced Emission Enhanced, Thermally Activated Delayed Fluorescent Material for Solution-Processed Multilayered Organic Light-Emitting Diodes. *Scientific Reports* **2017**, *7*, 41780.
63. Albrecht, K.; Matsuoka, K.; Yokoyama, D.; Sakai, Y.; Nakayama, A.; Fujita, K.; Yamamoto, K., Thermally activated delayed fluorescence OLEDs with fully solution processed organic layers exhibiting nearly 10% external quantum efficiency. *Chemical Communications* **2017**, *53*, 2439-2442.
64. Huang, M.; Li, Y.; Wu, K.; Luo, J.; Xie, G.; Li, L.; Yang, C., Carbazole-dendronized thermally activated delayed fluorescent molecules with small singlet-triplet gaps for solution-processed organic light-emitting diodes. *Dyes and Pigments* **2018**, *153*, 92-98.
65. Li, Y.; Xie, G.; Gong, S.; Wu, K.; Yang, C., Dendronized delayed fluorescence emitters for non-doped, solution-processed organic light-emitting diodes with high efficiency and low efficiency roll-off simultaneously: two parallel emissive channels. *Chemical Science* **2016**, *7*, 5441-5447.
66. N. J. Turro, V. R., J. C. Scaiano, Principle of Molecular Photochemistry: An Introduction (University Science Books, 2009), chap. 3, pp. 113–118.
67. Noda, H.; Nakanotani, H.; Adachi, C., Excited state engineering for efficient reverse intersystem crossing. *Science Advances* **2018**, *4*, eaao6910.
68. Etherington, M. K.; Gibson, J.; Higginbotham, H. F.; Penfold, T. J.; Monkman, A. P., Revealing the spin–vibronic coupling mechanism of thermally activated delayed fluorescence. *Nature Communications* **2016**, *7*, 13680.
69. Cui, L.-S.; Gillett, A. J.; Zhang, S.-F.; Ye, H.; Liu, Y.; Chen, X.-K.; Lin, Z.-S.; Evans, E. W.; Myers, W. K.; Ronson, T. K.; Nakanotani, H.; Reineke, S.; Bredas, J.-L.; Adachi, C.; Friend, R. H., Fast spin-flip enables efficient and stable organic electroluminescence from charge-transfer states. *Nature Photonics* **2020**, *14*, 636-642.
70. Wei, Q.; Imbrasas, P.; Caldera-Cruz, E.; Cao, L.; Fei, N.; Thomas, H.; Scholz, R.; Lenk, S.; Voit, B.; Reineke, S.; Ge, Z., Conjugation-Induced Thermally Activated Delayed Fluorescence: Photophysics of a Carbazole-Benzophenone Monomer-to-Tetramer Molecular Series. *The Journal of Physical Chemistry A* **2021**, *125*, 1345-1354.
71. Zhang, D.; Cai, M.; Zhang, Y.; Zhang, D.; Duan, L., Sterically shielded blue thermally activated delayed fluorescence emitters with improved efficiency and stability. *Materials Horizons* **2016**, *3*, 145-151.
72. Hirai, H.; Nakajima, K.; Nakatsuka, S.; Shiren, K.; Ni, J.; Nomura, S.; Ikuta, T.; Hatakeyama, T., One-Step Borylation of 1,3-Diaryloxybenzenes Towards Efficient Materials for Organic Light-Emitting Diodes. *Angewandte Chemie International Edition* **2015**, *54*, 13581-13585.
73. de Mello, J. C.; Wittmann, H. F.; Friend, R. H., An improved experimental determination of external photoluminescence quantum efficiency. *Advanced Materials* **1997**, *9*, 230-232.
74. Good, H. P.; Wild, U. P.; Haas, E.; Fischer, E.; Resewitz, E. P.; Lippert, E., The Fluorescence Lifetime of Trans-Stilbene and its Variation with Temperature. *Berichte der Bunsengesellschaft für physikalische Chemie* **1982**, *86*, 126-129.

Chapter 1a. Fine-tuning the hole-electron overlap by donor extensions of different strength

An efficient TADF emitter requires a small gap between the singlet and triplet states (ΔE_{ST}) to enable TADF and a high radiative decay rate.¹⁻² The size of the ΔE_{ST} gap and the radiative decay rate in the molecule are governed by the overlap of the electron and hole wavefunctions.¹⁻² A small ΔE_{ST} gap requires a minimal overlap between electron and hole densities, yet a strong wavefunction overlap is needed for a high radiative decay rate in the molecule. Therefore, a tricky part is to engineer just the right amount of overlap between electron and hole wavefunctions so that the ΔE_{ST} gap is small enough but the radiative decay rate is still high enough. One way to obtain the right amount of wavefunction overlap is by introducing a torsion between the donor and the acceptor moieties by the right amount of steric constraint to reduce the electronic coupling between the two parts of the molecule.³⁻⁶ However, one has to be careful not to induce too much torsion between the donor and acceptor units as the radiative decay rate becomes too small.

An alternative way to engineer the desired amount of wavefunction overlap is to increase the delocalization of the hole density over the donor unit.⁷ Implementation of this strategy is illustrated in dendrimers, which frequently contain dendritic donors surrounding an electron-acceptor.^{2, 8-11} A dendritic structure has advantages. First, it was shown that even more moderate donor-acceptor torsions enabling a small ΔE_{ST} gap in the dendrimers would still ensure sufficient overlap between electron and hole wavefunctions for a reasonable oscillator strength.⁴ Second, a further advantage of a dendritic structure as the emitter is the possibility to use it host-free in the emissive layer of the OLED.¹² Commonly, TADF emitters are dispersed in a host material to avoid concentration quenching. However, the dendritic structure itself is often sufficiently sterically crowded to prevent concentration quenching. Suppressed concentration quenching enables dendritic TADF emitters to be used without a separate host material (see also Chapter 1b).

To study the hole wavefunction delocalization on the ΔE_{ST} gap, TADF and PLQY, the donor group was extended of the sky-blue emitter **2CzPN** (Figure 1a.1).¹³⁻¹⁵ **2CzPN** consists of an electron-withdrawing phthalonitrile core with two carbazole donor moieties attached. These donors can be substituted comparatively easily at the 3,6-positions, allowing for the conjugated π -system to extend. **2CzPN** itself shows a high PLQY value of 89% and the presence of TADF despite a ΔE_{ST} gap of more than 0.2 eV in mCP film.¹⁴ It is not clear if extending the donor group of **2CzPN** could decrease the ΔE_{ST} gap and increase TADF. To gradually increase the donor strength, the central carbazole was extended using peripheral carbazoles (**Cz**), di(4-*tert*-butyl-phenyl)amines (**tBuDPA**) or phenoxazine (**PXZ**). The increasing strength of donor extensions was confirmed by David Hall (University of St Andrews) using the differential pulse voltammetry (the oxidation potential values of 1.15 V, 0.84 V and 0.66 V for the **Cz**, **tBuDPA**, **PXZ** units were obtained, respectively) and density functional theory (DFT) (*vide infra*).

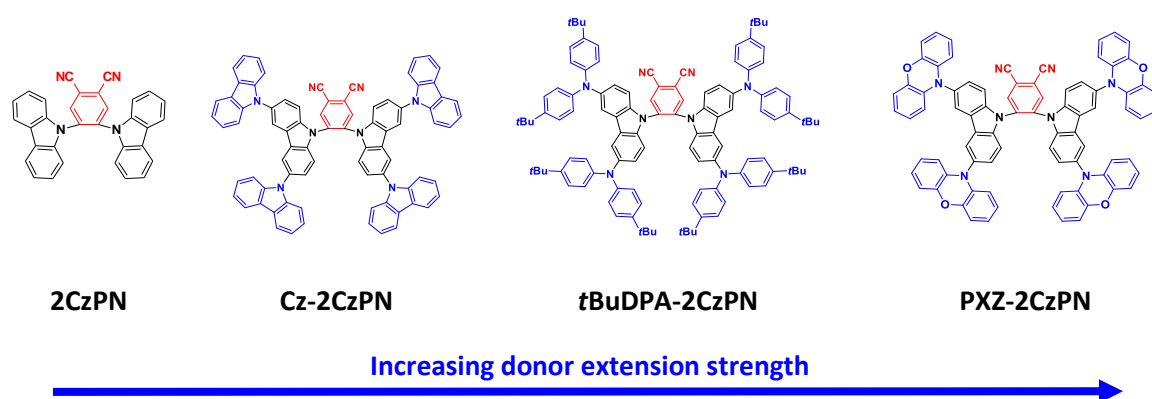


Figure 1a.1. Chemical structures of the investigated compounds. The parent **2CzPN** is extended using carbazole (**Cz**), *tert*-butyl-diphenylamine (**tBuDPA**) and phenoxazine (**PXZ**).

My photophysical study shows that the extension of the donor group allows for an enhancement of the intramolecular charge transfer (CT) character of the emitter and a progressively smaller ΔE_{ST} , from above 200 meV for the parent compound **2CzPN** to below 100 meV for extended compounds. While the TADF contribution is successfully increased in solution for **Cz-2CzPN**, the non-radiative decay is found to suppress a larger contribution of TADF in film for extended compounds. Overall, extending the donor group indeed reduces the ΔE_{ST} gap and shows promising results in terms of TADF for **Cz-2CzPN**.

Methods

Materials. The compounds for the investigation were synthesized by David Hall in the Prof. Eli Zysman-Colman group (University St Andrews, UK).

Photophysical measurements. The solutions of 0.05 mg/ml in toluene (corresponding to 10^{-4} - 10^{-5} M depending on molecular weight), as well as spin-coated 10 wt% films in mCP, were prepared and measured at different temperatures in the steady-state mode using the spectrofluorometer (Jasco FP-8600) and in the time-resolved mode using the iCCD camera (Andor iStar A-DH334T-18F-03) by exponentially increasing delay and gating times where the gating time is kept lower by 10 times compared to the delay time. For the steady-state mode, variable excitation wavelengths were used (see figure captions) while for the iCCD measurements samples were excited at 355 nm.

Photophysics in solution and film

The compounds are first measured in dilute toluene solution where intermolecular interactions can be expected to be suppressed (Figure 1a.2). This should provide a clear photophysical understanding related to monomolecular processes.

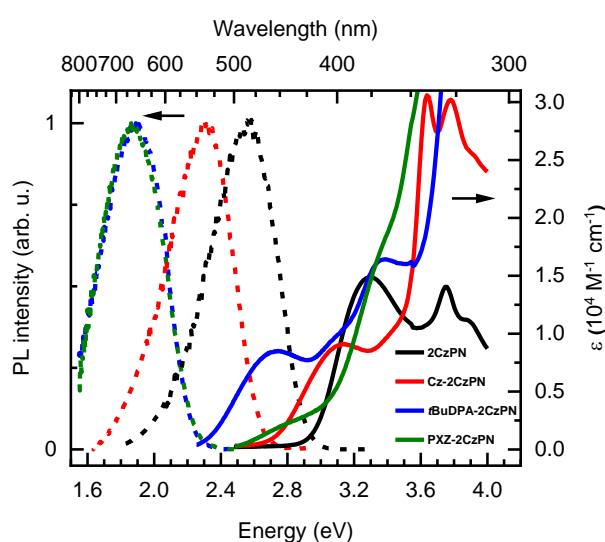


Figure 1a.2. Absorption and steady-state emission spectra of **2CzPN**, **Cz-2CzPN**, **tBuDPA-2CzPN**, **PXZ-2CzPN** in toluene at 300 K ($\lambda_{\text{exc}} = 300$ nm).

All compounds show a broad, unstructured, low-intensity absorption on the lower energy side (Figure 1a.2). Along the series, the absorption maxima shift to lower energy and reduce in intensity

(Table **1a.1**). I attribute these bands to a transition with a predominant CT character between the electron-donating donors and the electron-accepting phthalonitrile. The trend of the progressive decrease of the extinction coefficients of this low energy band reflects the increasing strength of the CT transition. The observation of extinction coefficients in the range of $10^4 \text{ M}^{-1} \text{ cm}^{-1}$ for the first three compounds in the series suggests there is still a reasonable wavefunction overlap between the donor and acceptor moieties.

Table 1a.1. Peak positions of the absorption and photoluminescence (PL) maxima, and the decadic molar extinction coefficient ϵ_{CT} for the compounds in dilute toluene solution.

	λ_{abs}	ϵ_{CT}	λ_{PL}
	300 K	($10^4 \text{ M}^{-1} \text{ cm}^{-1}$)	300 K
2CzPN	3.30 eV (376 nm)	1.49	2.56 eV (484 nm)
Cz-2CzPN	3.14 eV (395 nm)	0.90	2.32 eV (534 nm)
tBuDPA-2CzPN	2.72 eV (456 nm)	0.85	1.88 eV (660 nm)
PXZ-2CzPN	2.72 eV (456 nm)	0.18	1.88 eV (660 nm)

At higher energies ($E \geq 3.6 \text{ eV}$) in the absorption spectra, transitions localized on the conjugated donors are evident. For example, in the absorption spectrum of **2CzPN**, there is a feature at 3.75 eV (331 nm) which can be attributed to the carbazole absorption.¹⁶ As compared to the absorption of N-phenyl-carbazole at 3.65 eV,¹⁶ the shift to the blue side of the carbazole absorption in **2CzPN** by 10 meV could be related to the acceptor unit withdrawing the electron density from the carbazole. In the case of **Cz-2CzPN**, the only change in the structure compared to **2CzPN** are four additional outer carbazole units that are reflected in the appearance of an additional absorption peak at 3.65 eV (340 nm). To identify which peak belongs to outer and to inner carbazoles, the following argument is considered. Since the outer carbazole donates some of its electron density to the inner carbazole thus restoring the “normal” electron density of carbazole, the peak at 3.65 eV (340 nm) can now be identified to belong to the inner carbazole. Having donated some of the electron density to the inner carbazoles,

the outer carbazoles are now more electron-deficient, allowing to ascribe the peak at 3.75 eV to belong to outer carbazoles. In the case of **tBuDPA-2CzPN** and **PXZ-2CzPN**, there is a sharp increase in absorption with a peak at 4.10 eV (302 nm) and 3.88 eV (320 nm), representing locally-excited (LE) transitions from diarylamine and phenoxazine¹⁷ units (not shown), respectively. The absorption of the phthalonitrile acceptor is located at even higher energies with peaks from 4.6 eV (270 nm) onwards.¹⁸ Regarding the emission in toluene, all steady-state emission spectra are broad and do not have any pronounced structure, characteristic of emission from a CT state. The photoluminescence maxima shift to lower energies across the family of derivatives, analogous to the shifts in the absorption maxima of the low-energy CT bands.

To estimate the energy splitting between the lowest singlet and triplet states, ΔE_{ST} , the fluorescence and phosphorescence spectra are taken at 77 K to exclude different temperature-dependent energy shifts. This is displayed in Figure **1a.3**, with the room temperature steady-state emission added for comparison. The steady-state emission at 77 K contains contributions from the prompt emission and the delayed emission which is mostly phosphorescence (Ph). For **tBuDPA-2CzPN**, the low-temperature measurement was done at 5 K as TADF was found to be still competing in intensity with phosphorescence at 77 K. The decrease of temperature leads to a blue-shift of the steady-state emission. This is attributed to the freezing of the solvation shell at low temperatures that prevents the reorganization of the solvent molecules after photoexcitation of the emitter molecules.¹⁹ To obtain the phosphorescence spectrum without contribution from fluorescence, the emission with detection in the millisecond range was recorded. Table **1a.2** below summarizes the energies obtained for the onsets of the singlet and triplet states along with the singlet-triplet gaps that are determined from them.

Table 1a.2. Singlet and triplet energies in toluene solution and mCP film (10 wt%), estimated using the onset at 77K (5 K for **tBuDPA-2CzPN**).

Compound	toluene			mCP		
	S ₁ (eV)	T ₁ (eV)	ΔE _{ST} (eV)	S ₁ (eV)	T ₁ (eV)	ΔE _{ST} (eV)
2CzPN	3.03	2.73	0.30	2.85	2.62	0.23
Cz-2CzPN	2.85	2.69	0.16	2.69	2.62	0.07
tBuDPA-2CzPN	2.37	2.36	0.01	2.34	2.33	0.01
PXZ-2CzPN	2.57	2.56	0.01	2.40	2.37	0.03

To address the CT or LE nature of phosphorescence, the positions of phosphorescence in the donor-acceptor compounds were compared with phosphorescence in the donor and acceptor moieties themselves. For **2CzPN**, the maximum of phosphorescence is much lower in energy than both, the phosphorescence peak of the carbazole unit and the phthalonitrile unit (peaks at 2.64 eV vs 3.0 eV¹⁶ and 3.2 eV²⁰, (470 nm vs 410 nm and 390 nm) respectively). However, based on the structured phosphorescence emission, the phosphorescence in **2CzPN** can still be ascribed to have a significant LE character with some CT contribution. This is in agreement and supported by the quantum chemical calculations in the work by Wong *et al.*¹⁵ Based on the reduction/disappearance of the vibronic progression in the phosphorescence spectra along the series, the extended compounds can be ascribed to have a more significant CT contribution. The ΔE_{ST} values in solution are decreasing along the series from 300 meV for the parent compound **2CzPN** until 10 meV for **tBuDPA-2CzPN** and **PXZ-2CzPN**. This decrease reflects the increasing hole localization on the dendron donor. Thus, the concept underlying the chemical design is confirmed.

To understand how the photophysical properties in solution transfer into films, the compounds in 10 wt% mCP film were investigated, where mCP (1,3-Bis(N-carbazolyl)benzene) is a host matrix with sufficiently high triplet energy of 2.90 eV (Figure 1a.3).²¹ This provides insight into which properties to expect in the device.

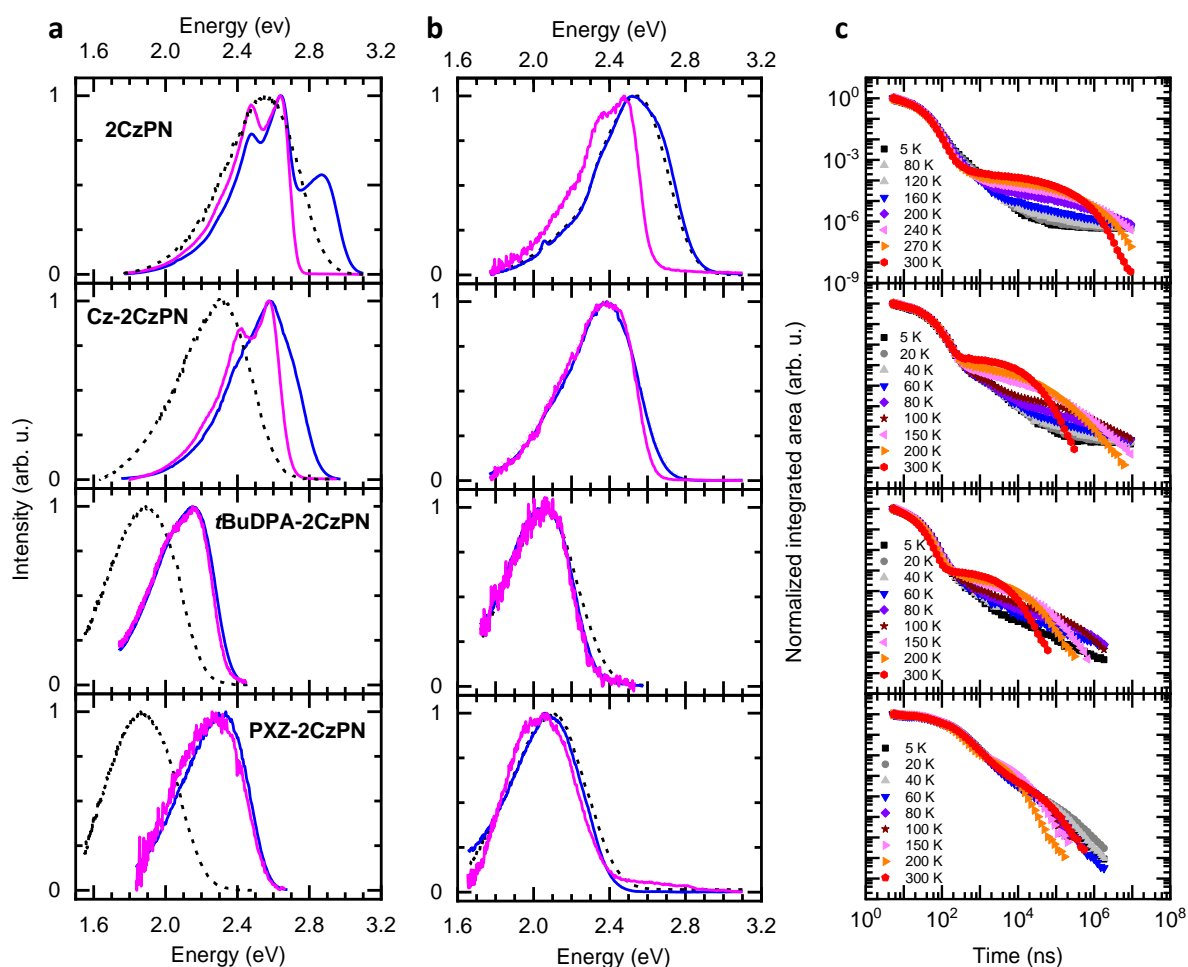


Figure 1a.3. PL emission and transient decay of **2CzPN**, **Cz-2CzPN**, **tBuDPA-2CzPN**, **PXZ-2CzPN**. Black dashed lines denote the steady-state PL at 300 K. Blue lines denote the steady-state emission at 77 K. Magenta lines denote the PL with detection in the ms range at 77 K. (a) PL emission in toluene for excitation at the maximum of the CT absorption band. (b) PL emission in 10 wt% mCP film ($\lambda_{\text{exc}} = 300$ nm). (c) Transient PL decay in 10 wt% mCP film at 300 K ($\lambda_{\text{exc}} = 355$ nm). *For **tBuDPA-2CzPN**, the steady-state emission and PL with the detection in the ms range is obtained at 5 K ($\lambda_{\text{exc}} = 355$ nm).

Figure **1a.3b** shows the thin film PL emission for the series at 300 K and 77 K (5 K for **tBuDPA-2CzPN**). The same trend in the singlet-triplet gap as in solution with ΔE_{ST} decreasing along the series is observed (within the experimental error margin of 10 meV, Table **1a.3**). In contrast to solution, the room-temperature steady-state spectra almost coincide with the low temperature steady-state spectra. This is attributed to the lack of solvent reorganization after excitation in the solid matrix.¹⁹ It implies that the spectra and the energy gap obtained at low-temperature also represent the room temperature situation.

For pronounced TADF, a small ΔE_{ST} value is a necessary but not sufficient condition. To evaluate the potential of a molecule as a TADF emitter, the relevant rate constants need to be considered, as reflected in the photoluminescence quantum yield (PLQY), delayed emission lifetimes, and the contribution of TADF to the total emission. With a view to application, the main focus is on the discussion of the TADF-related parameters in film, comparing with the solution data wherever needed. Figure **1a.3c** shows the transient PL decays for the compounds in 10 wt% mCP film. The analogous data for solution is given in Figure **1a.4**. The photophysical parameters obtained are summarized in Table **1a.3** for solution and Table **1a.4** for films.

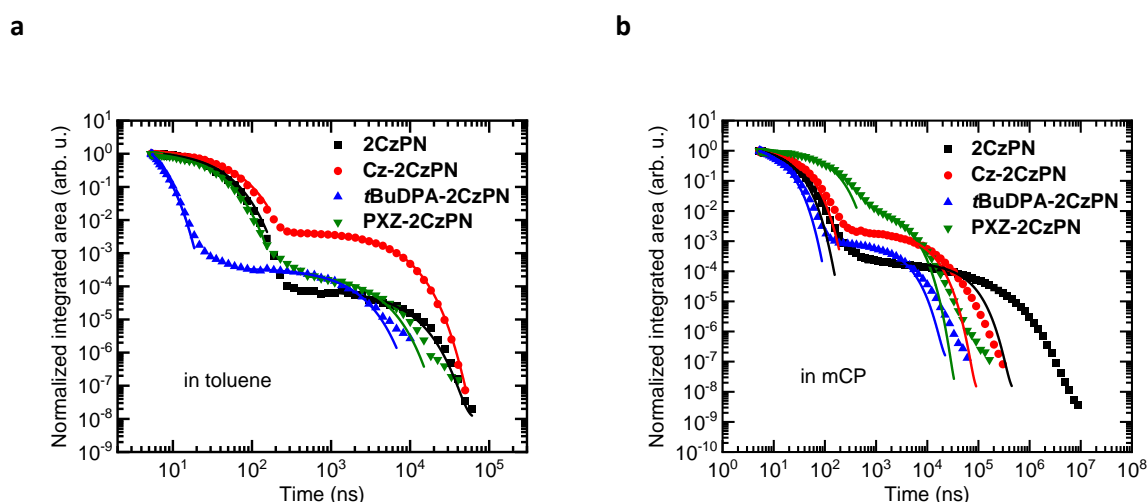


Figure **1a.4**. Transient PL decay analysis of **2CzPN**, **Cz-2CzPN**, **tBuDPA-2CzPN**, **PXZ-2CzPN** in (a) toluene and (b) mCP film (10 wt%) at 300 K. Mono-exponential fittings for both prompt and delayed components shown in solid lines. $\lambda_{exc} = 355$ nm.

For both, solution and film, two regimes in the PL decay can be identified. One is a prompt decay in the nanosecond range and the other one is a delayed emission taking place in the microsecond range. The delayed emission can be attributed to TADF based on the small ΔE_{ST} gap and the increase of the emission in the microsecond range with increasing temperature. From the temperature dependence of the delayed fluorescence (DF) in the film, the activation energies could also be calculated (Figure 1a.5). As with the singlet-triplet gap, the activation energy also reduces along the series. I attribute the lower activation energy than the estimated ΔE_{ST} gap to the presence of a higher-lying intermediate T_2 state, reducing the energy required for the RISC process (*vide infra*).¹

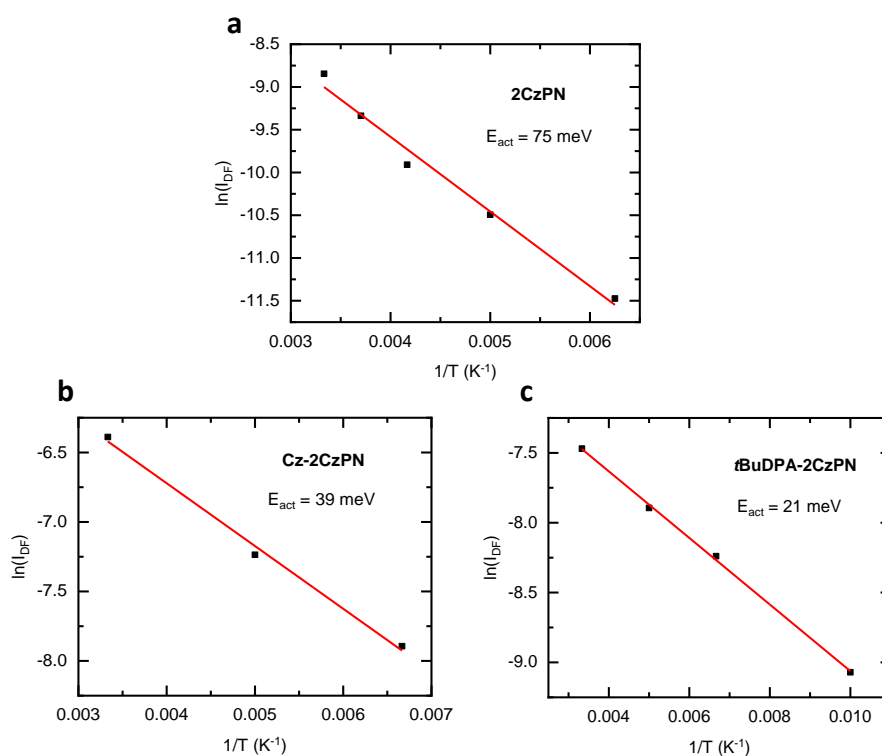


Figure 1a.5. Extraction of activation energy for (a) **2CzPN**, (b) **Cz-2CzPN** and (c) **tBuDPA-2CzPN** in mCP using the transient decay data in Figure 1a.3. The activation energy was determined using $I_{DF} = Ae^{\frac{-E_{act}}{k_B T}}$, where I_{DF} is the plateau of the delayed emission intensity (Figure 1a.3), A is a pre-exponential factor and k_B is Boltzmann's constant.

Table 1a.3. Quantum yields Φ , lifetimes τ and rates k for the compounds in toluene.

	$\Delta E_{ST}^{(a)}$	$\Phi_{PL}^{(b)}$	$\Phi_{DF}/\Phi_{PF}^{(c)}$	$\tau_{PF}^{(d)}$	$\tau_{DF}^{(e)}$	$k_r^S{}^{(f)}$	$k_{nr}^S{}^{(g)}$
	(meV)	(%)		(ns)	(μ s)	($\times 10^7, s^{-1}$)	($\times 10^7, s^{-1}$)
	± 10						
2CzPN	300	38	0.01	27	6.0	1.4	2.3
Cz-2CzPN	160	63	0.43	42	4.5	1.1	1.4
tBuDPA-2CzPN	10	2	0.01	2	1.2	1.0	49.0
PXZ-2CzPN	10	3	0.02	23	2.3	0.1	4.3

(a) $\Delta E_{ST} = S_1 - T_1$. Estimated from the onsets as in Table 1a.2.

(b) Total PLQY under N_2 . $\lambda_{exc} = 355$ nm.

(c) Ratio between the integrated area under the delayed and prompt emission.

(d) Prompt emission lifetime at 300 K extracted from a mono-exponential fitting (Figure 1a.4).

(e) Delayed emission lifetime at 300 K extracted from a mono-exponential fitting (Figure 1a.4).

(f) Constant of radiative decay rate extracted using $k_r^S = \Phi_{PF} / \tau_{DF}$.

(g) Constant of non-radiative decay rate extracted using $\tau_{PF} = 1 / (k_r^S + k_{nr}^S)$.

Table 1a.4. Quantum yields Φ , activation energies E_{act} , lifetimes τ and rates k for the compounds in mCP films.

	$\Delta E_{ST}^{(a)}$	E_{act}	$\Phi_{PL}^{(b)}$	$\Phi_{DF}/\Phi_{PF}^{(c)}$	$\tau_{PF}^{(d)}$	$\tau_{DF}^{(e)}$	$k_r^S^{(f)}$	$k_{nr}^S^{(g)}$	$\tau_{Ph}^{(h)}$	
	(meV)	(meV)	(%)		(ns)	(μ s)	($\times 10^7, s^{-1}$)	($\times 10^7, s^{-1}$)	(ms)	(ms)
	± 10								5 K	80 K
2CzPN	230	75 \pm 5	93	1.0	16	42.6	2.9	3.4	170	110
Cz-2CzPN	70	39 \pm 3	78	0.6	25	7.0	1.9	2.1	150	60
tBuDPA-2CzPN	10	21 \pm 1	14	0.1	10	2.3	1.2	8.8	3.5	-
PXZ-2CzPN	30	-	23	0.3	95	2.5	0.2	0.9	0.2	-

^(a) $\Delta E_{ST} = S_1 - T_1$. Estimated from the onsets as in Table 1a.2.

^(b) Total PLQY under N_2 . $\lambda_{exc} = 355$ nm.

^(c) Ratio between the integrated area under the delayed and prompt emission.

^(d) Prompt emission lifetime at 300 K extracted from a mono-exponential fitting (Figure 1a.4).

^(e) Delayed emission lifetime at 300 K extracted from a mono-exponential fitting (Figure 1a.4).

^(f) Constant of radiative decay rate of the singlet state extracted using $k_r^S = \Phi_{PF} / \tau_{DF}$.

^(g) Constant of non-radiative decay rate of the singlet state extracted using $\tau_{PF} = 1 / (k_r^S + k_{nr}^S)$.

^(h) Phosphorescence lifetime extracted from a mono-exponential fitting (Figure 1a.6).

Briefly commenting on the radiative decay rate from the singlet state, k_r^S is only slightly reduced relative to the parent compound for **Cz-2CzPN** and **tBuDPA-2CzPN**, yet significantly for **PXZ-2CzPN**. This indicates a too strong decoupling of the hole and electron wavefunctions in **PXZ-2CzPN**. For **tBuDPA-2CzPN**, the ΔE_{ST} is small and a high radiative rate from the CT singlet is maintained, yet a 7 times higher non-radiative CT singlet decay rate precludes a high photoluminescence quantum yield. This finding is consistent with the work by Yang *et al.* where they reported a diphenylsulfone core linked to acridine-based dendron donors.²²⁻²³ When they attached diphenylamine or carbazole as peripheral donor groups they also found a smaller ΔE_{ST} gap and lower PLQY in toluene for the former (40 meV, 12%) than for the latter (90 meV, 68%).²²⁻²³

Despite the small singlet-triplet gap for extended compounds, very little TADF in solution is observed except for **Cz-2CzPN** (Table **1a.3**). A low TADF yield in solution at room temperature has been also observed in previous works.^{15, 24} This could be explained by the quenching of the triplet state by collisional interactions (collisions with the different emitter or solvent molecules and cuvette), and by conformational degrees of freedom (*vide infra*). Thus, for solutions, the emission characteristics are largely dominated by the singlet state emission due to a strong quenching of the triplet state.

In the film, the rigid matrix removes the collisional quenching mechanism, so that TADF has a stronger contribution to the overall PLQY. Nevertheless, the ratio between the integrated emission intensities of delayed and prompt fluorescence is less than 4 for all compounds and the non-radiative losses cannot be assumed to be negligible (*vide infra*) so that the commonly used approximations to calculate the reverse intersystem crossing (RISC) rate do not apply.²⁵ An assessment of the efficiency of RISC is still possible by considering the DF/PF ratio and the DF lifetime together. As summarized in Table **1a.4**, the extended compounds show a shorter DF lifetime than the parent compound. While this by itself could indicate a faster RISC rate, the lower DF/PF ratios in the extended compounds indicate that there must be an additional dominant process present. It is concluded that the shorter lifetime of the DF thus rather indicates a quenching channel for the triplet states from which the DF is fed. This is confirmed by measuring the phosphorescence lifetimes (Figure **1a.6**).

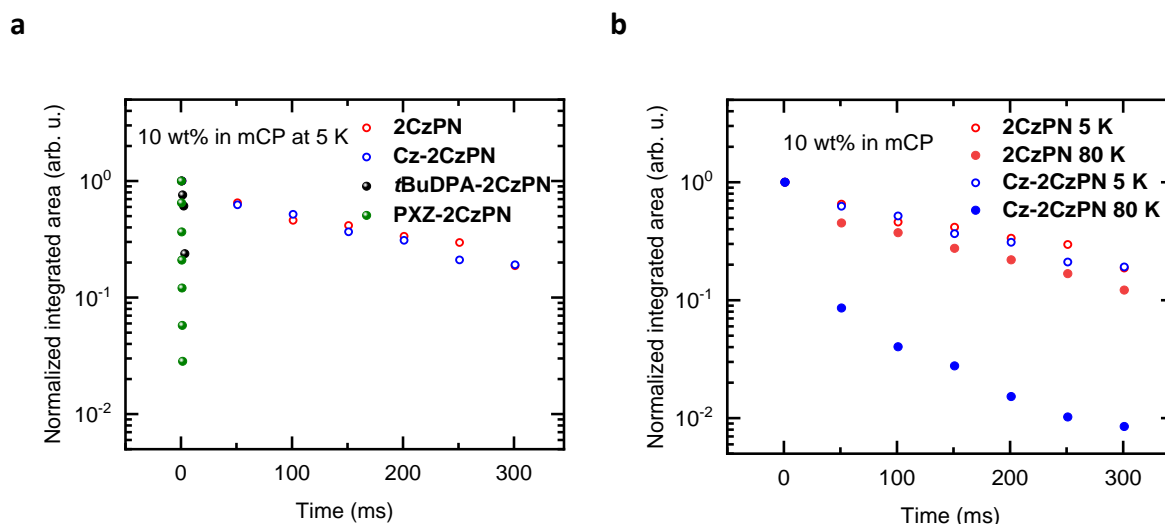


Figure 1a.6. PL transient decay recorded until hundreds ms range of **2CzPN**, **Cz-2CzPN**, **tBuDPA-2CzPN** and **PXZ-2CzPN** in mCP (10 wt%) at 5 K and 80 K. $\lambda_{\text{exc}} = 355 \text{ nm}$.

The triplet lifetime of **tBuDPA-2CzPN** and **PXZ-2CzPN** at 5 K is about 50 and 1000 times lower than that for the parent **2CzPN**. For **Cz-2CzPN**, it is comparable at 5K, yet reduces more strongly upon heating, for example, to 80K, thus also indicating thermally activated non-radiative decay channels. (Table 1a.4). The presence of these triplet quenching channels in the extended compound is disappointing. The nearly identical triplet energy of **2CzPN** and **Cz-2CzPN** excludes the energy-gap law as the origin. Most likely, the shorter triplet lifetime results from the higher conformational degrees of freedom in extended compounds, so that deactivation by torsional modes is facilitated. Overall, it is found that extending the donors indeed reduces the singlet-triplet gap, and concomitantly the activation energy for TADF. However, in the film, this advantage is compromised by an increased non-radiative decay from the triplet state, which occurs in different degrees for the different donor extensions.

To support the photophysical insights obtained in this chapter, the DFT calculation was carried out by David Hall (Figure 1a.7).

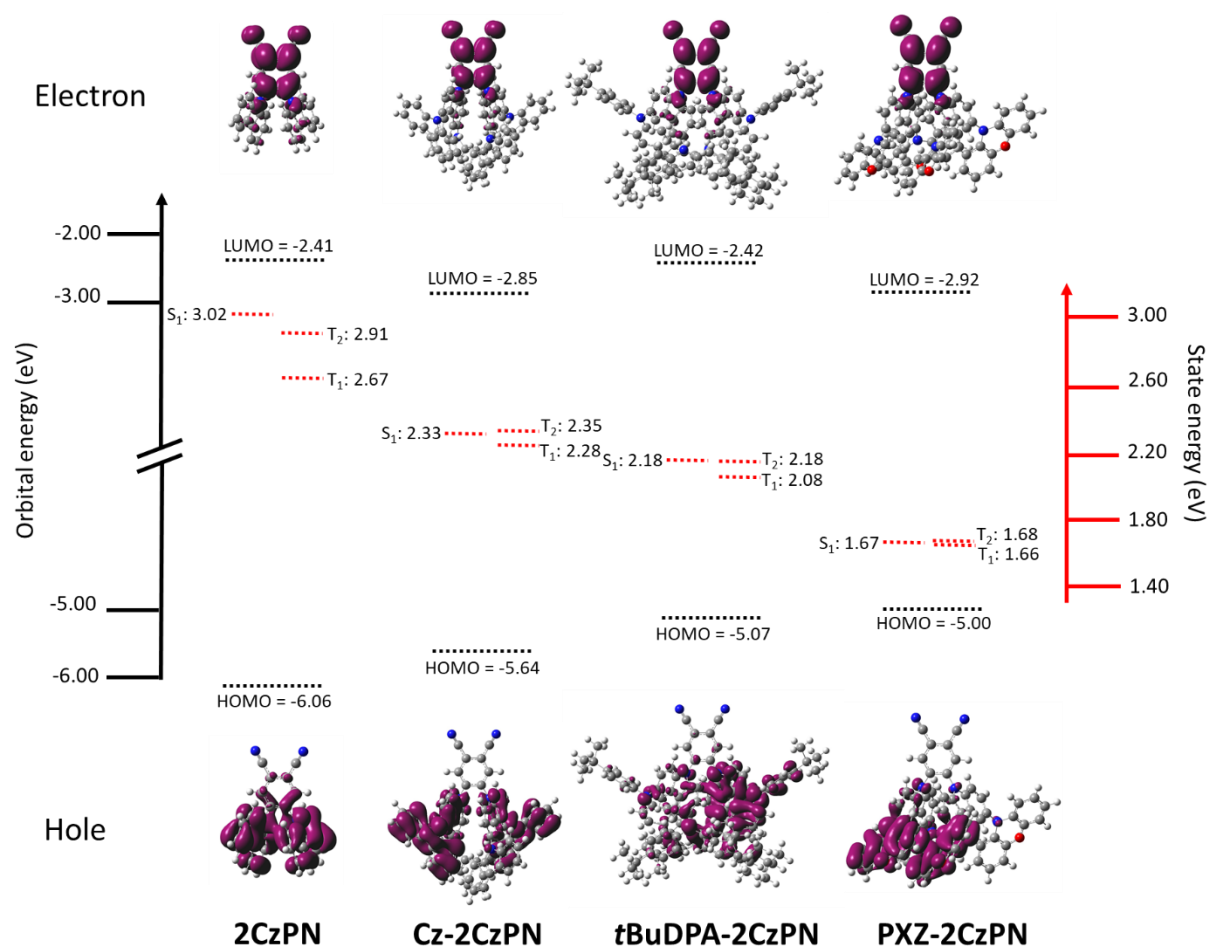


Figure 1a.7. Left axis in black: HOMO LUMO energies calculated for the ground state geometry. Right axis in red: vertical transition energies for S_1 , T_1 and T_2 . Also shown are the hole and electron densities S_1 . Calculated at the PBE0/6-31G(d,p) level, where f is the oscillator strength. This figure is presented with the permission of David Hall (University of St Andrews).

Figure 1a.7 presents the DFT results for the series of compounds investigated. The HOMO energies are increasing along the series, which is an expected result based on the fact that the parent compound was extended with units of increasing oxidation potential. It can also be seen that the S_1 energies and ΔE_{ST} gaps decrease along the series, consistent with the photophysical results. The electron and hole densities for the S_1 state indeed show a mixed CT and LE state transition, with less and less overlap towards the end of the series, demonstrating an increasing CT character and confirming the photophysical insights.

Concluding discussion

While it has been explored before that extending the donor group can be used as a way to activate TADF, often with the same unit for the inner and the outer donor,²⁶ the work presented in Chapter 1a is the first detailed photophysical study investigating the possibility to control TADF-related properties by fine-tuning the outer donor strength. In this work, the effects of the donor extension of increasing strength were investigated using **2CzPN** as a parent molecule on TADF-related properties. The results show that the relation between the ΔE_{ST} gap and the TADF contribution can indeed be controlled by the correct selection of the donor extension, with the carbazole-based extension providing the most suitable balance between the hole and electron densities. In solution, the derivative **Cz-2CzPN** significantly exceeds the PLQY and TADF properties of the parent **2CzPN**. However, it is also found that, in the film, a higher non-radiative rate of the triplet state prohibits a stronger role of TADF in the extended compound despite a reduced gap between the singlet and triplet state. The results presented in this chapter imply that the approach of fine-tuning the donor strength indeed can improve the TADF emission. Yet, for implementation, this still requires more control over the non-radiative decay of the triplet state in the film, for example, by ensuring that the dendron donors are sufficiently rigid.

References of Chapter 1a

1. Gibson, J.; Penfold, T. J., Nonadiabatic coupling reduces the activation energy in thermally activated delayed fluorescence. *Physical Chemistry Chemical Physics* **2017**, *19*, 8428-8434.
2. Miwa, T.; Kubo, S.; Shizu, K.; Komino, T.; Adachi, C.; Kaji, H., Blue organic light-emitting diodes realizing external quantum efficiency over 25% using thermally activated delayed fluorescence emitters. *Scientific Reports* **2017**, *7*, 284.
3. Kaji, H.; Suzuki, H.; Fukushima, T.; Shizu, K.; Suzuki, K.; Kubo, S.; Komino, T.; Oiwa, H.; Suzuki, F.; Wakamiya, A.; Murata, Y.; Adachi, C., Purely organic electroluminescent material realizing 100% conversion from electricity to light. *Nature Communications* **2015**, *6*, 8476.
4. Shizu, K.; Tanaka, H.; Uejima, M.; Sato, T.; Tanaka, K.; Kaji, H.; Adachi, C., Strategy for Designing Electron Donors for Thermally Activated Delayed Fluorescence Emitters. *The Journal of Physical Chemistry C* **2015**, *119*, 1291-1297.
5. Stachelek, P.; Ward, J. S.; dos Santos, P. L.; Danos, A.; Colella, M.; Haase, N.; Raynes, S. J.; Batsanov, A. S.; Bryce, M. R.; Monkman, A. P., Molecular Design Strategies for Color Tuning of Blue TADF Emitters. *ACS Applied Materials & Interfaces* **2019**, *11*, 27125-27133.
6. Rajamalli, P.; Chen, D.; Li, W.; Samuel, I. D. W.; Cordes, D. B.; Slawin, A. M. Z.; Zysman-Colman, E., Enhanced thermally activated delayed fluorescence through bridge modification in sulfone-based emitters employed in deep blue organic light-emitting diodes. *Journal of Materials Chemistry C* **2019**, *7*, 6664-6671.
7. Li, J.; Liao, X.; Xu, H.; Li, L.; Zhang, J.; Wang, H.; Xu, B., Deep-blue thermally activated delayed fluorescence dendrimers with reduced singlet-triplet energy gap for low roll-off non-doped solution-processed organic light-emitting diodes. *Dyes and Pigments* **2017**, *140*, 79-86.
8. Matsuoka, K.; Albrecht, K.; Yamamoto, K.; Fujita, K., Multifunctional Dendritic Emitter: Aggregation-Induced Emission Enhanced, Thermally Activated Delayed Fluorescent Material for Solution-Processed Multilayered Organic Light-Emitting Diodes. *Scientific Reports* **2017**, *7*, 41780.
9. Albrecht, K.; Matsuoka, K.; Yokoyama, D.; Sakai, Y.; Nakayama, A.; Fujita, K.; Yamamoto, K., Thermally activated delayed fluorescence OLEDs with fully solution processed organic layers exhibiting nearly 10% external quantum efficiency. *Chemical Communications* **2017**, *53*, 2439-2442.
10. Huang, M.; Li, Y.; Wu, K.; Luo, J.; Xie, G.; Li, L.; Yang, C., Carbazole-dendronized thermally activated delayed fluorescent molecules with small singlet-triplet gaps for solution-processed organic light-emitting diodes. *Dyes and Pigments* **2018**, *153*, 92-98.
11. Li, Y.; Xie, G.; Gong, S.; Wu, K.; Yang, C., Dendronized delayed fluorescence emitters for non-doped, solution-processed organic light-emitting diodes with high efficiency and low efficiency roll-off simultaneously: two parallel emissive channels. *Chemical Science* **2016**, *7*, 5441-5447.
12. Godumala, M.; Choi, S.; Cho, M. J.; Choi, D. H., Recent breakthroughs in thermally activated delayed fluorescence organic light emitting diodes containing non-doped emitting layers. *Journal of Materials Chemistry C* **2019**, *7*, 2172-2198.
13. Uoyama, H.; Goushi, K.; Shizu, K.; Nomura, H.; Adachi, C., Highly efficient organic light-emitting diodes from delayed fluorescence. *Nature* **2012**, *492*, 234-238.
14. Kim, G. H.; Lampande, R.; Im, J. B.; Lee, J. M.; Lee, J. Y.; Kwon, J. H., Controlling the exciton lifetime of blue thermally activated delayed fluorescence emitters using a heteroatom-containing pyridoindole donor moiety. *Materials Horizons* **2017**, *4*, 619-624.
15. Wong, M. Y.; Krotkus, S.; Copley, G.; Li, W.; Murawski, C.; Hall, D.; Hedley, G. J.; Jaricot, M.; Cordes, D. B.; Slawin, A. M. Z.; Olivier, Y.; Beljonne, D.; Muccioli, L.; Moral, M.; Sancho-Garcia, J.-C.; Gather, M. C.; Samuel, I. D. W.; Zysman-Colman, E., Deep-Blue Oxadiazole-Containing Thermally Activated Delayed Fluorescence Emitters for Organic Light-Emitting Diodes. *ACS Applied Materials & Interfaces* **2018**, *10*, 33360-33372.
16. Bagnich, S. A.; Athanasopoulos, S.; Rudnick, A.; Schroegel, P.; Bauer, I.; Greenham, N. C.; Strohriegel, P.; Köhler, A., Excimer Formation by Steric Twisting in Carbazole and Triphenylamine-Based Host Materials. *The Journal of Physical Chemistry C* **2015**, *119*, 2380-2387.

17. Mantsch, H. H.; Dehler, J., π -Electronic structure and reactivity of phenoxazine (1), phenothiazine (2), and phenoxthiin (3). *Canadian Journal of Chemistry* **1969**, *47*, 3173-3178.
18. Takei, K.; Kanda, Y., Phosphorescence spectra of benzonitrile and related compounds. *Spectrochimica Acta* **1962**, *18*, 1201-1216.
19. Lakowicz, J. R., *Principles of Fluorescence Spectroscopy*. 3rd ed.; Springer: Berlin, 2006.
20. Hayashi, H.; Nagakura, S., The E.S.R. and phosphorescence spectra of some dicyanobenzene complexes with methyl-substituted benzenes. *Molecular Physics* **1970**, *19*, 45-53.
21. Ren, X.; Li, J.; Holmes, R. J.; Djurovich, P. I.; Forrest, S. R.; Thompson, M. E., Ultrahigh Energy Gap Hosts in Deep Blue Organic Electrophosphorescent Devices. *Chemistry of Materials* **2004**, *16*, 4743-4747.
22. Gong, S.; Luo, J.; Wang, Z.; Li, Y.; Chen, T.; Xie, G.; Yang, C., Tuning emissive characteristics and singlet-triplet energy splitting of fluorescent emitters by encapsulation group modification: Yellow TADF emitter for solution-processed OLEDs with high luminance and ultraslow efficiency roll-off. *Dyes and Pigments* **2017**, *139*, 593-600.
23. Luo, J.; Gong, S.; Gu, Y.; Chen, T.; Li, Y.; Zhong, C.; Xie, G.; Yang, C., Multi-carbazole encapsulation as a simple strategy for the construction of solution-processed, non-doped thermally activated delayed fluorescence emitters. *Journal of Materials Chemistry C* **2016**, *4*, 2442-2446.
24. Lee, J.; Shizu, K.; Tanaka, H.; Nakanotani, H.; Yasuda, T.; Kaji, H.; Adachi, C., Controlled emission colors and singlet-triplet energy gaps of dihydrophenazine-based thermally activated delayed fluorescence emitters. *Journal of Materials Chemistry C* **2015**, *3*, 2175-2181.
25. Dias, F. B.; Penfold, T. J.; Monkman, A. P., Photophysics of thermally activated delayed fluorescence molecules. *Methods and Applications in Fluorescence* **2017**, *5*, 012001.
26. Park, W. J.; Lee, Y.; Kim, J. Y.; Yoon, D. W.; Kim, J.; Chae, S. H.; Kim, H.; Lee, G.; Shim, S.; Yang, J. H.; Lee, S. J., Effective thermally activated delayed fluorescence emitter and its performance in OLED device. *Synthetic Metals* **2015**, *209*, 99-104.

Chapter 1b. The optimal linkage position of the dendron donor group to the acceptor core

In Chapter 1a, I found that a carbazole-based extension of the donor group of **2CzPN** has the most promising effects in terms of a reduced ΔE_{ST} gap, increased PLQY and increased TADF contribution in solution compared to the parent **2CzPN**. However, in film, a non-radiative decay channel in **Cz-2CzPN** was also identified suppressing TADF.

In Chapter 1b, I aim to further investigate carbazole-based dendrons for TADF application, with a focus on a neat film photophysics to explore the possibility to use these dendrimer-type emitters host-free in the emissive layer of the OLED. To prevent excimer formation via carbazole-carbazole interactions in the neat films, *tert*-butyl groups are introduced on the carbazole-based dendron. Concerning the acceptor unit, triphenyltriazine (TRZ) is selected, allowing up to three symmetric or asymmetric functional groups, or dendrons, to be incorporated onto the TRZ moiety to tune the photophysical properties synergistically.¹⁻² To check the optimal connection geometry of the donor group to the acceptor unit, the dendron units were linked to the acceptor either via a *para*-phenylene or a *meta*-phenylene bridge, resulting in **tBuCz2pTRZ** and **tBuCz2mTRZ**, respectively. The photophysical properties of these two compounds were then compared to **tBuCz2m2pTRZ** which is based on a design that combines features of both **tBuCz2pTRZ** and **tBuCz2mTRZ** (Figure **1b.1**). It is known that while a *para*-connection leads to strong electronic coupling between donor and acceptor, which results in a high radiative decay rate for the intramolecular charge transfer (ICT) transition, a *meta*-connection has a weaker electronic coupling between donor and acceptor, resulting in a smaller ΔE_{ST} which is better for TADF.³ It is expected that a synergistic *para*- and *meta*-connection would inherit key properties from both dendrimers, including a high radiative decay rate and a small ΔE_{ST} gap. In addition to this, a two times larger number of dendron units in **tBuCz2m2pTRZ** is expected to further suppress guest to guest interactions and reduce concentration quenching.

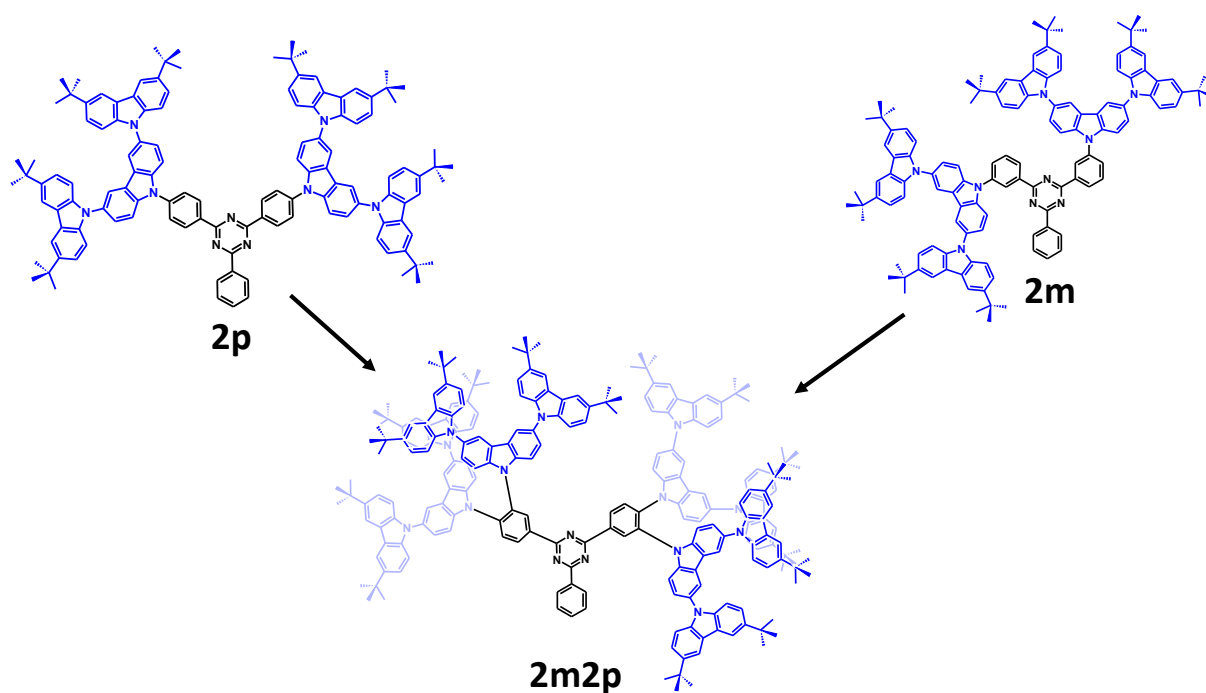


Figure 1b.1. Chemical structures of *tBuCz2pTRZ* (**2p**), *tBuCz2mTRZ* (**2m**) and *tBuCz2m2pTRZ* (**2m2p**). The dendron unit is coloured in blue.

I found that a synergistic *para*- and *meta*-connection of **tBuCz2m2pTRZ** indeed shows a combination of properties typical for *para*- and *meta*-connections, including a higher radiative decay rate compared to **tBuCz2mTRZ** alone and a smaller ΔE_{ST} gap compared to **tBuCz2pTRZ** alone (40 vs 90 meV, respectively). Most remarkably, **tBuCz2m2pTRZ** shows almost no loss of photoluminescence quantum efficiency via concentration quenching. Comparing a 1 wt% film dispersed in PMMA and the neat film, the PLQY of **tBuCz2m2pTRZ** is almost identical (90 vs 86%, respectively). A high PLQY accompanied by a minimal concentration quenching confirms that **tBuCz2m2pTRZ** is a suitable candidate to be used as a host-free emitter in the emissive layer of the OLED.

Methods

Materials. The compounds for the investigation were synthesized by Dr. Dianming Sun in the Prof. Eli Zysman-Colman group (University St Andrews, UK).

Photophysical measurements. Solution samples were prepared in toluene at 0.05 mg/mL (corresponding to the concentration of 10^{-5} M) for absorption and emission study. Doped films were

prepared by spin-coating 10 mg/mL chloroform solutions where 1 wt% of dendrimer was dispersed into PMMA. Neat films were prepared by spin-coating 10 mg/mL chloroform solutions of dendrimers. Samples were characterized using the same equipment as mentioned earlier (Methods section of the thesis and Chapter 1a).

Photophysics in solution and film

To exclude bimolecular interactions and to assess the properties of monomolecular species, the photophysical measurements were first done in dilute toluene solution (Figure 1b.2).

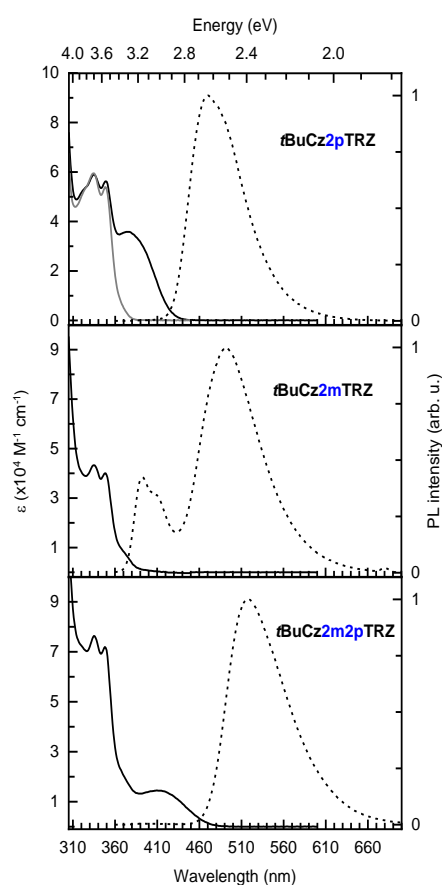


Figure 1b.2. Molar absorptivity and PL emission spectra in toluene ($\lambda_{\text{exc}} = 340 \text{ nm}$). The grey line represents the normalized molar absorptivity from the dendron unit (the structure of dendron is coloured in blue in Figure 1b.1).

In Figure 1b.2, the absorption spectra in toluene show very similar shapes for all three compounds. The grey line represents the absorption spectrum for the dendron unit (structure of the dendron unit is shown in Figure 1b.1 in blue). Since the absorption of the dendron units overlaps with the high-

energy part of the absorption of the three compounds, the peaks at 3.68 and 3.63 eV (337 and 342 nm) can be ascribed to the π - π^* transitions of the dendron unit. The broad band at 3.22 eV (385 nm) for **tBuCz2pTRZ** is assigned to the intramolecular charge-transfer (ICT) transition from the *para*-connected dendron donor to the TRZ acceptor, with a weak ICT absorption barely visible for **tBuCz2mTRZ**. The ICT absorption for **tBuCz2m2pTRZ** at 2.99 eV (415 nm) shows a molar absorptivity that has an extinction value between the one observed in the *para*- and *meta*-based dendrimers. Figure **1b.2** also shows the steady-state emission spectra of the three compounds in toluene. Two emission bands can be identified, a structured locally-excited (LE), which is clearly visible in **tBuCz2mTRZ**, and a structureless charge-transfer (CT) transition. The reason why the LE band is only clearly visible for **tBuCz2mTRZ** is straightforward to understand. The simultaneous emission from LE and CT states can be observed when the internal conversion from an LE to a CT state is slower than the radiative decay from the LE state. The conversion from an LE to a CT state implies an electron transfer, which depends strongly on the wavefunction overlap. This should therefore be faster for the compounds with a *para*-connection than with a *meta*-connection, consistent with a dominating CT emission in **tBuCz2pTRZ** and **tBuCz2m2pTRZ**. The simultaneous LE and CT state emission in **tBuCz2mTRZ** indicates that for some of the dendron donors the rate of ICT is slow compared to the radiative emission rate from the LE state. These units could therefore act as hole-transporting units or host moieties, given their suitably higher triplet energies for the ICT-based emission of the dendrimers.

Prompt and delayed emission were measured after pulsed excitation to gain deeper insight into the nature of the excited states of the emitters in solution and film. Figure **1b.3** shows the prompt emission spectra of the three dendrimers in 10^{-5} M toluene solution with a delay time of 30 ns and a gating time of 10 ns. The characteristically broad and unstructured prompt emission in toluene indicates a strong CT character for all three dendrimers. The prompt emission at both 300 K and 5 K are almost identical for **tBuCz2pTRZ**, while in contrast, there exists a significant blue-shift upon cooling from 300 K to 5 K for **tBuCz2mTRZ** and **tBuCz2m2pTRZ**, both of which contain electronically decoupled dendrons. The temperature-insensitive prompt emission for **tBuCz2pTRZ** could be attributed to a more significant LE character compared to other compounds. The singlet energies were then measured from the onset of

the prompt emission spectra at 5 K to be 2.92, 2.94 and 2.73 eV for **tBuCz2pTRZ**, **tBuCz2mTRZ** and **tBuCz2m2pTRZ**, respectively. The singlet energies of **tBuCz2pTRZ** are nearly isoenergetic to those of **tBuCz2mTRZ** at 5 K, indicating similar energy of their ¹CT states regardless of the electronic coupling between donor and acceptor. The spectra obtained at 5 K using a delay time of 30 ms with a gate width of 15 ms are ascribed to phosphorescence. Similar to the prompt emission, the phosphorescence spectra are also broad and structureless, indicating the emission from ³CT states. The phosphorescence spectrum of **tBuCz2mTRZ** closely resembles that of **tBuCz2pTRZ**, resulting in close-lying triplet states at 2.83 eV and 2.88 eV, for **tBuCz2pTRZ** and **tBuCz2mTRZ**, respectively, measured from the onset of these spectra. Taking the offset between the prompt emission and phosphorescence spectra, the ΔE_{ST} values of 90 meV and 60 meV were estimated for **tBuCz2pTRZ** and **tBuCz2mTRZ**. The T₁ state of **tBuCz2m2pTRZ** has its onset at 2.69 eV, resulting in a ΔE_{ST} gap of 40 meV. I discuss the reasons behind different ΔE_{ST} gaps for the compounds later after the data in film is introduced. In principle, the presence of the smaller gap between the singlet and triplet states should increase TADF contribution in **tBuCz2m2pTRZ**.

For host-free electroluminescent devices, it is essential to understand how the photophysical properties in solution translate into neat films. Therefore, the neat thin film photophysics of **tBuCz2pTRZ**, **tBuCz2mTRZ** and **tBuCz2m2pTRZ** was investigated next at 300 K and 5 K (Figure **1b.3**).

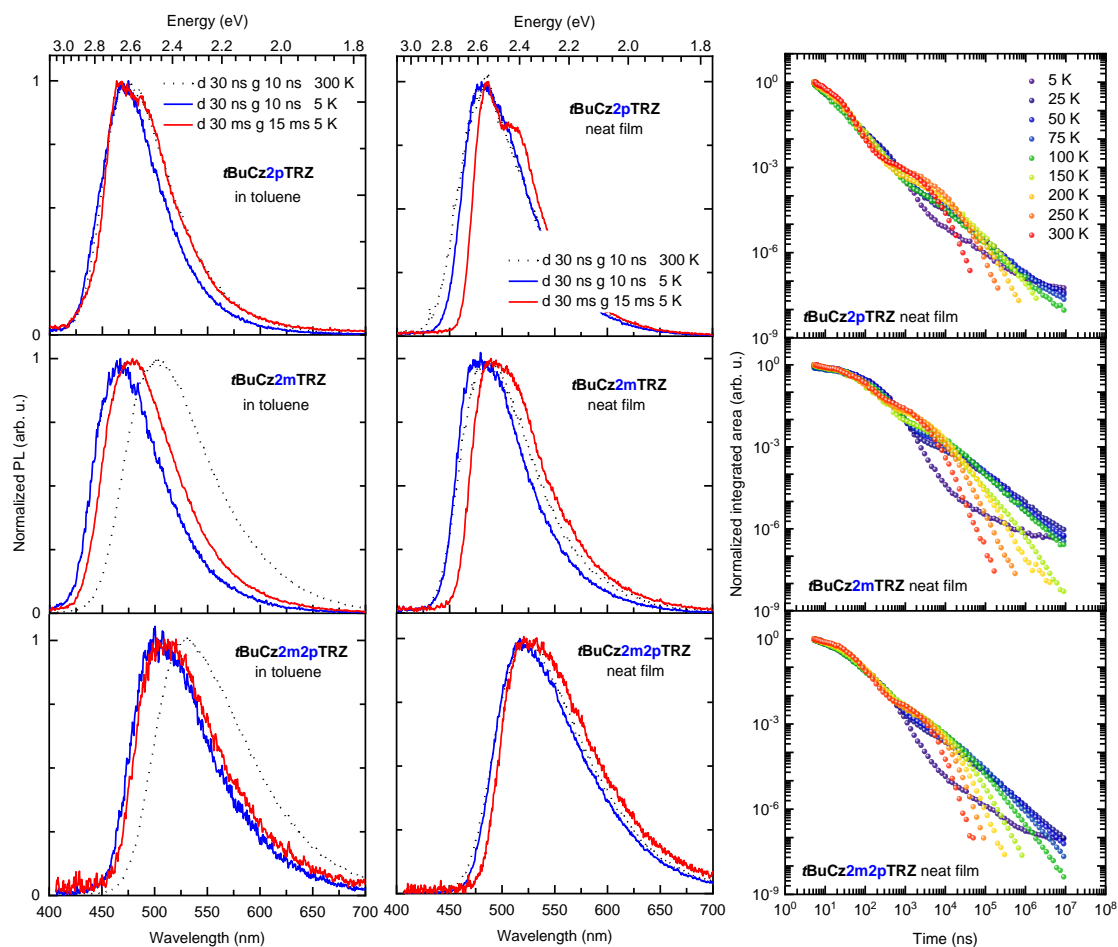


Figure 1b.3. Prompt emission with a delay (d) of 30 ns and gate (g) of 10 ns at 300 K (black dotted line) and at 5 K (blue solid line), phosphorescence with detection in the ms range ($d = 30$ ms, $g = 15$ ms) at 5 K (red solid line) of **tBuCz2pTRZ** (top), **tBuCz2mTRZ** (middle) and **tBuCz2m2pTRZ** (bottom) in toluene solution and neat film. On the right is the temperature-dependent time-resolved PL decay of neat films. The decays were obtained by integrating each time-resolved spectrum across the full spectral range ($\lambda_{exc} = 355$ nm).

Similar to the features observed in toluene, the prompt emission at both 300 K and 5 K in neat films is also broad and unstructured. The prompt emission of **tBuCz2pTRZ** still closely resembles that of **tBuCz2mTRZ**. The energy levels of the lowest singlet (1CT) states determined from the onsets of the corresponding prompt fluorescence spectra at 5 K are 2.78, 2.81 and 2.63 eV for **tBuCz2pTRZ**, **tBuCz2mTRZ** and **tBuCz2m2pTRZ**, respectively, values that are stabilized by about 140-160 meV compared to those in toluene glass. The spectra obtained at 5 K after a time delay of 30 ms are, again, ascribed to phosphorescence. The phosphorescence spectra for **tBuCz2pTRZ** and **tBuCz2mTRZ** are structured with a major peak at 486 nm (2.55 eV) and a low energy feature around 510 nm (2.43 eV)

that is ascribed to unresolved vibrational transition. The energies of the T_1 state of **tBuCz2pTRZ** and **tBuCz2mTRZ** were measured from the onsets at 2.69 and 2.72 eV, respectively, leading to the same ΔE_{ST} value of 90 meV. The similarities in their S_1 and T_1 states indicate that the *para*- or *meta*-connection between donor and acceptor has little effect on the nature of the excited states. The energy of the T_1 state of **tBuCz2m2pTRZ** is located at 2.59 eV, leading to the smallest ΔE_{ST} value of 40 meV, which is also the same as that determined in toluene glass.

Figure **1b.3** also shows the PL transient decay curves of neat films. The intensity of DF decreases upon cooling and vanishes at 5 K yet, for **tBuCz2mTRZ** and **tBuCz2m2pTRZ**, most thermal activation occurs between 5 and 25 K, implying a very efficient RISC even at low temperatures. Based on the low temperature for the thermal activation of the delayed emission, the actual singlet-triplet gaps for **tBuCz2mTRZ** and **tBuCz2m2pTRZ** are likely to be smaller than predicted by the difference in offsets between the singlet and triplet spectra at 5 K. A smaller ΔE_{ST} and thus a faster RISC rate can be explained considering two reasons. First, a part of the high RISC rate can be accounted for by the presence of higher-lying intermediate triplet states that reduces the energetic gap for the RISC process.⁴⁻⁶ Second, the smaller effective ΔE_{ST} in the solid-state can be explained by the presence of different molecular conformations with associated different singlet-triplet gaps.⁷⁻⁹ In fact, most of the TADF is likely to result from the fraction of the molecules that possess the smallest singlet-triplet gaps. The PL quantum yields (Φ_{PL}) of the neat films as well as other photophysical parameters are collated in Table **1b.1**.

Table 1b.1. Summary of the photophysical properties of the compounds as the neat films. Φ_{PL} in 1 wt% PMMA film is also provided for comparison. λ_{PL} represents the peak wavelength while S_1 and T_1 represent the singlet and triplet energies determined from the onset.

	λ_{PL} 300 K	S_1 5 K	T_1 5 K	$\Delta E_{ST}^{(a)}$	$\Phi_{PL}^{(b)}$	$\Phi_{PL}^{(c)}$	$\Phi_{DF}/\Phi_{PF}^{(d)}$	$\tau_{PF}^{(e)}$	$\tau_{DF}^{(f)}$	k_r^S (g)	k_{nr}^S (h)
					1 wt%	neat					
	(nm)	(eV)	(eV)	(meV)	(%)	(%)	(Φ_{DF})	(ns)	(μ s)	($\times 10^7, s^{-1}$)	($\times 10^7, s^{-1}$)
tBuCz2pTrz	481	2.78	2.69	90	86	61 (8)	0.15	11	1.2	4.8	4.3
tBuCz2mTrz	483	2.81	2.72	90	64	59 (33)	1.3	52	1.1	0.5	1.4
tBuCz2m2pTrz	520	2.63	2.59	40	90	86 (25)	0.4	31	1.1	2.0	1.2

(a) $\Delta E_{ST} = S_1 - T_1$. Estimated from the onsets of S_1 and T_1 at 5 K.

(b) Total PLQY under N_2 in a PMMA film at a 1 wt% doping concentration. $\lambda_{exc} = 340$ nm.

(c) Total PLQY under N_2 in the neat film. $\lambda_{exc} = 340$ nm.

(d) Ratio between the integrated area under the delayed and prompt emission.

(e) Prompt emission lifetime at 300 K extracted from a mono-exponential fitting.

(f) Delayed emission lifetime at 300 K extracted from a mono-exponential fitting.

(g) Constant of radiative decay rate of the singlet state extracted using $k_r^S = \Phi_{PF}/\tau_{DF}$.

(h) Constant of non-radiative decay rate of the singlet state extracted using $\tau_{PF} = 1 / (k_r^S + k_{nr}^S)$.

Under N₂, neat films of **tBuCz2pTRZ** and **tBuCz2mTRZ** have similar Φ_{PL} of 61% and 59%, respectively. For the neat film of **tBuCz2m2pTRZ**, the Φ_{PL} in N₂ is the highest among three dendrimers at 86%, indicative of effective suppression of quenching resulting from aggregation in the neat film for this compound. The Φ_{PL} was also compared by doping 1 wt% of the three dendrimers into a PMMA matrix to discriminate any potential efficiency loss due to concentration quenching. Photoluminescence quantum yields of 86%, 64% and 90% were obtained for **tBuCz2pTRZ**, **tBuCz2mTRZ** and **tBuCz2m2pTRZ** doped films, respectively, under N₂. A significant decrease of Φ_{PL} from 86% (doped film) to 61% (neat film) was observed for **tBuCz2pTRZ**, indicating significant non-radiative losses, while in contrast, **tBuCz2mTRZ** (64% in doped film vs 59% in neat film) and **tBuCz2m2pTRZ** (90% in doped film vs 86% in neat film) could still sustain their PL quantum yields. A smaller amount of concentration quenching when donor and acceptor units are linked via a *meta*-connection compared to a *para*-connection can be attributed to a more twisted geometry between donor and acceptor units, which is typical for *meta*-linked compounds.³ In principle, a more twisted geometry means that the exciton is less delocalized, thus suppressing the chance of efficiency loss via a triplet excimer formation.¹⁰ This explanation would also be consistent with the highest delayed emission yield in the *meta*-based compound (Table **1b.1**). Importantly, the results indicate that **tBuCz2m2pTRZ** inherits not only a high Φ_{PL} (86% in neat film) from **tBuCz2pTRZ**, but also from **tBuCz2mTRZ** an ability to suppress non-radiative losses. Furthermore, a two times larger amount of dendron units in **tBuCz2m2pTRZ** is an extra factor limiting guest to guest interactions, resulting in the best performance of **tBuCz2m2pTRZ** in terms of a suppressed concentration quenching. Compared to the works of other groups, **tBuCz2m2pTRZ** shows by far one of the highest photoluminescence quantum yields as a neat film,¹¹⁻¹² which could potentially lead to the highest-performing host-free OLEDs in the field.

Conclusion

Carbazole-based extended donor groups result in compounds with ΔE_{ST} gaps below 100 meV and moderate to high PLQYs, even in the neat films. It is found that, depending on how the donor unit is linked to the acceptor, different amount of radiative decay rates and TADF contributions are present. While **tBuCz2pTRZ** has the strongest radiative decay rate and the weakest TADF contribution, **tBuCz2mTRZ** has the weakest radiative decay rate and the strongest TADF contribution. Furthermore, it is found that *para*- and *meta*-type connections show different amounts of concentration quenching, which is significantly smaller for **tBuCz2mTRZ**. The combined molecule, **tBuCz2m2pTRZ**, shows photophysical properties that are typical for both *meta*- and *para*-type connections, resulting in a high PLQY and a minimal concentration quenching. The minimal concentration quenching in **tBuCz2m2pTRZ** is largely attributed to the presence of *meta*-linked dendrons. Overall, the carbazole-based dendron donor units accompanied by a suitable connection to the acceptor unit result in a good candidate for an efficient emitter that could be used host-free in the emissive layer of the OLED.

References of Chapter 1b

1. Matulaitis, T.; Imbrasas, P.; Kukhta, N. A.; Baronas, P.; Bučiūnas, T.; Banevičius, D.; Kazlauskas, K.; Gražulevičius, J. V.; Juršėnas, S., Impact of Donor Substitution Pattern on the TADF Properties in the Carbazolyl-Substituted Triazine Derivatives. *The Journal of Physical Chemistry C* **2017**, *121*, 23618-23625.
2. Braveenth, R.; Chai, K. Y., Triazine-Acceptor-Based Green Thermally Activated Delayed Fluorescence Materials for Organic Light-Emitting Diodes. *Materials* **2019**, *12*, 2646.
3. Xie, F.-M.; Zhou, J.-X.; Li, Y.-Q.; Tang, J.-X., Effects of the relative position and number of donors and acceptors on the properties of TADF materials. *Journal of Materials Chemistry C* **2020**, *8*, 9476-9494.
4. Chen, X.-K.; Zhang, S.-F.; Fan, J.-X.; Ren, A.-M., Nature of Highly Efficient Thermally Activated Delayed Fluorescence in Organic Light-Emitting Diode Emitters: Nonadiabatic Effect between Excited States. *The Journal of Physical Chemistry C* **2015**, *119*, 9728-9733.
5. Noda, H.; Chen, X.-K.; Nakanotani, H.; Hosokai, T.; Miyajima, M.; Notsuka, N.; Kashima, Y.; Brédas, J.-L.; Adachi, C., Critical role of intermediate electronic states for spin-flip processes in charge-transfer-type organic molecules with multiple donors and acceptors. *Nature Materials* **2019**, *18*, 1084-1090.
6. Cui, L.-S.; Gillett, A. J.; Zhang, S.-F.; Ye, H.; Liu, Y.; Chen, X.-K.; Lin, Z.-S.; Evans, E. W.; Myers, W. K.; Ronson, T. K.; Nakanotani, H.; Reineke, S.; Bredas, J.-L.; Adachi, C.; Friend, R. H., Fast spin-flip enables efficient and stable organic electroluminescence from charge-transfer states. *Nature Photonics* **2020**, *14*, 636-642.
7. Stavrou, K.; Franca, L. G.; Monkman, A. P., Photophysics of TADF Guest-Host Systems: Introducing the Idea of Hosting Potential. *ACS Applied Electronic Materials* **2020**, *2*, 2868-2881.
8. Zhang, Z.; Kumar, S.; Bagnich, S.; Spuling, E.; Hundemer, F.; Nieger, M.; Hassan, Z.; Köhler, A.; Zysman-Colman, E.; Bräse, S., OBO-Fused Benzo[fg]tetracene as Acceptor With Potential for Thermally Activated Delayed Fluorescence Emitters. *Frontiers in Chemistry* **2020**, *8*, 563411.
9. Woo, S.-J.; Kim, J.-J., TD-DFT and Experimental Methods for Unraveling the Energy Distribution of Charge-Transfer Triplet/Singlet States of a TADF Molecule in a Frozen Matrix. *The Journal of Physical Chemistry A* **2021**, *125*, 1234-1242.
10. Bagnich, S. A.; Athanasopoulos, S.; Rudnick, A.; Schroegel, P.; Bauer, I.; Greenham, N. C.; Strohriegl, P.; Köhler, A., Excimer Formation by Steric Twisting in Carbazole and Triphenylamine-Based Host Materials. *The Journal of Physical Chemistry C* **2015**, *119*, 2380-2387.
11. Jhulki, S.; Cooper, M. W.; Barlow, S.; Marder, S. R., Phosphorescent and TADF polymers and dendrimers in solution-processed self-host organic light-emitting diodes: structure analysis and design perspectives. *Materials Chemistry Frontiers* **2019**, *3*, 1699-1721.
12. Liu, D.; Tian, W.; Feng, Y.; Zhang, X.; Ban, X.; Jiang, W.; Sun, Y., Achieving 20% External Quantum Efficiency for Fully Solution-Processed Organic Light-Emitting Diodes Based on Thermally Activated Delayed Fluorescence Dendrimers with Flexible Chains. *ACS Applied Materials & Interfaces* **2019**, *11*, 16737-16748.

Chapter 2. How does TADF depend on the length of the oligomer chain?

In Chapter 1, I focused on the changes to TADF-related properties when the donor group is extended or linked to the acceptor via a phenylene bridge in a different position. In Chapter 2, I now investigate how TADF-related properties change based on the length of the oligomer chain.

TADF emitters can thermally up-convert dark triplet excitons (T_1) to emissive singlet excitons (S_1) through reverse intersystem crossing (RISC), and the efficiency of this process is governed by the singlet-triplet energy gap, ΔE_{ST} , and the magnitude of the spin-orbit coupling (SOC) between these two states.¹⁻² Based on El Sayed's rule,³⁻⁴ the spin-flip between the states of the same nature is inefficient and requires a higher-lying triplet state of a different orbital character for efficient spin-orbit coupling (SOC) between triplet and singlet manifolds.⁵⁻⁷ To maximise the chance of having a triplet state of a SOC-suitable character (for example, LE), a possible solution could be to employ chemical designs that have a high number of intermediate triplet states. There are a few strategies to achieve a higher number of intermediate triplet states that are based on a larger number of either donor or donor and acceptor units.⁸⁻¹² In principle, a higher number of repetitive units should result in a larger number of quasi-degenerate states that also results in a higher number of intermediate triplet states.⁸

One known design strategy to produce a system that possesses intermediate triplet states is based on a multi-donor to a single acceptor system like poly(carbazole)-substituted benzonitrile (BN) derivatives.⁸⁻⁹ For example, according to DFT calculations, the number of intermediate triplet states increases from two to three when the number of donor carbazoles is increased from four in 2,3,5,6-tetra(9*H*-carbazol-9-yl)benzonitrile (**4CzBN**) to five in 2,3,4,5,6-penta-(9*H*-carbazol-9-yl)benzonitrile (**5CzBN**).¹³ The chemical structures of **4CzBN** and **5CzBN** are given in Figure 2.1.

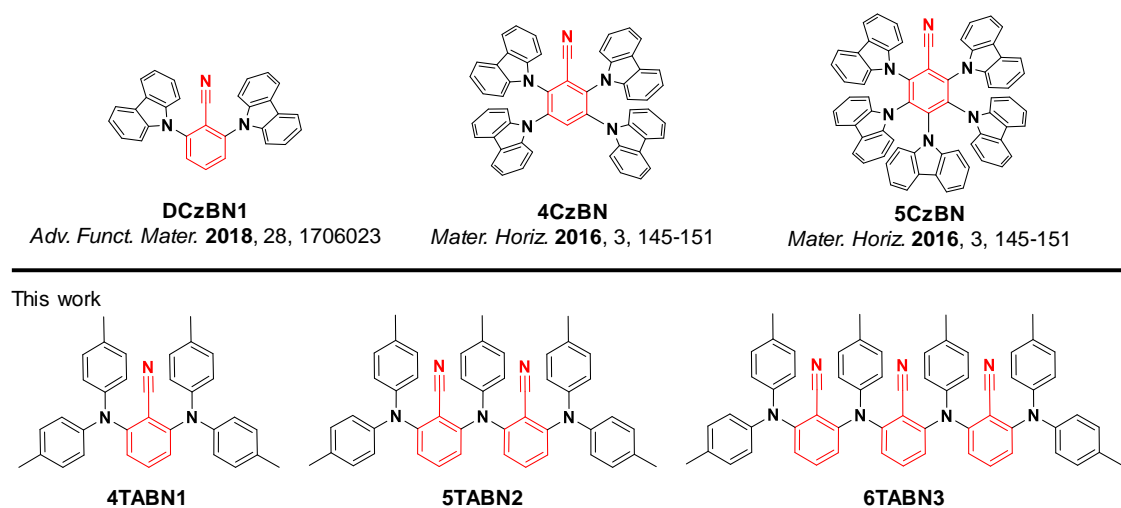


Figure 2.1. Chemical structures of the literature compounds and the compounds investigated in this work.

Another strategy to ensure a larger number of intermediate triplet states is to increase the number of repetitive donors and acceptor units within the main chain polymer. The possibility of employing multi donor-acceptor units for a TADF emitter was investigated by Adachi *et al.* in 2016.¹⁰ While the group reports TADF-active polymers that perform well as solution-processed OLEDs, the number of intermediate triplet states in their polymers is not investigated either using a theoretical or photophysical study. Furthermore, the fine-tuning of the TADF-properties in their polymers resulted in a strong redshift of photoluminescence.¹⁰

To experimentally study TADF-related properties as a function of molecular chain length with the same repeating donor and acceptor units, a series of compounds of increasing molecular size is selected. The group of compounds selected is the donor-acceptor type oligomers that have benzonitrile (BN) as the acceptor units which are connected via the amine donors, acting as bridges to adjacent BN acceptors (Figure 2.1). The *ortho*-substitution pattern of the donors should translate to highly twisted conformations of the emitters, which is expected to be beneficial to both reduce ΔE_{ST} and avoid an undesired redshift of the emission. Since the first member of the series, **4TABN1**, is similar to the previously reported **DCzBN1**,¹⁴ the photophysical properties of **4TABN1** are also cross-compared to **DCzBN1** in this chapter (Figure 2.1).

I found that increasing the oligomer length demonstrates positive effects not only in terms of suppressed aggregation in larger oligomers but also in terms of the enhancement of TADF-related properties. The intersystem crossing rate and reverse intersystem crossing rate are found to increase with increasing oligomer size which is explained by a higher number of intermediate triplet states as also predicted by the quantum chemical calculations. Most importantly, I discover that increasing the oligomer size with repeating donor-acceptor units enhances TADF-related properties and suppresses aggregation at no cost to the blue photoluminescence emission wavelength.

Methods

Materials. The compounds for the investigation were synthesized by Dr. Subeesh Suresh in the Prof. Eli Zysman-Colman group (University St Andrews, UK).

Photophysical measurements. The solutions of 0.05 mg/mL in toluene corresponding to around 10^{-5} M depending on molecular weight as well as spin-coated 10 wt% films in DPEPO were prepared. PL measurements were carried out as detailed in Methods section of the thesis and Chapter 1a.

Photophysical properties

The photophysical investigation is started with absorption and photoluminescence measurements of the compounds in toluene solution to allow the evaluation of the monomolecular properties (Figure 2.2).

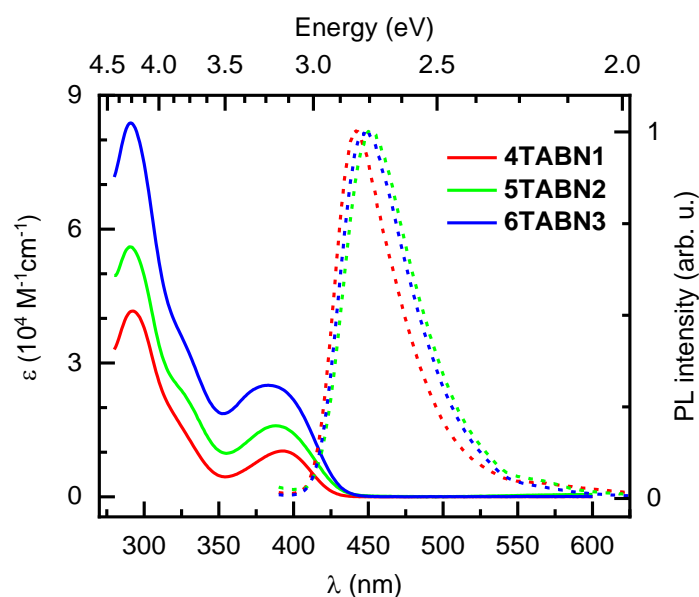


Figure 2.2. Absorption and steady-state photoluminescence emission in toluene at room temperature ($\lambda_{\text{exc}} = 370 \text{ nm}$).

Figure 2.2 presents the room temperature absorption and photoluminescence (PL) spectra of the compounds. All molecules show the same absorption profile but differ in the band intensity. Taking into account the nature of the donor and acceptor units, the band at 4.23 eV (293 nm) can be assigned to the π - π^* absorption of the donor unit,¹⁵ with the absorption of the acceptor occurring at the energy higher than 4.5 eV.¹⁶ The intensity of this LE absorption band corresponds to the increase of the donor units in the molecule along the series. Figure 2.2 also reveals a broad, low intensity and structureless absorption band at 3.15 eV (394 nm) which I assign to the intramolecular charge transfer (ICT) state. The intensity of the ICT absorption band also increases with the increasing number of donor and acceptor units. A small blue-shift of the ICT absorption band with increasing oligomer length suggests a larger twisting of the molecules in larger oligomers. The PLQYs of the compounds in the oxygen-free toluene were determined to be comparable along the series, with the values of 18, 14 and 15% for **4TABN1**, **5TABN2** and **6TABN3**, respectively. All three compounds show broad and structureless PL spectra that are typical for the emission from the CT states.¹⁷ Since there is only a minor (around 50 meV) steady-state PL emission energy shift along the series, it implies that the emission colour is largely preserved along the series. The absorption and steady-state PL energies are summarized in Table 2.1 below.

Table 2.1. Extinctions coefficients and energetic positions of photoluminescence as obtained from the optical spectroscopy of the compounds in toluene and 10 wt% DPEPO films.

	In toluene					In 10 wt% DPEPO film				
	$\lambda_{\text{abs}}^{(a)}$	$\epsilon_{\text{CT}}^{(b)}$	$\lambda_{\text{PL}}^{(c)}$	$S_1^{(d)}$	$T_1^{(d)}$	$\Delta E_{\text{ST}}^{(e)}$	$\lambda_{\text{PL}}^{(c)}$	$S_1^{(d)}$	$T_1^{(d)}$	$\Delta E_{\text{ST}}^{(e)}$
	300 K	(10^4 M^{-1} cm^{-1})	300 K	(eV)	(eV)	(eV)	300 K	(eV)	(eV)	(eV)
				77 K	77 K	± 0.01		77 K	77 K	± 0.01
4TABN1	3.16 eV (393 nm)	1.03	2.81 eV (441 nm)	2.95	2.76	0.19	2.67 eV (464 nm)	2.92	2.71	0.21
5TABN2	3.19 eV (389 nm)	1.59	2.76 eV (449 nm)	2.93	2.76	0.17	2.64 eV (470 nm)	2.89	2.72	0.17
6TABN3	3.24 eV (383 nm)	2.47	2.74 eV (452 nm)	2.95	2.77	0.18	2.66 eV (466 nm)	2.89	2.72	0.17

^a Peak maximum of CT absorption, ^b decadic molar extinction coefficient, ^c Peak maximum of steady-state emission, ^d S_1 and T_1 energetic positions as determined from the onset, ^e $\Delta E_{\text{ST}} = S_1 - T_1$.

To estimate the singlet-triplet gaps of the compounds in solution, the samples are next cooled down to 77 K (Figure 2.3).

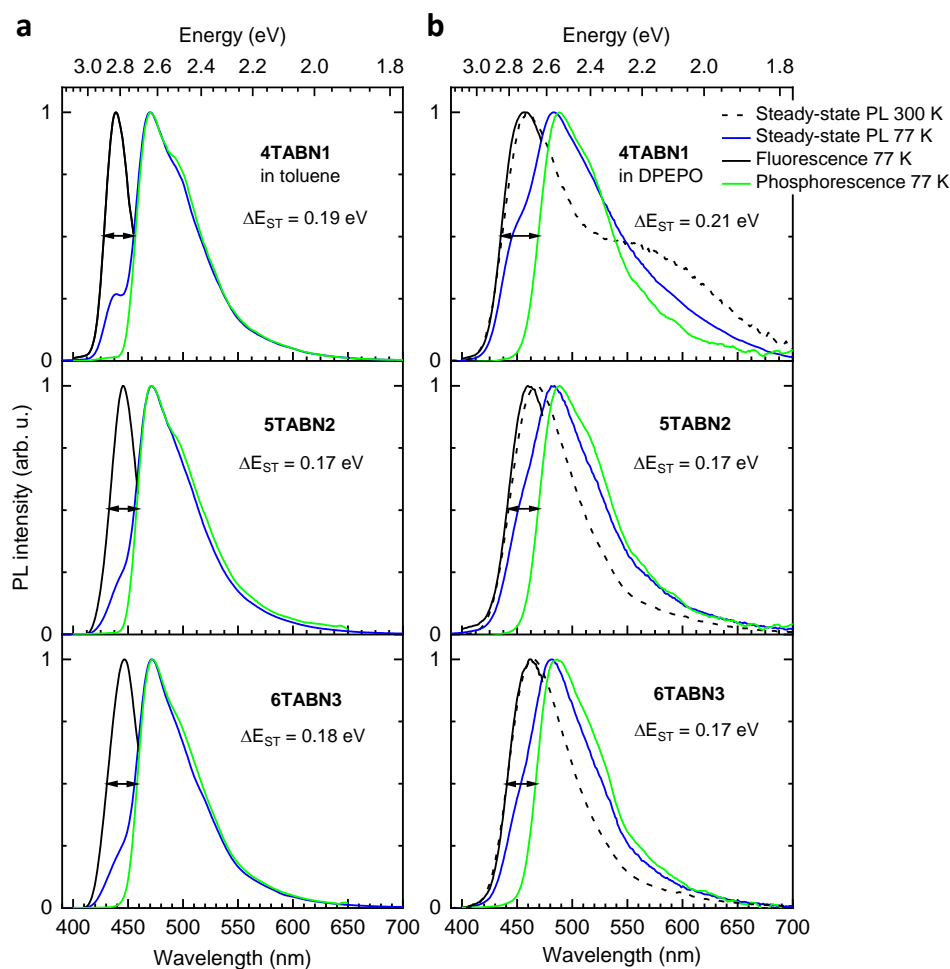


Figure 2.3. Steady-state emission (blue line), phosphorescence (delay 150 ms, gate 50 ms, green line) and fluorescence (black line) obtained as the difference between the steady-state emission and phosphorescence at 77 K in (a) toluene solution and (b) 10 wt% film in DPEPO. The black dashed line represents the steady-state emission at 300 K. $\lambda_{exc} = 300$ nm.

Figure 2.3a shows the spectra of the steady-state emission in toluene glass at 77 K (blue line). The fluorescence spectra (black line) in Figure 2.3 were obtained from the difference between the steady-state emission and phosphorescence spectra. It is evident that the steady-state emission is dominated by phosphorescence, with fluorescence being observed only as a weak high-energy shoulder. This implies that the main channel of deactivation of the singlet excited state is intersystem crossing (ISC) that leads to the population of the triplet state. The energy of the S_1 state estimated from the onset of the fluorescence spectrum is at 2.95 eV for **4TABN1** and **6TABN3** and at 2.93 eV for **5TABN2**. When comparing with the 300 K data (Figure 2.2), there is no spectral shift of fluorescence that accompanies

the change in temperature of the sample from 300 to 77 K which is typically observed for the emission from a CT state.¹⁷ Such behaviour is rather congruent with emission from an LE state. At the same time, fluorescence arises at excitation of the low energy absorption band that was attributed to the CT state. However, the experimentally obtained extinction coefficient for this band is more typical for a π - π^* state.¹⁸ Based on the coexistence of features that are typical for CT and π - π^* state, I assign the singlet transition to a mixed CT/LE nature. The phosphorescence spectra, recorded with a delay of 150 ms after excitation and a gate of 50 ms are also shown in Figure **2.3a**. The structured phosphorescence spectra of the three compounds all align with the first maximum λ_{PL} of 2.62 eV (473 nm). While the origin of phosphorescence can be ascribed neither to donor nor acceptor individually, it must come from a new CT or LE state. Similar to fluorescence, phosphorescence is also ascribed to have a mixed CT/LE state character. The phosphorescence spectra being the same in shape and position for all molecules reveals that the donor-acceptor units are not strongly coupled with one another. This conclusion is also supported by the analysis of their absorption spectra, where no new features appear along the series. The phosphorescence spectra are shifted to lower energy by 0.17-0.19 eV compared to fluorescence. This gives the separation energy, ΔE_{ST} , between the lowest singlet and triplet state. Comparing to the reference **DCzBN1** ($\Delta E_{\text{ST}} = 0.31$ eV, in toluene, Figure **2.1**),¹⁴ the ΔE_{ST} values for **4TABN1**, **5TABN2** and **6TABN3** in toluene are smaller which is more promising for TADF.

To assess the potential of these compounds as emitters for OLEDs, the photophysical properties as 10 wt% blend films in DPEPO (Bis[2-(diphenylphosphino)phenyl] ether oxide) were evaluated (Figure **2.3b**). DPEPO was selected as a host because of its sufficiently high lowest triplet state energy of around 3.0 eV.¹⁹ Similar to solution, all compounds show a broad and structureless high energy band with maxima that are redshifted by around 0.1 eV relative to their solution-state PL spectra (Table **2.1**). The energy of the S_1 states, obtained using the onset of the fluorescence spectra, being slightly lower in energy than the corresponding values in solution can be attributed to a strong polarity of DPEPO molecules.²⁰ Similar to solution, the phosphorescence spectra are shifted to lower energy by a comparable amount, yielding the ΔE_{ST} gaps in the range between 0.17 and 0.21 eV. Compared to

solution, the difference in ΔE_{ST} values of 10 wt% DPEPO films between **4TABN1** and the remaining compounds is more pronounced (210 vs 170 meV). In addition to the high energy band at around 2.70 eV (460 nm), **4TABN1** in 10 wt% DPEPO film shows a significant low energy band at around 2.30 eV (540 nm) which was not observed in solution. For longer oligomers, **5TABN2** and **6TABN3**, the low energy band is absent. To understand the origin of the low energy band in **4TABN1**, the PL steady-state emission was measured at several different concentrations (Figure 2.4).

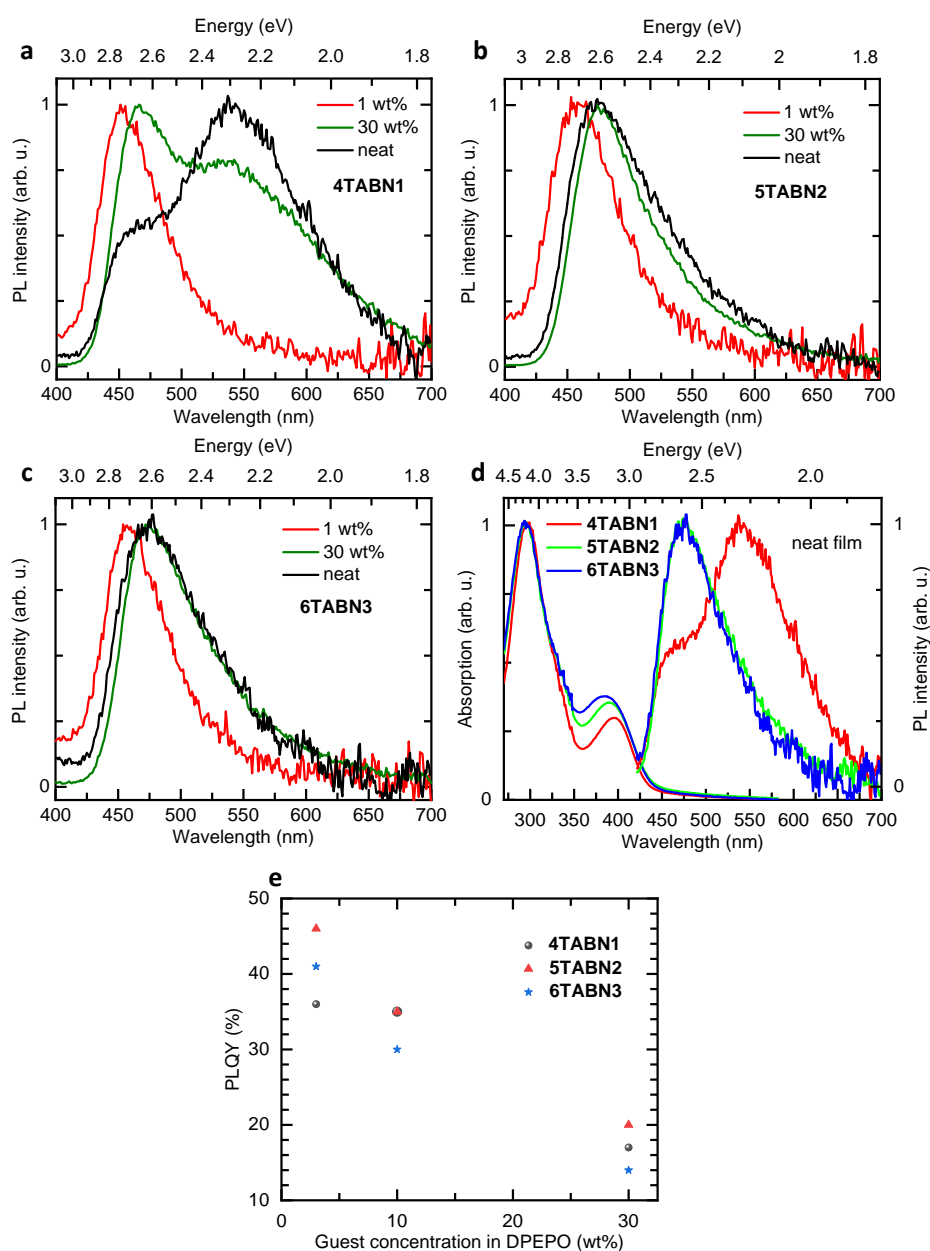


Figure 2.4. The steady-state PL emission of the compounds at different concentrations at RT ($\lambda_{exc} = 315$ nm), the absorption spectra of the neat films and the PLQY dependence on the guest concentration in DPEPO.

Figure 2.4 shows the steady-state emission of the compounds at 1 wt%, 30 wt% doping concentrations, as well as neat films. The redshift of the high energy band with increasing concentration can be attributed to spectral diffusion.²¹ It is also evident that a significant low energy band is present for **4TABN1**, becoming more pronounced with increasing emitter concentration in the film. The low energy band can be ascribed to aggregation. To examine the nature of this aggregate, the absorption spectrum of the neat film was measured (Figure 2.4d). Interestingly, no difference in the neat film absorption can be seen as compared to solution (see also Figure 2.2). This can be ascribed to either a low concentration of aggregate in the film which becomes hardly detectable in the absorption spectra or the formation of excimer. For **5TABN2** and especially **6TABN3**, the low energy feature is strongly suppressed (Figure 2.4). The photoluminescence quantum yields (PLQY) in oxygen-free conditions at 3, 10 and 30 wt% doping concentrations are also shown in Figure 2.4. Although the low energy peak is no longer visible in **5TABN2** and **6TABN3**, the decrease in PLQY with increasing emitter concentration is similar for all compounds, suggesting that there is still some aggregation in the latter two compounds.

To evaluate TADF properties of the doped films, the evolution of the time-resolved PL decays as a function of temperature is investigated (Figure 2.5).

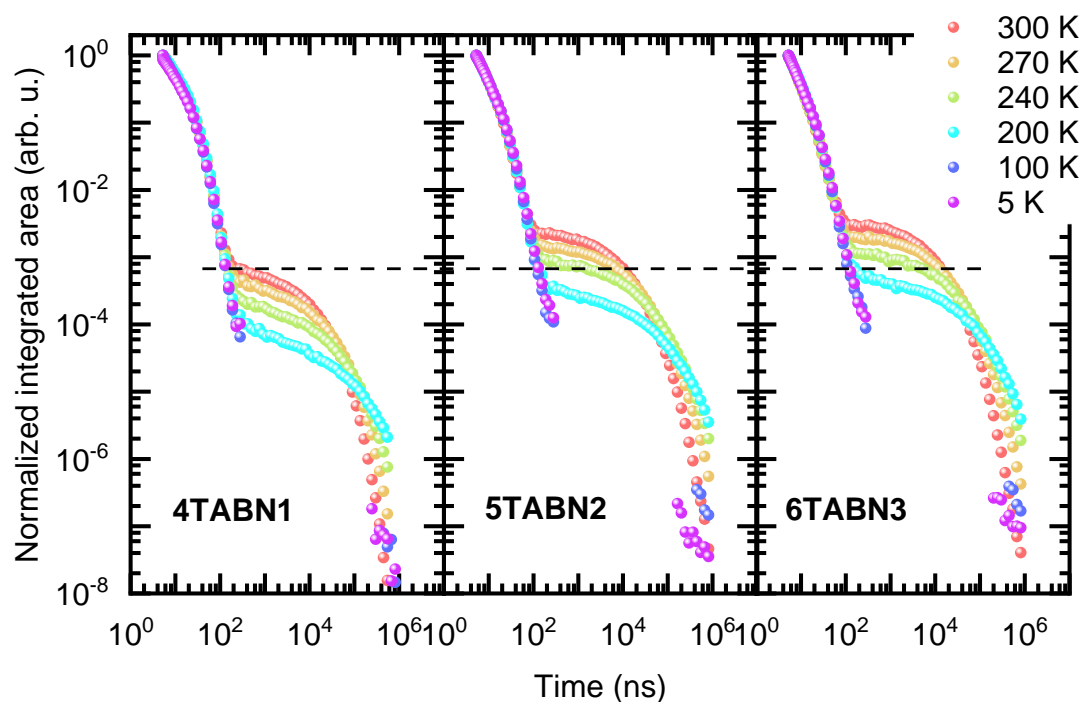


Figure 2.5. Transient photoluminescence decay of the blend films in 10 wt% DPEPO films ($\lambda_{exc} = 355$ nm). Integrated across the full spectral range.

Figure 2.5 presents the transient photoluminescence decay of the 10 wt% DPEPO doped films of the compounds. Each decay consists of two regimes: the prompt fluorescence, lasting up until around 100 ns, and the delayed fluorescence, on the order of microseconds. The prompt fluorescence is insensitive to temperature, but the intensity of the delayed fluorescence increases with increasing temperature, which is consistent with a thermally activated delayed fluorescence. From a visual inspection of the delayed fluorescence of the three compounds, it can be seen that the amplitude of the delayed intensity is higher for **5TABN2** and **6TABN3**, which is consistent with a slightly smaller ΔE_{ST} in these two compounds. The photophysical parameters extracted from the analysis of the transient photoluminescence decay curves according to Refs ²²⁻²³ are summarized in Table 2.2 below.

Table 2.2. Efficiencies and rate constants of **4TABN1**, **5TABN2** and **6TABN3** films in DPEPO (10 wt%).

	$\Phi_{\text{PL}}^{(a)}$	$\Phi_{\text{DF}}/\Phi_{\text{PF}}^{(b)}$	$\tau_{\text{PF}}^{(c)}$	$\tau_{\text{DF}}^{(d)}$	$k_r^{\text{S}(e)}$	$k_{\text{nr}}^{\text{S}(f)}$	$\Phi_{\text{ISC}}^{(g)}$	$k_{\text{ISC}}^{(h)}$	$k_{\text{rISC}}^{(i)}$
	(%)		(ns)	(μs)	($\times 10^7$, s^{-1})	($\times 10^7$, s^{-1})		($\times 10^8$, s^{-1})	($\times 10^4$, s^{-1})
4TABN1	35	0.53	11.0	28	2.1	3.7	0.36	0.3	5.3
5TABN2	35	1.99	7.0	29	1.7	1.9	0.75	1.1	9.2
6TABN3	30	2.49	7.0	26	1.2	2.1	0.77	1.1	12.4

^a total PLQY ($\lambda_{\text{exc}} = 315 \text{ nm}$); ^b ratio of the integrated areas of delayed and prompt emission; ^c lifetime of prompt emission estimated using a mono-exponential fit at 300 K; ^d average lifetime of delayed emission at 300 K; ^e constant of radiative decay rate of singlet excitons; ^f constant of non-radiative decay rate of singlet exciton excluding k_{ISC} ; ^g intersystem crossing yield; ^h constant of intersystem crossing rate; ⁱ constant of reverse intersystem crossing rate.

Starting from the singlet state properties, the radiative decay rates do not show an increasing trend in contrast to what one might expect from an increasing extinction coefficient along the series (Figure 2.2, Table 2.1). This could be explained by the fact that the donor-acceptor units are not strongly conjugated with other units in the oligomers and thus show comparable radiative decay rates, typical for a monomer. To support this claim, the extinction coefficients presented in Figure 2.2 are divided by 1.5, 2.5 and 3.5, numbers that represent the amount of “repetition” in oligomers, where an integer number stands for a full D-A pair while 0.5 represents the remaining part of the molecule. After such correction of the extinction spectra, comparable extinction coefficients are found for all molecules, consistent with comparable radiative decay rates along the series (Table 2.2). Furthermore, it should be recalled that neither S_1 nor T_1 shows a redshift along the series, also confirming the absence of significant conjugation along the series (Table 2.1). The analysis of the delayed part of the transient PL is not straightforward. Since a mono-exponential fit defines only 60% of the total delayed emission, the average lifetime for the delayed part was calculated. While the average lifetimes of the delayed part are quite similar for all compounds and have no particular trend, the ratio of integrated areas between the delayed and prompt part is increasing along the series. This ratio is more than four times larger for **6TABN3** compared to **4TABN1**. Table 2.2 also shows an increase in rate constant and

yield of intersystem crossing (ISC) along the series. I ascribe this to the increasing number of intermediate triplet states along the series (*vide infra*). According to Fermi's golden rule, the transition probability between the initial and final state is defined by the number of final states. Therefore, as the number of intermediate triplet states increases along the series, the ISC rate also increases. The presence of intermediate triplet states in larger oligomers has also benefits for the reverse intersystem crossing rate. The increase in the RISC rate could be explained by the presence of intermediate triplet states that reduce the effective ΔE_{ST} , thus enhancing the RISC process. As a result, the RISC rate is more than two times larger in **6TABN3** compared to **4TABN1**. Generally, the increase of RISC rate by two times requires the change in the ΔE_{ST} value of only around 20 meV at room temperature which is consistent with the ΔE_{ST} values estimated for emitters in DPEPO (210 vs 170 meV, Table **2.1**).

From the photophysical investigation so far, I demonstrated that the PL emission wavelength is largely similar for all compounds, with the presence of the additional low energy band in **4TABN1** which is ascribed to aggregation. While in solution comparable ΔE_{ST} gaps were found along the series, in film the ΔE_{ST} gaps were discovered to be slightly smaller for **5TABN2** and **6TABN3** (210 meV vs 170 meV). After analysing the transient PL decay in films, I showed that the ISC and RISC rates are increasing along the series. I attributed the increase of the ISC and RISC processes to a larger number of intermediate triplet states in larger oligomers. To confirm the presence of an increasing number of intermediate triplet states along the series, the density functional theory (DFT) calculation was performed for the compounds by David Hall (University of St Andrews, UK) (Figure **2.6**).

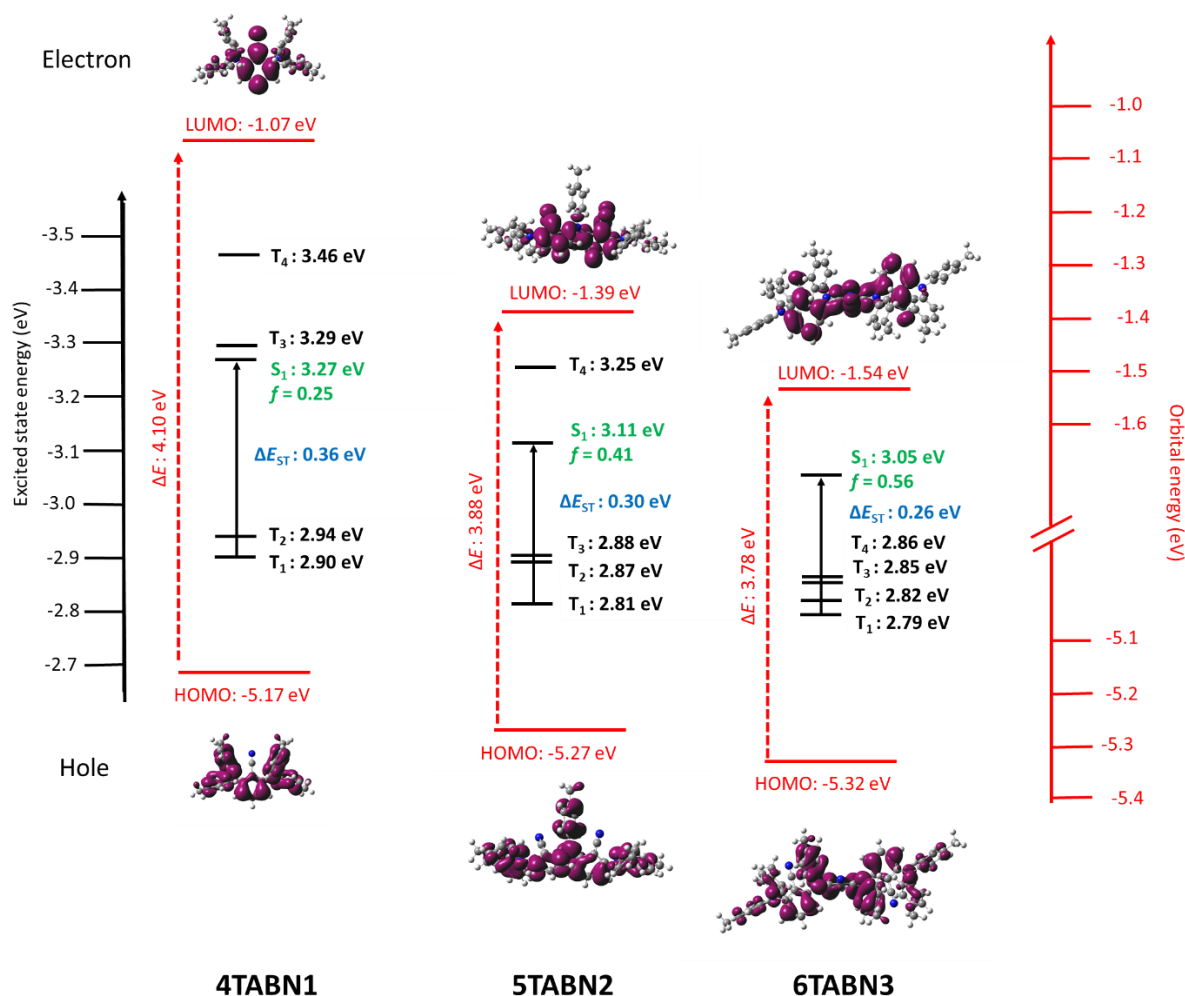


Figure 2.6. Left axis in black: HOMO LUMO energies calculated for the ground state geometry. Right axis in red: vertical transition energies for S₁, T₁ and T₂. Also shown are the hole and electron densities S₁. Calculated at the PBE0/6-31G(d,p) level, where *f* is the oscillator strength. This figure is presented with the permission of David Hall (University of St Andrews).

Before I analyse the triplet states as predicted by the DFT, I briefly discuss the singlet state properties. Surprisingly, the DFT shows that there is a reasonable stabilization of the S₁ energies from 3.27 eV to 3.11 eV and 3.05 eV for **4TABN1**, **5TABN2** and **6TABN3**, respectively, along with an increasing oscillator strength along the series. From the photophysical study, the S₁ energies and the oscillator strengths are predicted to be comparable along the series, ascribing this to the lack of conjugation between different D-A units in oligomers. This disagreement between theory and experiment could be assigned to DFT calculations being performed for the gas phase while the experiments were done in a liquid or solid-state. The molecules in the liquid or solid-state should face more significant interactions with the environment than in the gas phase that could lead to larger molecular torsions decreasing the

conjugation. Regarding the triplet state properties, the higher-lying triplet states (T_3 - T_4) are stabilized more significantly compared to S_1 along the series. For example, the energy of T_3 changes from 3.29 eV to 2.88 eV and 2.85 eV along the series, with T_3 being more than 200 meV below S_1 for **5TABN2** and **6TABN3**, respectively. Given such a large and unambiguous energetic difference between S_1 and T_3 , the predicted higher-lying triplet states are nevertheless expected to play a role as intermediate triplet states in larger oligomers, even when the DFT predicts more conjugation in the oligomers than experimentally shown. The DFT shows that the number of intermediate triplet states increases along the series (Figure 2.6), with 1, 2, and 3 intermediate triplet states for **4TABN1**, **5TABN2**, **6TABN3**, respectively. This supports the experimentally determined ISC rate which increases along the series. Regarding the ΔE_{ST} gaps predicted by the DFT, they decrease from 0.37 eV to 0.30 eV and 0.26 eV for **4TABN1**, **5TABN2** and **6TABN3**, respectively. If the energy difference between the lowest singlet and the highest intermediate triplet states are evaluated, then the $\Delta E_{ST}'$ values reduce to 0.33 eV, 0.23 eV and 0.19 eV for **4TABN1**, **5TABN2** and **6TABN3**, respectively. A lower energetic difference between the singlet and triplet states in larger oligomers also supports the experimentally increasing RISC rate along the series.

In summary, by the photophysical investigation, increasing ISC and RISC rates were found along the series, with no significant changes to monomolecular photoluminescence emission. Consistent with this work, a previously reported multi-donor approach where the number of carbazole units was increased from four to five also shows the enhancement of the RISC rate of around two times (in toluene) going from **4CzBN** to **5CzBN** (Figure 2.1).²⁴ Unfortunately, the PL emission wavelength is not preserved in their approach and redshifts by around 20 nm from 442 nm to 464 nm in toluene.²⁴ Opposite to only increasing the number of donor units in the molecule, multi donor and acceptor-based TADF emitters were also reported by Adachi *et al.* in a polymer architecture, yet the tuning of TADF-parameters resulted in a redshift of photoluminescence.¹⁰ With the approach presented in this work, it is demonstrated that the TADF-related parameters can be successfully fine-tuned without the redshift of photoluminescence. The unfortunate aspect of the approach investigated in this work is a

rather low PLQY of the compounds. However, as the photoluminescence properties are largely governed by the monomer properties, further optimisation is expected by employing more efficient monomer units.

Conclusion

In this chapter, an extendable molecular design consisting of repetitive donor-acceptor units to target intermediate triplet states was investigated. The effects on the RISC-related parameters as a function of increasing oligomer size were studied. An increasing ISC and RISC rates along the series were found, with no significant change to monomolecular photoluminescence spectra. Furthermore, increasing the oligomer length was found to suppress the low energy emission band, assigned to aggregation. Overall, this chapter demonstrates a successful way to increase the number of intermediate triplet states for the enhanced TADF-properties in the molecule without changing the blue photoluminescence emission wavelength.

References of Chapter 2

1. Hosokai, T.; Matsuzaki, H.; Nakanotani, H.; Tokumaru, K.; Tsutsui, T.; Furube, A.; Nasu, K.; Nomura, H.; Yahiro, M.; Adachi, C., Evidence and mechanism of efficient thermally activated delayed fluorescence promoted by delocalized excited states. *Science Advances* **2017**, *3*, e1603282.
2. N. J. Turro, V. R., J. C. Scaiano, Principle of Molecular Photochemistry: An Introduction (University Science Books, 2009), chap. 3, pp. 113–118.
3. El-Sayed, M. A., Spin–Orbit Coupling and the Radiationless Processes in Nitrogen Heterocyclics. *The Journal of Chemical Physics* **1963**, *38*, 2834–2838.
4. El-Sayed, M. A., Triplet state. Its radiative and nonradiative properties. *Accounts of Chemical Research* **2002**, *1*, 8–16.
5. Noda, H.; Nakanotani, H.; Adachi, C., Excited state engineering for efficient reverse intersystem crossing. *Science Advances* **2018**, *4*, eaao6910.
6. Etherington, M. K.; Gibson, J.; Higginbotham, H. F.; Penfold, T. J.; Monkman, A. P., Revealing the spin–vibronic coupling mechanism of thermally activated delayed fluorescence. *Nature Communications* **2016**, *7*, 13680.
7. Wang, M.; Chatterjee, T.; Foster, C. J.; Wu, T.; Yi, C.-L.; Yu, H.; Wong, K.-T.; Hu, B., Exploring mechanisms for generating spin-orbital coupling through donor–acceptor design to realize spin flipping in thermally activated delayed fluorescence. *Journal of Materials Chemistry C* **2020**, *8*, 3395–3401.
8. Yin, C.; Zhang, D.; Duan, L., A perspective on blue TADF materials based on carbazole-benzonitrile derivatives for efficient and stable OLEDs. *Applied Physics Letters* **2020**, *116*, 120503.
9. Uoyama, H.; Goushi, K.; Shizu, K.; Nomura, H.; Adachi, C., Highly efficient organic light-emitting diodes from delayed fluorescence. *Nature* **2012**, *492*, 234–238.
10. Lee, S. Y.; Yasuda, T.; Komiyama, H.; Lee, J.; Adachi, C., Thermally Activated Delayed Fluorescence Polymers for Efficient Solution-Processed Organic Light-Emitting Diodes. *Advanced Materials* **2016**, *28*, 4019–4024.
11. Cui, L.-S.; Gillett, A. J.; Zhang, S.-F.; Ye, H.; Liu, Y.; Chen, X.-K.; Lin, Z.-S.; Evans, E. W.; Myers, W. K.; Ronson, T. K.; Nakanotani, H.; Reineke, S.; Bredas, J.-L.; Adachi, C.; Friend, R. H., Fast spin-flip enables efficient and stable organic electroluminescence from charge-transfer states. *Nature Photonics* **2020**, *14*, 636–642.
12. Wei, Q.; Imbrasas, P.; Caldera-Cruz, E.; Cao, L.; Fei, N.; Thomas, H.; Scholz, R.; Lenk, S.; Voit, B.; Reineke, S.; Ge, Z., Conjugation-Induced Thermally Activated Delayed Fluorescence: Photophysics of a Carbazole-Benzophenone Monomer-to-Tetramer Molecular Series. *The Journal of Physical Chemistry A* **2021**, *125*, 1345–1354.
13. Zhang, D.; Cai, M.; Zhang, Y.; Zhang, D.; Duan, L., Sterically shielded blue thermally activated delayed fluorescence emitters with improved efficiency and stability. *Materials Horizons* **2016**, *3*, 145–151.
14. Chan, C. Y.; Cui, L. S.; Kim, J. U.; Nakanotani, H.; Adachi, C., Rational Molecular Design for Deep-Blue Thermally Activated Delayed Fluorescence Emitters. *Advanced Functional Materials* **2018**, *28*, 1706023.
15. Bagnich, S. A.; Athanasopoulos, S.; Rudnick, A.; Schroegel, P.; Bauer, I.; Greenham, N. C.; Strohriegel, P.; Köhler, A., Excimer Formation by Steric Twisting in Carbazole and Triphenylamine-Based Host Materials. *The Journal of Physical Chemistry C* **2015**, *119*, 2380–2387.
16. Mordzinski, A.; Sobolewski, A. L.; Levy, D. H., Dual Fluorescence in Aromatic Nitriles: The Role of the Charge-Transfer State. *The Journal of Physical Chemistry A* **1997**, *101*, 8221–8226.
17. Rodella, F.; Bagnich, S.; Duda, E.; Meier, T.; Kahle, J.; Athanasopoulos, S.; Köhler, A.; Strohriegel, P., High Triplet Energy Host Materials for Blue TADF OLEDs—A Tool Box Approach. *Frontiers in Chemistry* **2020**, *8*, 657.
18. Platt, J. R., Classification and Assignments of Ultraviolet Spectra of Conjugated Organic Molecules. *Journal of the Optical Society of America* **1953**, *43*, 252.

19. Zhang, Q.; Komino, T.; Huang, S.; Matsunami, S.; Goushi, K.; Adachi, C., Triplet Exciton Confinement in Green Organic Light-Emitting Diodes Containing Luminescent Charge-Transfer Cu(I) Complexes. *Advanced Functional Materials* **2012**, *22*, 2327-2336.
20. Stavrou, K.; Franca, L. G.; Monkman, A. P., Photophysics of TADF Guest–Host Systems: Introducing the Idea of Hosting Potential. *ACS Applied Electronic Materials* **2020**, *2*, 2868-2881.
21. Hoffmann, S. T.; Bäessler, H.; Koenen, J.-M.; Forster, M.; Scherf, U.; Scheler, E.; Strohriegel, P.; Köhler, A., Spectral diffusion in poly(para-phenylene)-type polymers with different energetic disorder. *Physical Review B* **2010**, *81*, 115103.
22. Baleizão, C.; Berberan-Santos, M. N., Thermally activated delayed fluorescence as a cycling process between excited singlet and triplet states: Application to the fullerenes. *The Journal of Chemical Physics* **2007**, *126*, 204510.
23. Dias, F. B.; Penfold, T. J.; Monkman, A. P., Photophysics of thermally activated delayed fluorescence molecules. *Methods and Applications in Fluorescence* **2017**, *5*, 012001.
24. Noda, H.; Chen, X.-K.; Nakanotani, H.; Hosokai, T.; Miyajima, M.; Notsuka, N.; Kashima, Y.; Brédas, J.-L.; Adachi, C., Critical role of intermediate electronic states for spin-flip processes in charge-transfer-type organic molecules with multiple donors and acceptors. *Nature Materials* **2019**, *18*, 1084-1090.

Chapter 3. How does TADF depend on the nature of the host?

In the previous chapters, I studied TADF-related properties in relation to the extension of the donor group, the linkage position of the donor group to the acceptor and the size of the oligomer. So far, the focus was on understanding the properties of the guest, with no strong emphasis on how the environment affects the TADF-related properties of the guest-host system which can also play a role. I dedicate Chapter 3 to explore how the host material itself affects TADF-related properties of the guest-host systems.

Even though much effort was dedicated to developing new stable blue-emitting materials as well as suitable hosts, efficient and stable blue OLEDs remain a challenge.¹⁻³ While there are several stable and efficient blue emitters reported so far,^{1, 3-4} there is a lack of good host materials for blue-emitting guests. For example, **DPEPO** is still one of the most used host materials for blue emitters despite reported stability issues.^{2, 5} Stavrou *et al.* have recently investigated a variety of host materials, including **DPEPO**, also in terms of TADF of a donor-acceptor type emitter **DMAC-TRZ**.⁶ The group reports that while the intersystem crossing (ISC) rate of the guest is similar using different hosts, this is not the case for the reverse intersystem crossing (RISC) rate.⁶ They find that while the emissive triplet state is LE in nature and does not depend on the host, the singlet state energy strongly depends on the physical properties of the host such as polarity, rigidity and the amount of guest to guest interactions.⁶ Environment-dependent singlet state energy leads to different singlet-triplet gaps of the guest, which is also the reason behind different RISC rates of the guest-host systems.⁶

The host materials investigated by Stavrou *et al.* are all themselves TADF-inactive, *i.e.*, they possess a large singlet-triplet gap.⁶ TADF-active hosts, however, have a bipolar nature, *i.e.*, are of a donor-acceptor type and thus can transport both electrons and holes, reducing the roll-off in the device due to a good charge balance.⁷⁻⁸ Unfortunately, it has been not yet investigated if using a TADF-active host has any improvement in TADF-related properties of the guest-host system from the photophysical

point of view. One could draw the following energy schemes for TADF-active and TADF-inactive host materials as in Figure 3.1.

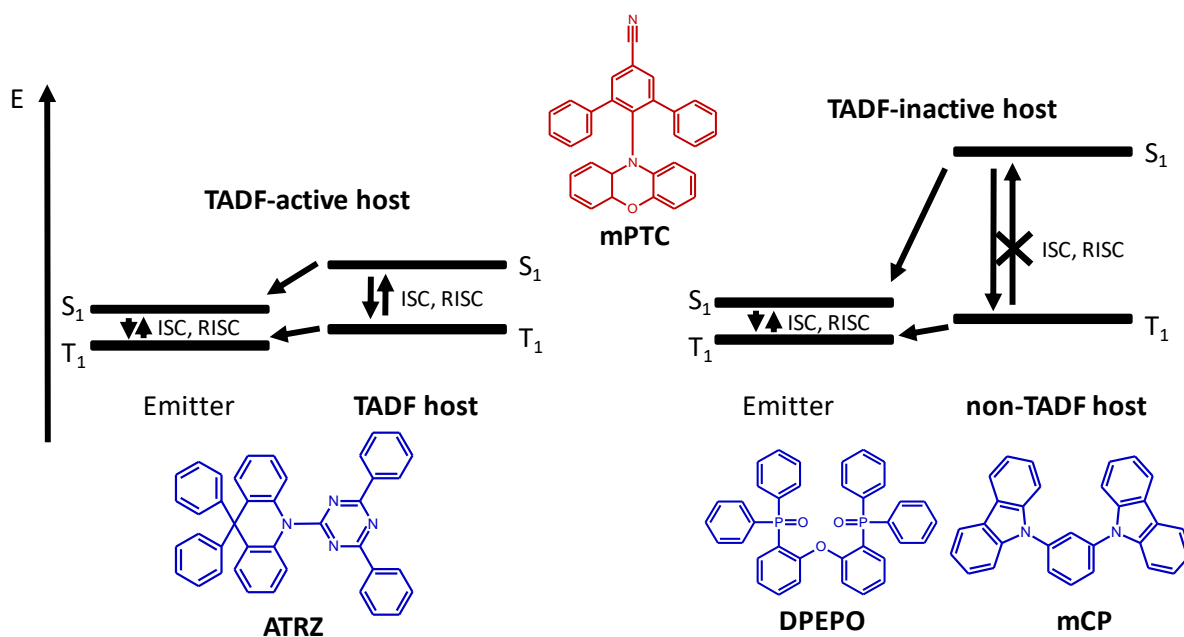


Figure 3.1. Comparison of energy schemes for TADF-active and TADF-inactive host materials in guest-host systems. The molecular structures of the emitter molecule **mPTC** and three host molecules, **ATRZ**, **DPEPO** and **mCP**.

As shown in Figure 3.1, the difference between TADF-active and TADF-inactive hosts is the energy difference between the singlet and triplet states. If this energy difference is low enough (<200 meV), the triplet state of the host has another conversion pathway which is the reverse intersystem crossing to the singlet state of the host. From the singlet state of the host, the energy could then be transferred to the singlet state of the guest. Intuitively, having a TADF-active host reduces the time the triplet exciton spends in the triplet state of the host. This could be especially important when the triplet-triplet energy transfer between host and guest is slow, increasing the chance that the triplet exciton is lost via a non-radiative decay pathway. To investigate if there is any advantage of using a TADF-active host in terms of TADF-related properties, PLQY and EQE of the guest-host system, a TADF-active host **ATRZ**⁹ was compared to large S₁-T₁ gaps and thus TADF-inactive hosts **DPEPO** and **mCP**.¹⁰⁻¹² In principle, **ATRZ** is also a bipolar host while **DPEPO** and **mCP** are unipolar host materials.^{5, 9, 13} Since there is a shortage of high triplet energy host materials that could be used for blue-emitting guests, this chapter

is specifically focused on the high triplet energy host materials. All selected host materials have a high triplet energy of more than 2.9 eV making them suitable for blue guests.⁹⁻¹² A commercial sky-blue emitter, **mPTC**,¹⁴ was selected for testing TADF-active and TADF-inactive hosts. **mPTC** is suitable for the selected host materials in terms of triplet energies and HOMO/LUMO levels for the device preparation. To prevent strong guest to guest interactions leading to concentration quenching and/or triplet-triplet annihilation (TTA),¹⁵ **mPTC** was dispersed in the host materials at the doping concentrations of 5, 10 and 15% by weight both in films and devices.

In this chapter I show that the comparison of TADF-active (**ATRZ**) and TADF-inactive (**DPEPO** and **mCP**) hosts indeed shows differences in photophysics and device performance with **mPTC** as an emitter. Even though the ΔE_{ST} gap of **mPTC** remains similar for both TADF-active and TADF-inactive hosts, TADF of the guest-host system is found to be more pronounced when the TADF-active host **ATRZ** is used, especially at lower doping concentrations. From electroluminescence measurements, I find that devices with a TADF-active host **ATRZ** show a higher efficiency at a lower doping concentration compared to other host materials.

Methods

Materials. Emitter, **mPTC**, was purchased from Lumtec. Hosts, **DPEPO** and **mCP**, were purchased from TCI and Ossila, respectively. The host, **ATRZ**, was synthesized by Francesco Rodella in Prof. Strohriegel's group.⁹

Photophysical and device measurements. For solution measurements, 0.05 mg/mL **mPTC** solution in toluene was prepared. For film measurements, films were spin-casted from a 2.5 mg/mL **mPTC** and host solution. The photophysical measurements were done using similar techniques as introduced earlier in this work (Methods section of the thesis and Chapter 1a). For the steady-state mode, variable excitation wavelengths were used (see figure captions) while for the iCCD measurements samples were excited at 355 nm. OLED devices were fabricated using pre-cleaned indium-tin oxide (ITO) coated glass substrates with ITO thickness of 90 nm. The OLED devices had a circular pixel diameter of 3 mm. While the PEDOT:PSS layer was solution-processed, the remaining layers were thermally evaporated

using a deposition chamber from Kurt J. Lesker at 10^{-7} mbar using the deposition rate of $0.1 - 1.0 \text{ \AA/s}$ for organic layers, 0.15 \AA/s for lithium fluoride (LiF) and 4 \AA/s for aluminium (Al) (full device structure presented later). Device measurements were performed using the characterization platform *Paicos* from Fluxim AG.

Photophysics in solution and film

In Ref⁹, our group studied the photophysics of **ATRZ** in solution and reported the singlet-triplet gap of 0.18 eV which is promising for TADF. However, no TADF-related data of **ATRZ** was reported in Ref⁹. Therefore, the photophysical study is started with an investigation of whether **ATRZ** actually shows TADF (Figure 3.2). For this reason, **ATRZ** was dispersed in UGH-3 at 10 wt% and the corresponding film was measured at 77 K to estimate the ΔE_{ST} gap. UGH-3 (1,3-bis(triphenylsilyl)benzene) was selected as a host for **ATRZ** because of sufficiently high triplet energy (3.50 eV).¹⁶ Next, the transient decay profile was measured at 300 K to confirm the presence of the delayed emission.

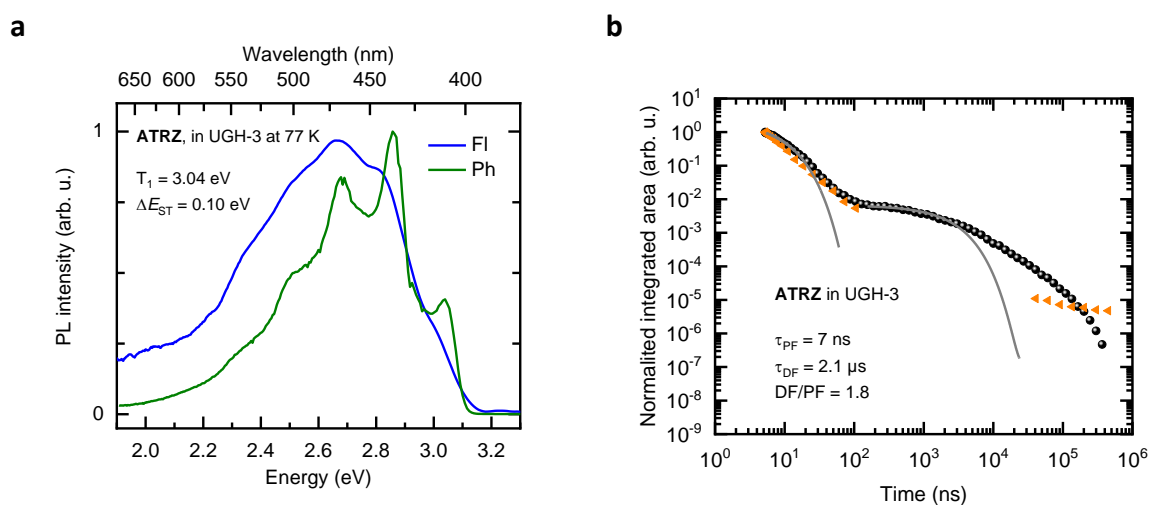


Figure 3.2. (a) Prompt (delay 5 ns, gate 10 ns) and delayed (delay 50 ms, gate 100 ms) emission spectra of **ATRZ** in UGH-3 (10 wt%) at 77 K, $\lambda_{\text{exc}} = 300 \text{ nm}$; (b) transient photoluminescence decay profile of **ATRZ** in UGH-3 (10 wt%) at 300 K (black) and 77 K (orange), $\lambda_{\text{exc}} = 355 \text{ nm}$. The prompt (PF) and delayed (DF) emission parts are fitted using a mono-exponential fit (grey lines). τ represents the lifetime while DF/PF is the ratio between the areas defined by the delayed and prompt emission.

Figure 3.2 shows the low-temperature photoluminescence spectra and the photoluminescence transient decay of **ATRZ** dispersed in UGH-3. The steady-state emission at 77 K (not shown), consisting of fluorescence and delayed emission, was found to overlap with the phosphorescence spectrum of

ATRZ, implying a strong intersystem crossing in **ATRZ**. The fluorescence spectrum could only be resolved in the time-resolved mode, with a time delay of 5 ns. The structured delayed emission at 77 K with a 50 ms delay is assigned to phosphorescence. From the onset of fluorescence and phosphorescence spectra, the singlet-triplet gap can be estimated to be 0.10 eV, suitable for TADF. The PL transient decay profile shown in Figure 3.2 demonstrates two regimes, a prompt emission lasting until around 80 ns and the emission taking place in the microsecond range. The intensity of the delayed part increases with temperature, therefore, the origin of the delayed part is ascribed to TADF which is also consistent with a reasonably small ΔE_{ST} gap of 0.10 eV. This implies that **ATRZ** is indeed TADF-active. The other two hosts, **DPEPO** and **mCP**, are known to have very large ΔE_{ST} gaps (>500 meV),¹⁰⁻¹² making the triplet upconversion to the singlet state using the ambient energy at room temperature impossible.

Next, before dispersing **mPTC** in different hosts, the monomolecular properties of **mPTC** itself are evaluated. The absorption and room temperature steady-state emission of **mPTC** are measured in dilute toluene solution such as to avoid significant guest to guest interactions (Figure 3.3).

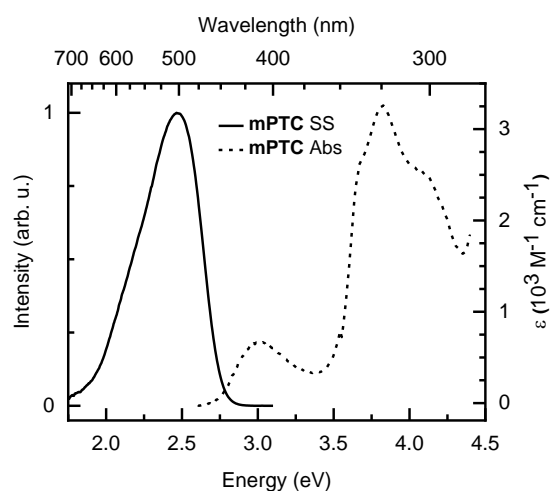


Figure 3.3. Absorption and steady-state (SS) emission spectra of **mPTC** in toluene (0.05 mg/mL) at 300 K. $\lambda_{exc} = 300$ nm.

Figure 3.3 presents the absorption (UV-vis) and the steady-state PL emission spectra of **mPTC**. Starting from the high energy bands, the absorption peak at around 3.8 eV can be ascribed to the phenoxazine

unit,¹⁷ since the absorption of benzonitrile occurs at higher energies (>4.3 eV).¹⁸ There is also a low-intensity absorption peak at around 3.0 eV which, based on the broad and unstructured shape, can be assigned to the charge-transfer transition between the donor and acceptor unit. The maximum of the steady-state emission spectrum at 300 K is located at 2.46 eV. The shape of the steady-state emission spectrum of **mPTC** at room temperature is broad with no pronounced structure. Complemented with quantum chemical calculations by Chen *et al.*,¹⁴ this allows to identify the PL emission at 300 K to correspond to a charge-transfer transition in the molecule.

Next, to compare the photophysical properties of TADF-active and TADF-inactive host materials, **mPTC** was dispersed in **ATRZ**, **DPEPO** and **mCP** at 5, 10 and 15 wt% doping concentrations. The steady-state emission spectra and the photoluminescence transient decay at 300 K were studied under identical conditions for all films (Figure 3.4).

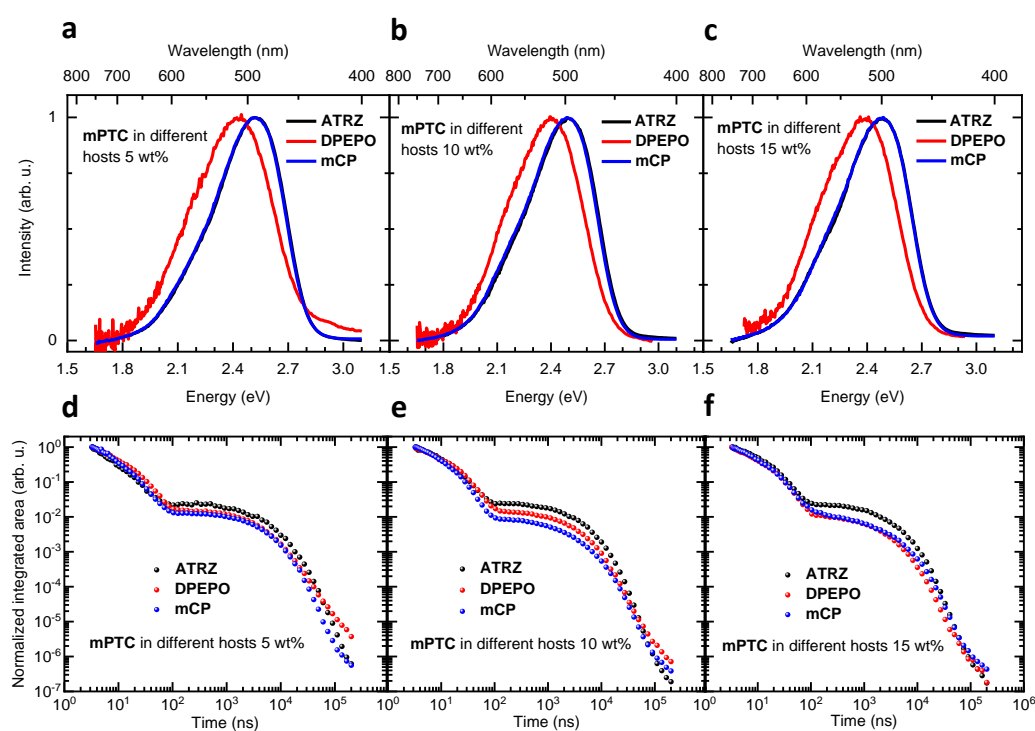


Figure 3.4. **a-c** The steady-state emission spectra of **mPTC** doped films in **ATRZ**, **DPEPO** and **mCP** at 5, 10 and 15% doping concentrations by weight at 300 K, $\lambda_{\text{exc}} = 300$ nm. **d-e** The transient PL decay of **mPTC** doped films in **ATRZ**, **DPEPO** and **mCP** at 300 K, $\lambda_{\text{exc}} = 355$ nm.

Figure 3.4 a-c presents the steady-state emission spectra of **mPTC** doped thin films at 300 K. The peak positions of the steady-state emission spectra are 2.52, 2.49 and 2.48 eV at 5, 10 and 15 wt% doping concentrations for films with **ATRZ** and **mCP** as a host, respectively, and 2.43, 2.40 and 2.38 eV at 5, 10 and 15 wt% doping concentrations for films with **DPEPO**, respectively. The full width at half maximum (FWHM) is 0.45 eV for films with **ATRZ** and **mCP** as a host, respectively, and 0.50 eV for films with **DPEPO**. The PL steady-state emission spectra of **mPTC** doped films in **DPEPO** are redshifted by around 0.10 eV compared to **ATRZ** and **mCP**. **DPEPO** is known to be a polar host matrix,¹⁹ thus the redshift of the steady-state emission of **mPTC** films in **DPEPO** can be attributed to the stabilization of the excited state energy due to a polar environment.²⁰ In addition to the redshift when **DPEPO** is used as a host, the FWHM of the films with **DPEPO** is broader by 0.05 eV, which I also assign to the polar character of **DPEPO**. The redshift of the PL emission for films with **mCP** as a host is absent, which is consistent to lower polarity of **mCP** as compared to **DPEPO**.²¹ Since **ATRZ** as a host shows similar effects on the PL emission as **mCP**, this implies that the polarity of **ATRZ** and **mCP** is comparable. Figure 3.4 d-f presents the transient PL decay profile of **mPTC** doped films at 300 K. The transient PL decay in the microsecond range has a significant contribution to the total emission (Table 3.1). To confirm the TADF origin of the delayed emission, the 5 wt% **mPTC** films were next measured at different temperatures (Figure 3.5).

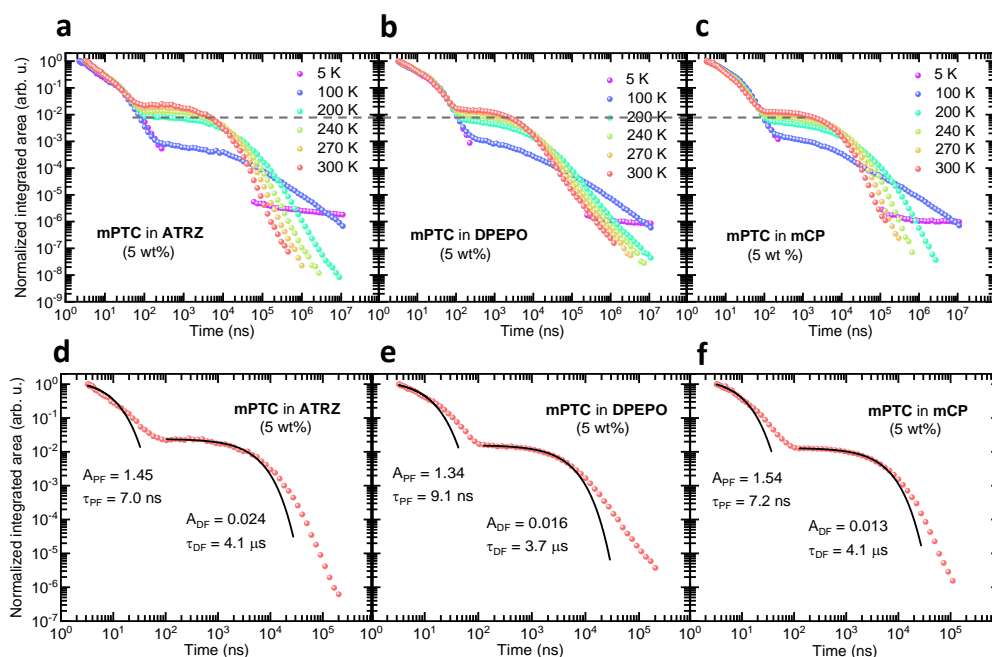


Figure 3.5. **a-c** Transient photoluminescence decay of 5 wt% **mPTC** films in **ATRZ**, **DPEPO** and **mCP** at multiple temperatures; **d-f** fitting example of 5 wt% **mPTC** films. $\lambda_{exc} = 355$ nm. A is a pre-exponential factor while τ is the lifetime of the prompt (PF) or delayed emission (DF).

All samples demonstrate an increase in the intensity of the delayed emission with increasing temperature, allowing to assign the origin of the delayed emission to TADF. Noteworthy is that for films with **DPEPO** the decay is slightly more extended at long delay times (μ s range) compared to films with **ATRZ** and **mCP** as a host. In general, the extended delayed emission decay profile in films can be associated with a lack of freedom for the guest molecules to reorganize and achieve an equilibrium dihedral angle between the donor and acceptor units, leading to a distribution of molecular conformations with different ΔE_{ST} gaps and RISC rates.⁶ The presence of this distribution of molecular conformations leads to a deviation from a mono-exponential behaviour in the delayed part of the transient PL decay and depends on the properties of the host such as polarity and rigidity.⁶ For **mPTC** in **DPEPO**, I ascribe a more extended delayed emission decay profile for the guest-host system to a higher polarity of **DPEPO**, as it can decrease the ability for the **mPTC** molecules to freely reorganize and achieve an equilibrium dihedral angle. Both the prompt and the delayed emission profiles can be approximated using a mono-exponential fit as shown in Figure 3.5. A mono-exponential fit for the delayed part is estimated to account for more than 80% of the delayed emission, therefore, the

calculation of the average lifetime is not required. To estimate the ΔE_{ST} values of **mPTC** films in different hosts, the prompt emission spectra and the spectra with a delay of 10 ms are measured at 5 K (Figure 3.6). At such low temperatures as 5 K, any TADF emission should be suppressed, allowing to ascribe the emission with a delay of 10 ms at 5 K to phosphorescence.

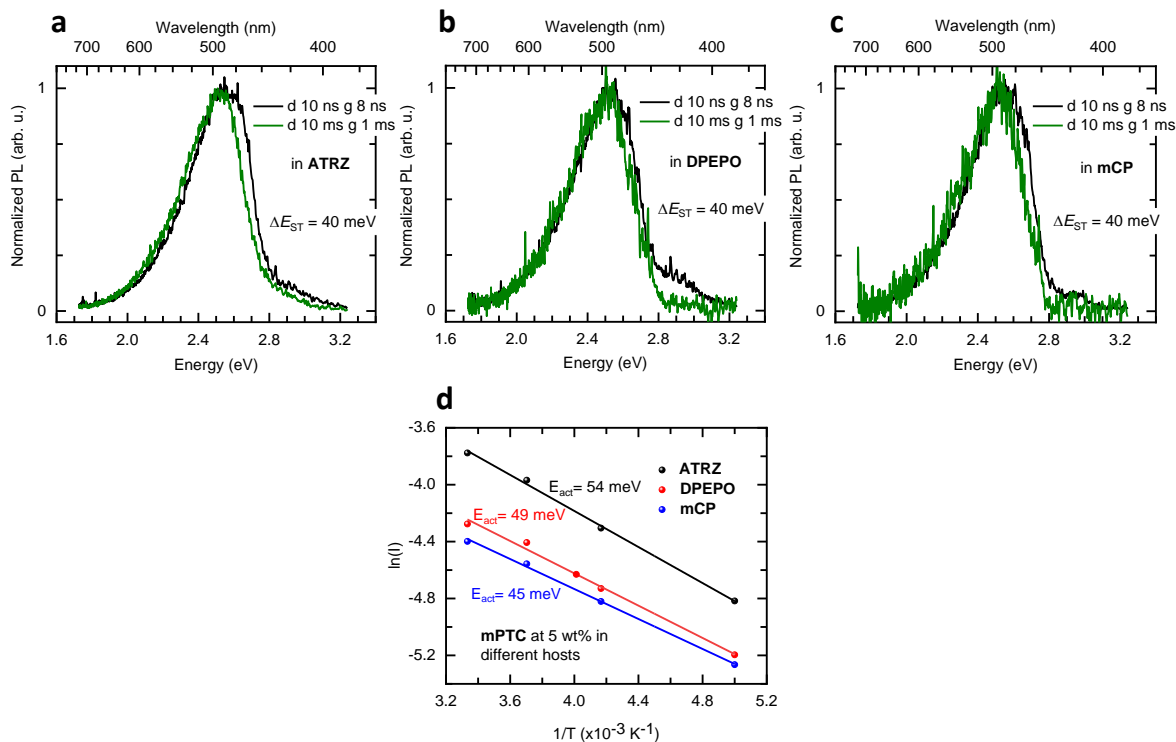


Figure 3.6. (a)-(c) Time-resolved photoluminescence emission spectra of 5 wt% **mPTC** films in **ATRZ**, **DPEPO** and **ATRZ** at 5 K, where d is the delay time and g is the gating time. $\lambda_{exc} = 355$ nm, (d) the plateau of the delayed emission intensity versus temperature, allowing to extract the activation energy for 5 wt% **mPTC** film in different hosts. The activation energy was determined using $I_{DF} = Ae^{\frac{-E_{act}}{k_B T}}$, where I_{DF} is the plateau of the delayed emission intensity (Figure 3.5), A is a pre-exponential factor and k_B is Boltzmann's constant.

For all films, the ΔE_{ST} values, as estimated from the prompt emission and phosphorescence onsets at 5 K, are in the range of 40 meV, small enough for TADF. To get a more accurate estimation of the singlet-triplet energetic separation, the activation energies are also calculated for the 5 wt% **mPTC** films as shown in Figure 3.6. Plotting the plateau positions of the delayed emission against different temperatures allows estimating the activation energy. The activation energies are in the range of 50 meV for all samples, consistent with the ΔE_{ST} values estimated from the onset positions at 5 K. The

photophysical parameters extracted from the transient PL analysis as well as the results of the PLQY measurements in oxygen-free conditions are summarized in Table 3.1 and Table 3.2 below.

Table 3.1. Summary of photophysical properties of **mPTC** doped films.

Host	mPTC (%)	$\tau_p^{(a)}$ (ns)	$\tau_d^{(b)}$ (μ s)	$\Phi_{PF} + \Phi_{DF}^{(c)}$ (%)	$\Phi_{DF} / \Phi_{PF}^{(d)}$	$\Phi_{PF}^{(e)}$ (%)	$\Phi_{DF}^{(f)}$ (%)
ATRZ	5	7.0	4.1	52	11.6	4.1	47.9
ATRZ	10	10.6	3.1	47	6.6	6.2	41.2
ATRZ	15	11.4	2.5	43	4.8	7.5	35.8
DPEPO	5	9.1	3.7	82	5.9	11.9	70.1
DPEPO	10	10.4	2.7	70	3.5	15.6	54.7
DPEPO	15	8.7	1.9	68	2.2	21.5	46.4
mCP	5	7.2	4.1	68	5.4	10.6	57.8
mCP	10	8.1	2.3	61	2.2	19.1	42.3
mCP	15	9.4	1.8	61	2.5	17.5	43.4

(a) Lifetime of prompt emission extracted using a mono-exponential fitting.

(b) Lifetime of delayed emission extracted using a mono-exponential fitting.

(c) Total PLQY consisting of prompt emission yield and delayed emission yield. $\lambda_{exc} = 315$ nm.

(d) Ratio of delayed emission versus prompt emission yield calculated comparing the areas of the delayed and prompt part in the transient decay profile.

(e) Yield of prompt emission.

(f) Yield of delayed emission.

Table 3.1 summarizes the prompt and delayed emission lifetimes and yields for **mPTC** films in different hosts. While the prompt emission lifetime does not have any particular tendency with increasing doping concentration, the delayed emission lifetime decreases with increasing doping concentration for **mPTC** films in all hosts. Shorter delayed emission lifetimes and also decreased PLQY values at higher doping concentrations are associated with concentration quenching.²² The highest PLQY values (68-82%) are found when **DPEPO** is used as a host while the lowest PLQY values (43-52%) are observed when **ATRZ** is used as a host. I attribute lower PLQY values of the guest-host system with **ATRZ** as a host compared to when **DPEPO** or **mCP** is used as a host to a strong intersystem crossing in **ATRZ** itself (see also the discussion below Figure 3.2), leading to a higher triplet state involvement in the guest-host system with **ATRZ** as a host and thus more energy loss. Next, the relative prompt and delayed emission yields are evaluated by comparing the areas under the transient decay profile of prompt and delayed emission to the total emission. The most significant difference between films with **ATRZ** and

other hosts is almost a three times smaller prompt emission yield. This can be explained by the amount of overlap between the PL emission of the host and the absorption of **mPTC**, essentially defining the efficiency of the singlet-singlet energy transfer between host and guest. To study the overlap of the PL emission of the hosts and the absorption of the guest, the PL emission of hosts was compared to the absorption of **mPTC** (Figure 3.7).

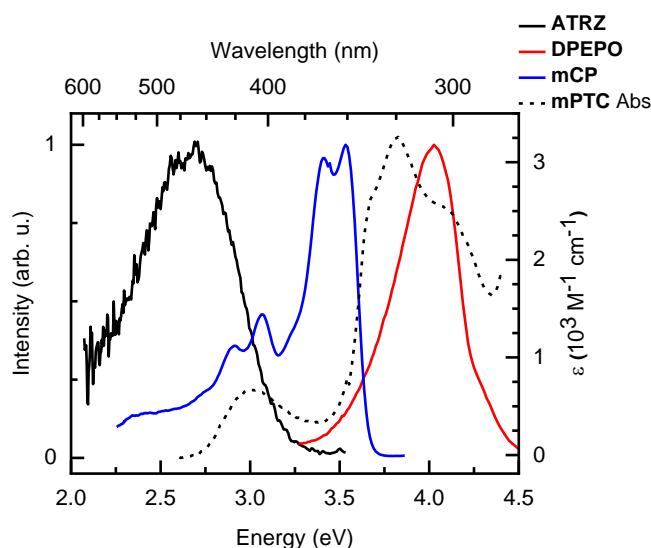


Figure 3.7. The steady-state emission of **ATRZ**, **DPEPO** and **mCP** in UGH-3 (10 wt%) and the absorption of **mPTC** in toluene at 300 K. The samples with **ATRZ** and **mCP** were excited at 300 nm while the sample with **DPEPO** was excited at 250 nm.

For **ATRZ**, with the PL emission peak at around 2.6 eV, only the high energy tail of the PL emission of **ATRZ** overlaps with the absorption of **mPTC** which has the lowest absorption peak at around 3.0 eV (Figure 3.7). In the case of **DPEPO** and **mCP**, the PL emission peaks are more in the blue range, with values of around 4.0 eV and 3.5 eV, respectively (Figure 3.7), allowing for a stronger overlap with the absorption of **mPTC**. To evaluate the overlap between emission of hosts and absorption of **mPTC**, the spectral overlap integral $(J = \int f_D(\lambda)\varepsilon_A(\lambda)\lambda^4 d\lambda)$ was calculated, where f_D corresponds to the normalized host emission spectrum, and ε_A is the molar extinction coefficient of the emitter.²³ The spectral overlap integral was calculated to correspond to the ratio of 1:2:5.5 for **ATRZ**, **mCP** and **DPEPO**, respectively. This implies that the lowest overlap between the PL emission of the host and absorption of **mPTC** is for **ATRZ** and the highest for **DPEPO**, largely consistent with the trends of prompt emission

yields of **mPTC** films in different hosts (Table 3.1). Next, TADF-related parameters are assessed using the approach by Dias *et al.*²⁴ and tabulated in Table 3.2.

Table 3.2. Summary of rate constants of **mPTC** doped films.

Host	mPTC (%)	$k_r^{(a)}$ ($\times 10^7 \text{ s}^{-1}$)	$\Phi_{\text{ISC}}^{(b)}$	$k_{\text{ISC}}^{(c)}$ ($\times 10^7 \text{ s}^{-1}$)	$k_{\text{IC}}^{(d)}$ ($\times 10^6 \text{ s}^{-1}$)	$k_{\text{RISC}}^{(e)}$ ($\times 10^6 \text{ s}^{-1}$)
ATRZ	5	0.6	0.92	13.2	5.4	3.1
ATRZ	10	0.6	0.87	8.2	6.6	2.5
ATRZ	15	0.7	0.83	7.3	8.6	2.3
DPEPO	5	1.3	0.86	9.4	2.9	1.9
DPEPO	10	1.5	0.78	7.5	6.4	1.7
DPEPO	15	2.4	0.69	7.9	11.5	1.7
mCP	5	1.5	0.84	11.7	6.9	1.6
mCP	10	2.4	0.69	8.5	15.0	1.4
mCP	15	1.9	0.71	7.6	11.9	1.9

(a) Rate constant for radiative decay.

(b) Intersystem crossing yield.

(c) Rate constant for intersystem crossing.

(d) Rate constant for internal conversion.

(e) Rate constant for reverse intersystem crossing.

Table 3.2 summarizes the common parameters used to compare rate constants in TADF materials. When comparing three different host materials, **mPTC** films in **ATRZ** show the lowest radiative decay rate, k_r , yet the intersystem crossing efficiency, Φ_{ISC} , is the highest compared to other hosts. The intersystem crossing rate, k_{ISC} , and the internal conversion rate, k_{IC} , show a similar trend and are similar for all host materials, implying that the non-radiative losses are comparable for all investigated guest-host systems. The reverse intersystem crossing rate, k_{RISC} , is highest for **mPTC** films with **ATRZ** as a host, especially at a 5 wt% doping concentration, where the RISC rate is around two times higher compared to other host materials. Since the ΔE_{ST} gaps and the activation energies are independent of the host, a higher RISC rate in the **mPTC** films with **ATRZ** as a host is an unexpected result. I attribute a higher RISC rate for films with **ATRZ** as a host to a poor singlet-singlet energy transfer between host and guest, increasing the amount of energy stored in the triplet state of **ATRZ** itself via intersystem crossing (see also Figure 3.7). Since the singlet-singlet energy transfer is not very effective, the triplet excitons from **ATRZ** can then be transferred to the triplet state of **mPTC**, resulting in a higher TADF contribution of

the guest-host system as a whole. It is now not clear how using a TADF-active **ATRZ** and non-TADF-active **DPEPO** and **mCP** as hosts reflect on the device performance, so the discussion is continued after the presentation of the device data.

Organic light-emitting diodes

To evaluate the performance of **mPTC** in different host materials, I performed the OLED study. The device structure was kept simple and similar for all host materials: ITO/PEDOT:PSS (40 nm)/TAPC (15 nm)/5, 10, 15 wt% **mPTC:ATRZ**, **DPEPO** and **mCP** (25 nm)/TPBi (40 nm)/LiF (1.5 nm)/Al (100 nm), where indium tin oxide (ITO) is the anode, PEDOT:PSS and 1,1-Bis[(di-4-tolylamino)phenyl]cyclohexane (TAPC) acts as the hole injection materials, **mPTC** is the emitter, **ATRZ**, **DPEPO** and **mCP** are the hosts, 2,2',2''-(1,3,5-Benzinetriyl)-tris(1-phenyl-1-H-benzimidazole) (TPBi) acts as the electron-transporting material and LiF modifies the work function of the aluminum cathode. The evaporation process was performed with the help of Dr. Julian Kahle. I then characterized the fabricated OLEDs in terms of electroluminescence (EL) emission spectra, external quantum efficiency (EQE) and also current-voltage-luminance (IVL) characteristics (Figure 3.8).

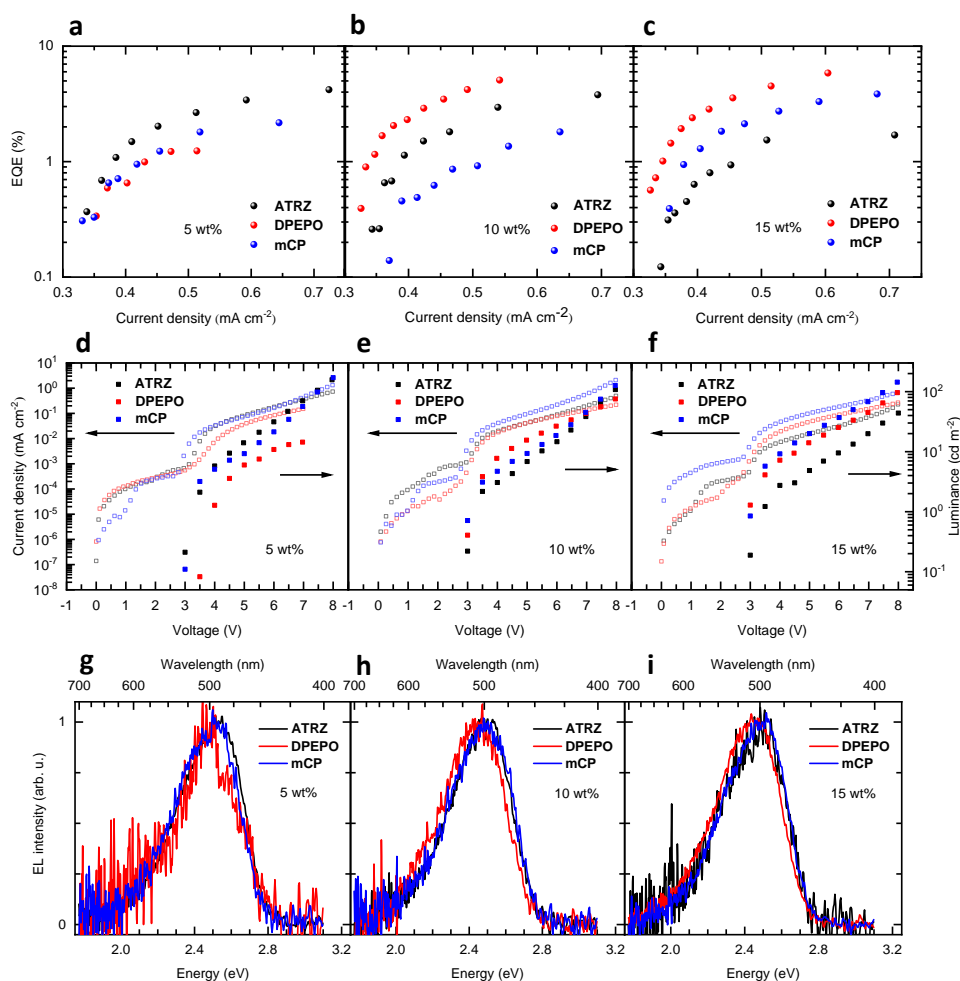


Figure 3.8. Characterization of *mPTC*-based OLEDs using **ATRZ**, **DPEPO** and **mCP** as host materials at 5, 10 and 15 wt% doping concentrations: **a-c** EQE versus current density; **d-f** IVL characteristics; **g-i** EL emission spectra.

The EL emission spectra are consistent with the photoluminescence spectra presented earlier. As can be seen from the current-voltage-luminance (IVL) characteristics, the onset voltage for all devices is around 3 V. The efficiency for all devices was compared at the same current density, *i.e.*, 0.5 mA cm^{-2} . From Figure 3.8, at 5 wt% doping concentration, the best performing device is using **ATRZ** as a host, with an EQE of 2.7% compared to 1.2% and 1.8% for devices with **DPEPO** and **mCP** as a host, respectively. At 15 wt% doping concentration, the best performing device is with **DPEPO** as a host, with an EQE of 4.5% compared to 1.5% and 2.6% for devices with **ATRZ** and **mCP** as a host, respectively. In short, *mPTC* devices with **ATRZ** as a host perform best at a low doping concentration while devices with **DPEPO** and **mCP** show better performance at higher doping concentrations.

Discussion

Comparison between photophysical and device data shows that the PLQY trend (highest PLQY with **DPEPO**, lowest with **ATRZ**) only matches with the EQE values at larger doping concentrations. Even though **mPTC** films with **ATRZ** as a host have the lowest PLQY in films at 5 wt% doping, the devices with **ATRZ** as a host show the highest efficiency at 5 wt% doping. This disagreement between the PLQY and EQE at a 5 wt% **mPTC** doping concentration can be explained considering the following two effects. First, as already discussed in the photophysics section, films with **ATRZ** show a more pronounced TADF at lower **mPTC** doping concentrations compared to other hosts. Second, different electronic nature of the hosts needs to be considered. While **ATRZ** is a bipolar host material, **DPEPO** and **mCP** are unipolar host materials, allowing for efficient transport for one type of charge carrier (electron for **DPEPO** and hole for **mCP**).²⁵⁻²⁶ This means that to increase the amount of minority charge carriers and to achieve a better balance between electrons and holes, larger doping concentrations are needed. For this reason, devices with **DPEPO** and **mCP** are not so efficient at low doping concentrations. For **ATRZ**, the bipolar nature should allow for a more balanced transportation of electrons and holes. At low doping concentrations, the charge carrier transport is mostly occurring through the host since there are not enough guest molecules for efficient charge hopping. At higher doping concentrations, more transport will be occurring through the guest having a detrimental effect on the charge transport through the host. Different modes of transport cause imbalances between holes and electrons leading to the loss of efficiency at higher doping concentrations when **ATRZ** is used as a host.

In principle, due to a better photophysical and device performance at lower doping concentrations, **ATRZ** could be attractive for systems where only low doping concentrations are acceptable, for example, for TADF emitters based on multi-resonant structures that are suffering from severe concentration quenching due to their rigid and planar nature (also discussed in the next chapter).²⁷⁻²⁸

Summary

In this chapter, the effects of the host material were investigated on TADF of the guest-host system. Three host materials were selected for investigation. TADF-active **ATRZ** and TADF-inactive **DPEPO** and **mCP** were investigated as host materials to find out if using a TADF-active host has any advantages for the guest-host system both in terms of photophysics and device performance. From the photophysical measurements, it was found that **mPTC** films with **ATRZ** as a host show the lowest PLQY values compared to other hosts but have strongest TADF, especially at lower doping concentrations. It was also observed that **DPEPO** as a host causes a small redshift of the PL emission and also extends the transient PL decay at longer delay times which can be ascribed to a higher polarity of **DPEPO** compared to **ATRZ** and **mCP**. Combining photophysical measurements with electroluminescence measurements, it was discovered that opposite to lower PLQY values in films, a TADF-active host **ATRZ** actually shows higher EQE values in devices with **mPTC** at lower doping concentrations compared to TADF-inactive hosts **DPEPO** and **mCP**. This was attributed to the stronger TADF of the guest-host system when **ATRZ** is used as a host and also the bipolar electronic nature of **ATRZ**.

References of Chapter 3

1. Cai, X.; Su, S.-J., Marching Toward Highly Efficient, Pure-Blue, and Stable Thermally Activated Delayed Fluorescent Organic Light-Emitting Diodes. *Advanced Functional Materials* **2018**, *28*, 1802558.
2. Chatterjee, T.; Wong, K.-T., Perspective on Host Materials for Thermally Activated Delayed Fluorescence Organic Light Emitting Diodes. *Advanced Optical Materials* **2019**, *7*, 1800565.
3. Wong, M. Y.; Zysman-Colman, E., Purely Organic Thermally Activated Delayed Fluorescence Materials for Organic Light-Emitting Diodes. *Advanced Materials* **2017**, *29*, 1605444.
4. Bui, T.-T.; Goubard, F.; Ibrahim-Ouali, M.; Gimes, D.; Dumur, F., Thermally Activated Delayed Fluorescence Emitters for Deep Blue Organic Light Emitting Diodes: A Review of Recent Advances. *Applied Sciences* **2018**, *8*, 494.
5. Ihn, S.-G.; Lee, N.; Jeon, S. O.; Sim, M.; Kang, H.; Jung, Y.; Huh, D. H.; Son, Y. M.; Lee, S. Y.; Numata, M.; Miyazaki, H.; Gómez-Bombarelli, R.; Aguilera-Iparraguirre, J.; Hirzel, T.; Aspuru-Guzik, A.; Kim, S.; Lee, S., An Alternative Host Material for Long-Lifespan Blue Organic Light-Emitting Diodes Using Thermally Activated Delayed Fluorescence. *Advanced Science* **2017**, *4*, 1600502.
6. Stavrou, K.; Franca, L. G.; Monkman, A. P., Photophysics of TADF Guest–Host Systems: Introducing the Idea of Hosting Potential. *ACS Applied Electronic Materials* **2020**, *2*, 2868-2881.
7. Zhang, D.; Zhao, C.; Zhang, Y.; Song, X.; Wei, P.; Cai, M.; Duan, L., Highly Efficient Full-Color Thermally Activated Delayed Fluorescent Organic Light-Emitting Diodes: Extremely Low Efficiency Roll-Off Utilizing a Host with Small Singlet–Triplet Splitting. *ACS Applied Materials & Interfaces* **2017**, *9*, 4769-4777.
8. Lin, C.-C.; Huang, M.-J.; Chiu, M.-J.; Huang, M.-P.; Chang, C.-C.; Liao, C.-Y.; Chiang, K.-M.; Shiau, Y.-J.; Chou, T.-Y.; Chu, L.-K.; Lin, H.-W.; Cheng, C.-H., Molecular Design of Highly Efficient Thermally Activated Delayed Fluorescence Hosts for Blue Phosphorescent and Fluorescent Organic Light-Emitting Diodes. *Chemistry of Materials* **2017**, *29*, 1527-1537.
9. Rodella, F.; Bagnich, S.; Duda, E.; Meier, T.; Kahle, J.; Athanasopoulos, S.; Köhler, A.; Strohriegel, P., High Triplet Energy Host Materials for Blue TADF OLEDs—A Tool Box Approach. *Frontiers in Chemistry* **2020**, *8*, 657.
10. Han, C.; Zhao, Y.; Xu, H.; Chen, J.; Deng, Z.; Ma, D.; Li, Q.; Yan, P., A Simple Phosphine-Oxide Host with a Multi-insulating Structure: High Triplet Energy Level for Efficient Blue Electrophosphorescence. *Chemistry - A European Journal* **2011**, *17*, 5800-5803.
11. Mai, V. T. N.; Ahmad, V.; Mamada, M.; Fukunaga, T.; Shukla, A.; Sobus, J.; Krishnan, G.; Moore, E. G.; Andersson, G. G.; Adachi, C.; Namdas, E. B.; Lo, S.-C., Solid cyclooctatetraene-based triplet quencher demonstrating excellent suppression of singlet–triplet annihilation in optical and electrical excitation. *Nature Communications* **2020**, *11*, 5623.
12. Fan, C.; Wei, Y.; Ding, D.; Xu, H., Linkage engineering in hosts for dramatic efficiency enhancement of blue phosphorescent organic light-emitting diodes. *Optics Express* **2015**, *23*, 12887.
13. Cheng, T.-Y.; Lee, J.-H.; Chen, C.-H.; Chen, P.-H.; Wang, P.-S.; Lin, C.-E.; Lin, B.-Y.; Lan, Y.-H.; Hsieh, Y.-H.; Huang, J.-J.; Lu, H.-F.; Chao, I.; Leung, M.-k.; Chiu, T.-L.; Lin, C.-F., Carrier Transport and Recombination Mechanism in Blue Phosphorescent Organic Light-Emitting Diode with Hosts Consisting of Cabazole- and Triazole-Moiety. *Scientific Reports* **2019**, *9*, 3654.
14. Chen, D.-Y.; Liu, W.; Zheng, C.-J.; Wang, K.; Li, F.; Tao, S. L.; Ou, X.-M.; Zhang, X.-H., Isomeric Thermally Activated Delayed Fluorescence Emitters for Color Purity-Improved Emission in Organic Light-Emitting Devices. *ACS Applied Materials & Interfaces* **2016**, *8*, 16791-16798.
15. Moon, J. S.; Ahn, D. H.; Kim, S. W.; Lee, S. Y.; Lee, J. Y.; Kwon, J. H., δ -Carboline-based bipolar host materials for deep blue thermally activated delayed fluorescence OLEDs with high efficiency and low roll-off characteristic. *RSC Advances* **2018**, *8*, 17025-17033.
16. Wang, Y.; Yun, J. H.; Wang, L.; Lee, J. Y., High Triplet Energy Hosts for Blue Organic Light-Emitting Diodes. *Advanced Functional Materials* **2020**, *31*, 2008332.
17. Mantsch, H. H.; Dehler, J., π -Electronic structure and reactivity of phenoxazine (1), phenothiazine (2), and phenoxthiin (3). *Canadian Journal of Chemistry* **1969**, *47*, 3173-3178.

18. Hirt, R. C.; Howe, J. P., The Ultraviolet Absorption Spectrum of Benzonitrile Vapor. *The Journal of Chemical Physics* **1948**, *16*, 480-485.
19. dos Santos, P. L.; Ward, J. S.; Bryce, M. R.; Monkman, A. P., Using Guest–Host Interactions To Optimize the Efficiency of TADF OLEDs. *The Journal of Physical Chemistry Letters* **2016**, *7*, 3341-3346.
20. Xie, G.; Chen, D.; Li, X.; Cai, X.; Li, Y.; Chen, D.; Liu, K.; Zhang, Q.; Cao, Y.; Su, S.-J., Polarity-Tunable Host Materials and Their Applications in Thermally Activated Delayed Fluorescence Organic Light-Emitting Diodes. *ACS Applied Materials & Interfaces* **2016**, *8*, 27920-27930.
21. Kumar; Pereira, Effect of the Host on Deep-Blue Organic Light-Emitting Diodes Based on a TADF Emitter for Roll-Off Suppressing. *Nanomaterials* **2019**, *9*, 1307.
22. Kim, H. S.; Park, S.-R.; Suh, M. C., Concentration Quenching Behavior of Thermally Activated Delayed Fluorescence in a Solid Film. *The Journal of Physical Chemistry C* **2017**, *121*, 13986-13997.
23. Köhler, A.; Bässler, H., *Electronic Processes in Organic Semiconductors: An Introduction*. 2015.
24. Dias, F. B.; Penfold, T. J.; Monkman, A. P., Photophysics of thermally activated delayed fluorescence molecules. *Methods and Applications in Fluorescence* **2017**, *5*, 012001.
25. Zhang, J.; Ding, D.; Wei, Y.; Xu, H., Extremely condensing triplet states of DPEPO-type hosts through constitutional isomerization for high-efficiency deep-blue thermally activated delayed fluorescence diodes. *Chemical Science* **2016**, *7*, 2870-2882.
26. Jou, J.-H.; Wang, W.-B.; Chen, S.-Z.; Shyue, J.-J.; Hsu, M.-F.; Lin, C.-W.; Shen, S.-M.; Wang, C.-J.; Liu, C.-P.; Chen, C.-T.; Wu, M.-F.; Liu, S.-W., High-efficiency blue organic light-emitting diodes using a 3,5-di(9H-carbazol-9-yl)tetraphenylsilane host via a solution-process. *Journal of Materials Chemistry* **2010**, *20*, 8411.
27. Madayanad Suresh, S.; Hall, D.; Beljonne, D.; Olivier, Y.; Zysman-Colman, E., Multiresonant Thermally Activated Delayed Fluorescence Emitters Based on Heteroatom-Doped Nanographenes: Recent Advances and Prospects for Organic Light-Emitting Diodes. *Advanced Functional Materials* **2020**, 1908677.
28. Hall, D.; Suresh, S. M.; dos Santos, P. L.; Duda, E.; Bagnich, S.; Pershin, A.; Rajamalli, P.; Cordes, D. B.; Slawin, A. M. Z.; Beljonne, D.; Köhler, A.; Samuel, I. D. W.; Olivier, Y.; Zysman-Colman, E., Improving Processability and Efficiency of Resonant TADF Emitters: A Design Strategy. *Advanced Optical Materials* **2019**, *8*, 1901627.

Chapter 4. TADF based on multi-resonant structures

Part of the work investigated in this chapter has been published and can be found online under Ref¹ and Ref².

Conventional donor-acceptor type TADF emitters usually have a dominant charge-transfer character due to a significant separation of hole and electron densities. The spectra of conventional donor-acceptor type emitters are usually broad, with a full width at half maximum (FWHM) ranging up to 100 nm, making it challenging to achieve a good colour purity in devices.³ In 2015, a new molecular design for TADF emitters (currently known as “resonance TADF”) was presented by Hatakeyama *et al.*⁴ The first reported TADF emitter based on a multi-resonant structure consists of the electron-donating oxygen and electron-withdrawing boron moieties.⁴ This emitter was reported to emit in the deep-blue range (399 nm), have a sufficiently small singlet-triplet gap (0.15 eV) together with a high PLQY (73%) and an attractive FWHM (40 nm).⁴ Later works by multiple groups featured more emitters based on resonance TADF that allowed not only for a sufficiently small ΔE_{ST} and a high efficiency but also a narrow FWHM (<40 nm).⁵⁻¹² Thanks to quantum chemical calculations, it was demonstrated that a small ΔE_{ST} and high PLOY in selected resonance TADF molecules is achieved via a short-range charge transfer and delocalized hole and electron wavefunctions, providing a small exchange interaction yet maintaining a sufficient radiative decay rate.³

Even though resonance TADF materials seem to solve the trade-off problem between a small ΔE_{ST} for efficient TADF and a sufficient oscillator strength for a high radiative decay rate, there are also problems associated with resonance TADF emitters. For example, many examples of resonance TADF emitters involve a highly planar structure making them prone to aggregation. For example, Figure 4.1 illustrates the aggregation problem of a deep-blue emitter even in dilute solution.

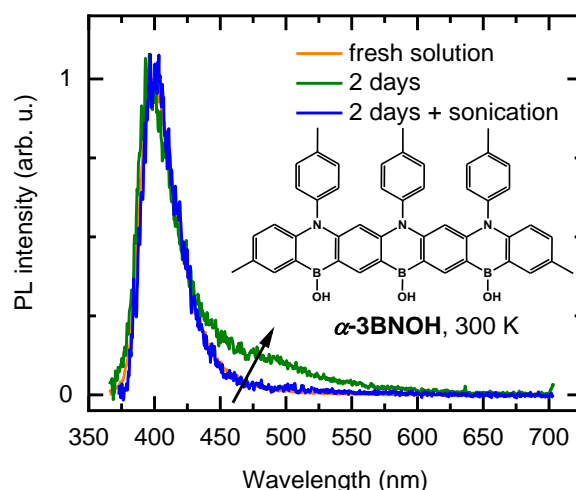


Figure 4.1. PL emission spectra of α -3BNOH in THF (7.6×10^{-6} M) at 300 K taken with a delay of 100 ns and a gate of 400 ns, $\lambda_{\text{exc}} = 355$ nm.

Figure 4.1 shows the photoluminescence emission spectrum of a resonance TADF emitter α -3BNOH in THF solution at different times after the preparation of the sample. First, a fresh solution is measured which shows a PL emission maximum at 400 nm which is attributed to the monomolecular emission species. Second, after the measurement is repeated after two days, the emission shoulder at around 480 nm appears in addition to the peak at 400 nm. After the solution is sonicated, the redshifted shoulder disappears. Based on the appearance of the additional redshifted emission with time and its disappearance after sonication, the emission shoulder at around 480 nm is assigned to aggregation. The rigid and planar structure of the α -3BNOH core even in the presence of phenyl-based groups makes the molecule prone to aggregation. This is a good example of the aggregation problem in resonance TADF emitters and the reason why only low doping concentrations are acceptable to use in films or devices. Although the paper involving the detailed investigation of α -3BNOH is not discussed further in this thesis, the published manuscript can be found online following Ref¹.

A possible way to reduce aggregation in resonance TADF emitters is shielding of the core by bulky groups which would limit guest to guest interactions. However, it is not clear how such modification would impact the TADF properties and the efficiency in the molecule. To look at this question in more detail, two resonance TADF emitters were investigated, namely, DiKTa and Mes₃DiKTa (Figure 4.2).

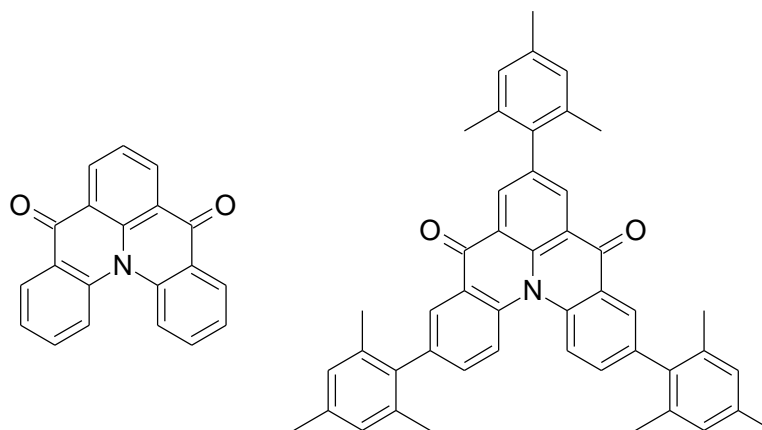


Figure 4.2. Molecular structures of **DiKta** and **Mes₃DiKta** (left and right, respectively).

Figure 4.2 shows the chemical structures of the two emitters investigated in solution and film to evaluate the effects on aggregation, TADF properties and PLQY when additional mesityl group are introduced on a rigid molecular unit. The mesityl groups were chosen because of two reasons. First, the mesityl groups were expected to adopt an orthogonal conformation with respect to **DiKta**. This should prevent delocalization of the electronic density from **DiKta** onto the mesityl groups, and thus keep the PL emission properties unchanged. Second, the steric bulk of mesityl groups should prevent aggregation by suppressing guest to guest interactions.¹³

I found that the addition of mesityl groups does not significantly change the photoluminescence efficiency, ΔE_{ST} gaps and TADF properties but has remarkable effects on aggregation and concentration quenching. The addition of mesityl units leads to the suppression of the aggregate emission and a strong decrease in concentration quenching. For example, at a 10 wt% doping, **Mes₃DiKta** shows a PLQY value which is almost three times higher compared to **DiKta**. Both in toluene solution and mCP film, **DiKta** and **Mes₃DiKta** were shown to have similar singlet-triplet gaps of around 200 meV, sufficiently low for TADF.

Methods

Materials. The compounds for the investigation were synthesized by David Hall in the Prof. Eli Zysman-Colman group (University St Andrews, UK).²

Photophysical measurements. The solutions of 0.05 mg/mL in toluene, as well as spin-coated 3.5 wt% films in mCP, were prepared and measured using similar instruments and techniques as mentioned earlier (Methods section of the thesis and Chapter 1a).

Photophysical properties

To evaluate the monomolecular properties of the emission, the photophysical investigation is started with solution measurements (Figure 4.3a and 4.3c).

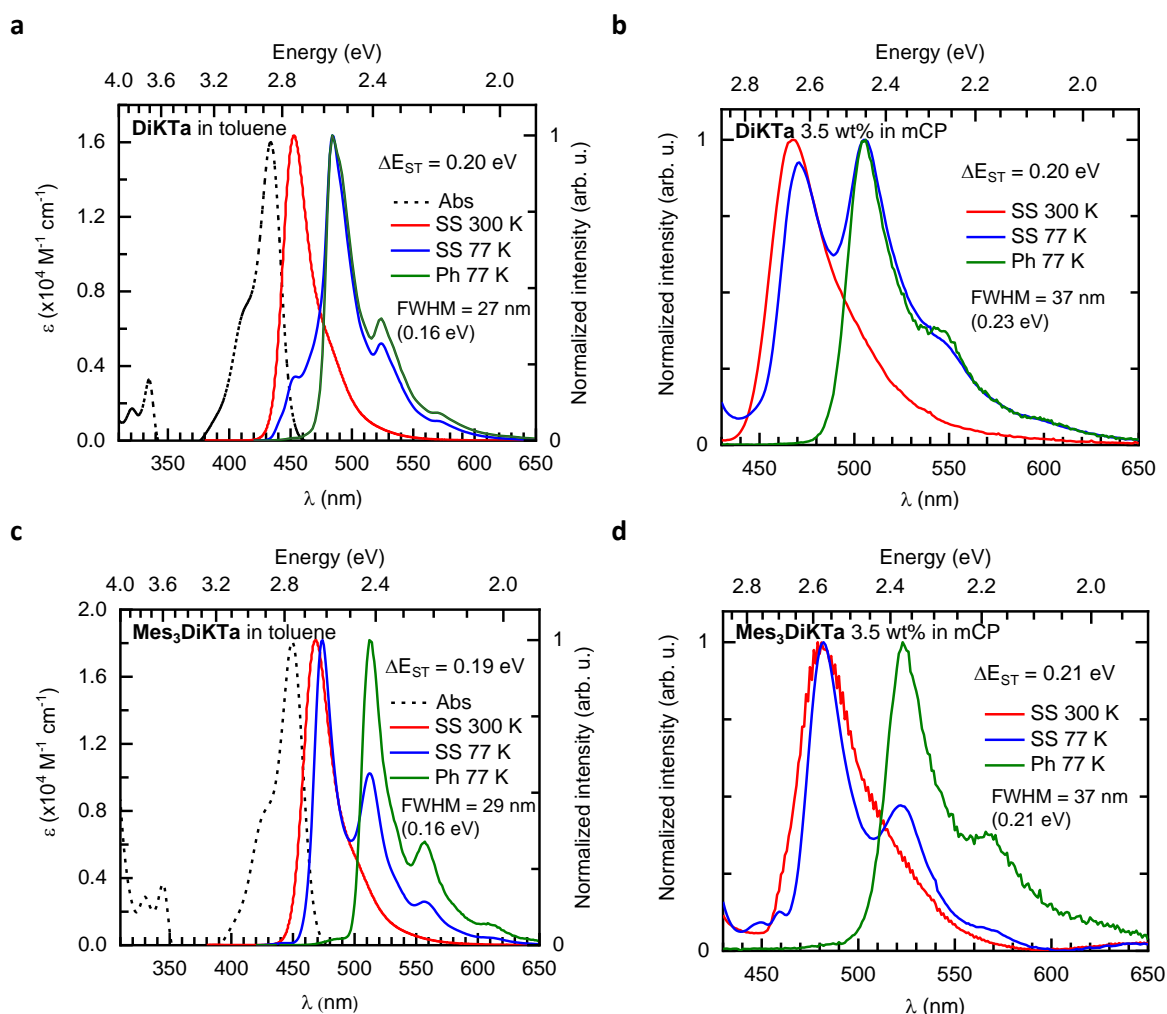


Figure 4.3. Absorption at 300 K, steady-state (SS) emission and phosphorescence spectra in toluene (0.05 mg/mL) and mCP film (3.5 wt%). $\lambda_{\text{exc}}(\text{SS})$ is 335 nm (345 nm) for DiKTa (Mes₃DiKTa). $\lambda_{\text{exc}}(\text{Ph})$ is 400 nm (415 nm) for DiKTa (Mes₃DiKTa).

Figure 4.3a and 4.3c present the absorption, steady-state emission and phosphorescence spectra of the compounds at 300 K and 77 K in toluene. The extinction coefficient at the energetically lowest absorption peak in **Mes₃DiK₂Ta** is similar to that of **DiK₂Ta**, indicating that the introduction of mesityl groups does not reduce the oscillator strength. The small energy difference between the absorption and the steady-state emission spectra for both compounds in toluene suggests a weak geometrical relaxation of the compounds after excitation. A weak geometrical relaxation after excitation and narrow emission spectra imply a rigid nature of the molecules, similar for both compounds. A small redshift in absorption and photoluminescence of **Mes₃DiK₂Ta** can be attributed to a small delocalization of the electronic density also onto the part of the mesityl group.² To estimate the separation between the singlet and triplet states, the solution is cooled down to 77 K. Once the solution is cooled down, the emission profile with a pronounced vibronic progression appears in the steady-state emission spectra. To resolve the phosphorescence spectra out of the steady-state emission, the light output is recorded after a 70 ms delay. Comparing the distance between the energetically lowest emission peaks of the steady-state emission and phosphorescence at 77 K, the singlet-triplet gap can be estimated. The ΔE_{ST} of 0.19 eV is estimated for both compounds in solution, indicative of a suitable singlet-triplet separation for the RISC process. The photophysical parameters extracted from the solution data are summarized in Table 4.1.

To understand how the properties in solution translate into the solid-state, films doped with a 3.5 wt% of the emitter in mCP host were prepared. A low concentration of the emitter was selected to avoid efficiency loss via concentration quenching. The host mCP was selected as the host material because of its high triplet energy (2.9 eV), suitable for the energy transfer from host to guest. Comparing to low-temperature solution data, for **DiK₂Ta**, the singlet and triplet energy peaks in film are located at a slightly lower energy (Figure 4.3, Table 4.1 and 4.2). Whereas for **Mes₃DiK₂Ta**, the shift of singlet and triplet positions to lower energies in the transition from solution to film is negligible, indicating that mesityl groups have a screening effect from the environment. The ΔE_{ST} values in film are the same as in solution, confirming a suitable singlet-triplet separation for the RISC process also in film. Both emitters show a high PLQY in film (75% and 80% for **DiK₂Ta** and **Mes₃DiK₂Ta** at 3.5 wt% doping

concentration, respectively), allowing us to expect good efficiency in an OLED. The photophysical parameters extracted from the film data are summarized in Table 4.2. To assess the TADF properties in the molecule, the photoluminescence transient decay measurements were conducted both in solution and film (Figure 4.4).

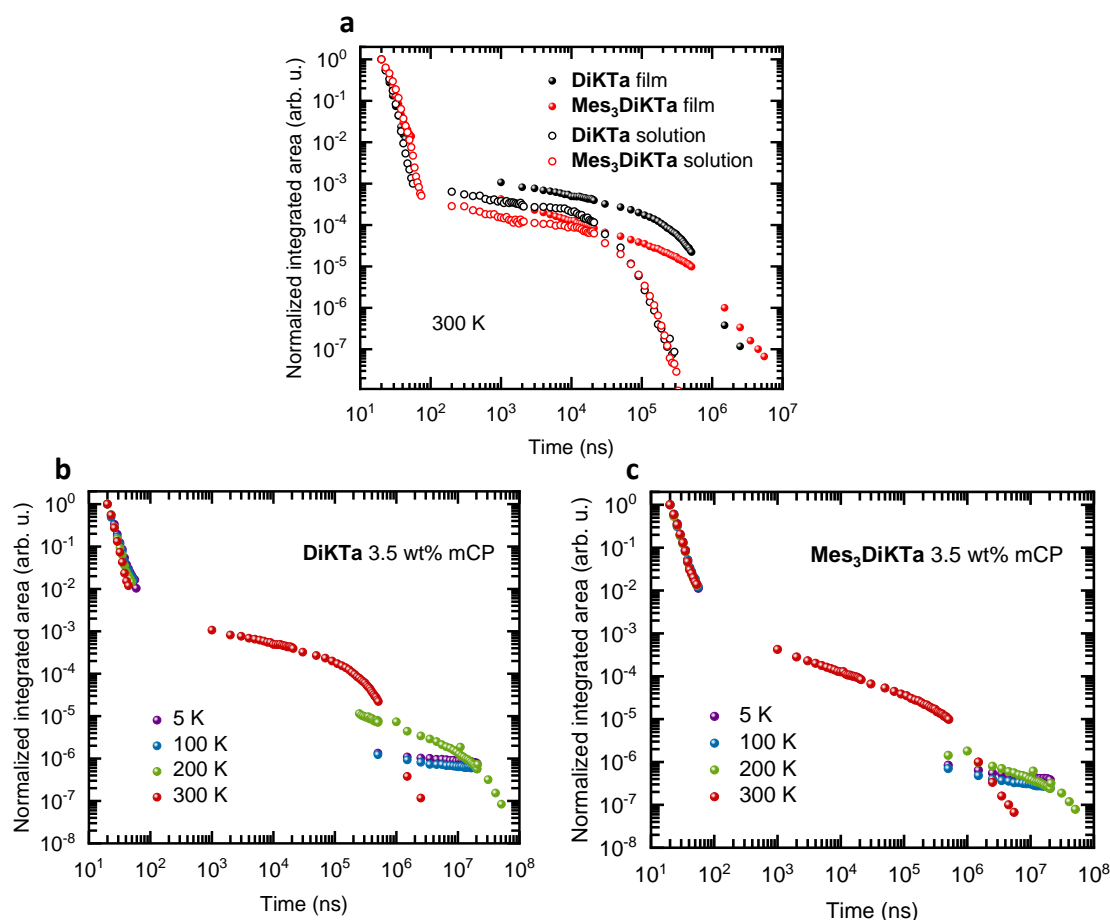


Figure 4.4. PL transient decay in solution and film at different temperatures. $\lambda_{\text{exc}} = 355 \text{ nm}$.

Figure 4.4 shows the PL transient decay profiles of the compounds in solution and film at different temperatures. Two regimes can be identified, a prompt part lasting until around 100 ns, and the delayed part taking place in the microsecond range. Based on the increase/appearance of the delayed intensity with temperature, the delayed emission at 300 K is assigned to TADF. The multi-exponential behaviour of the delayed part is associated with the distribution of molecular conformations owing different ΔE_{ST} gaps.¹⁴⁻¹⁵ Therefore, to estimate the lifetime of the delayed part and to take into account all of the molecular conformations involved in the delayed process, the average lifetime is calculated.

The delayed emission detected in the millisecond range at 5 K and 100 K is attributed to phosphorescence, as there is not enough thermal energy for TADF given that the ΔE_{ST} gap is around 200 meV for both compounds. This is further supported by longer delayed emission lifetimes at 5 and 100 K. Extracted lifetimes, TADF contributions to the total emission as well as rate constants are summarized in Table 4.1, Table 4.2, and Table 4.3 together with the photophysical data mentioned earlier.

Table 4.1. Photophysical parameters of **DiKTa** and **Mes₃DiKTa** in toluene at 300 K (unless indicated otherwise).

	λ_{abs}	λ_{PL}^a	S_1^b	T_1^c	ΔE_{ST}^d	Φ_{PL}^e	$\Phi_{DF}/$	τ_p^g	τ_d^g	k_r^S	k_{nr}^S
	(nm)	(nm)	(eV)	(eV)	(eV)	(%)	Φ_{PF}^f	(ns)	(μ s)	($\times 10^7$	($\times 10^7$
			77 K	77 K	77 K					s ⁻¹)	s ⁻¹)
DiKTa	434	453	2.74	2.56	0.18	26	0.03	5.1	23	4.9	14.7
Mes₃DiKTa	449	468	2.62	2.42	0.20	37	0.03	6.7	33	5.4	9.6

^a $\lambda_{exc} = 335$ nm (345 nm for **Mes₃DiKTa**). ^b Obtained from the peak of the PL steady-state spectrum, $\lambda_{exc} = 335$ nm (345 nm for **Mes₃DiKTa**). ^c Obtained from the peak of the PL emission spectrum with a 70 ms delay, $\lambda_{exc} = 400$ nm (415 nm for **Mes₃DiKTa**). ^d $\Delta E_{ST} = E(S_1) - E(T_1)$. ^e Calculated in oxygen-free solvent, $\lambda_{exc} = 360$ nm. ^f Ratio of delayed emission versus prompt emission yield calculated comparing the areas of the delayed and prompt part in the transient decay profile. ^g $\lambda_{exc} = 355$ nm, prompt and delayed fluorescence decays were fitted using mono-exponential fits.

Table 4.2. Photophysical parameters of **DiKTa** and **Mes₃DiKTa** in mCP film (3.5 wt%) at 300 K (unless indicated otherwise).

	λ_{PL}^a	S_1^b	T_1^c	ΔE_{ST}^d	Φ_{PL}^e	$\Phi_{DF}/$	τ_p^g	τ_d^g	k_r^S	k_{nr}^S
	(nm)	(eV)	(eV)	(eV)	(%)	Φ_{PF}^f	(ns)	(μ s)	($\times 10^7$	($\times 10^7$
		77 K	77 K	77 K					s ⁻¹)	s ⁻¹)
DiKTa	463	2.64	2.46	0.18	75	0.22	4.4	200	14.0	8.8
Mes₃DiKTa	477	2.57	2.37	0.20	80	0.10	5.9	390	12.3	4.6

^a $\lambda_{exc} = 335$ nm. ^b Obtained from the peak of the PL steady-state spectrum, $\lambda_{exc} = 335$ nm. ^c Obtained from the peak of the PL emission spectrum with a 70 ms delay, $\lambda_{exc} = 415$ nm. ^d $\Delta E_{ST} = E(S_1) - E(T_1)$. ^e Calculated under N_2 , $\lambda_{exc} = 335$ nm. ^f Ratio of delayed emission versus prompt emission yield calculated comparing the areas of the delayed and prompt part in the transient decay profile. ^g $\lambda_{exc} = 355$ nm, prompt component fitted using a mono-exponential, delayed obtained using an average lifetime.

Starting from the properties of the singlet state, the experimental radiative decay rate is similar for both compounds and it coincides well with the extinction coefficient of around $2 \times 10^4 \text{ M}^{-1} \text{ cm}^{-1}$, yielding a theoretical radiative decay rate value in the range of 10^7 - 10^8 s^{-1} for both compounds.¹⁶ To understand the origin of the non-radiative decay rate, two parameters need to be considered, namely, the internal conversion of the excited singlet state to the ground state and the intersystem crossing to the triplet state (ISC). Since the internal conversion channel can be assumed as negligible due to the rigid nature of the molecules, the dominating channel for the non-radiative decay rate of the singlet state is the intersystem crossing. This can be supported by comparing the steady-state emission for both compounds at 77 K (Figure 4.3). The steady-state emission spectra consist of emission from the singlet state and emission from the triplet state (phosphorescence). For both compounds, the phosphorescence spectra contribute significantly to the steady-state emission, meaning a significant ISC in the molecules. For **DiKTa** in solution, the non-radiative decay rate of the singlet state is around three times higher compared to the radiative decay of the singlet state (Table 4.1), indicating a strong energy loss to the triplet state. This is supported by Figure 4.3a, where the steady-state emission at 77 K shows that the dominating emission is phosphorescence. For **DiKTa** in film, the non-radiative decay rate from the singlet state is reduced while the radiative decay of the singlet state is increased compared to solution, meaning a stronger contribution of fluorescence in the steady-state emission which is indeed supported by Figure 4.3b. For **Mes₃DiKTa**, the non-radiative decay rate is around two times smaller compared to **DiKTa**, indicating a smaller amount of ISC which can again be supported by the steady-state emission spectra at 77 K (Table 4.3). Assuming the internal conversion to be negligible enables to approximate the intersystem crossing yield as $(1 - \Phi_{\text{PE}})$,¹⁷ also allowing for the simplified calculation of the RISC-related parameters (Table 4.3).

Concerning the triplet state properties, for both compounds, the delayed lifetime is significantly shorter in solution as compared to film where the delayed lifetime is around one order of magnitude longer. The shorter delayed lifetime in solution has been observed before.¹⁸⁻¹⁹ I associate it with the collisional quenching of the triplet state via collisions between molecules or collisions between

molecules and the cuvette. Collisional quenching essentially quenches the triplet state, preventing the molecule from showing a higher TADF contribution in solution. In the solid-state, this collisional quenching mechanism is suppressed which is supported by the decreased non-radiative decay rate of the triplet state (Table 4.3). Preserving the population of the triplet state that can participate in the TADF process increases the TADF contribution in film. However, even though the TADF contribution is increased in film compared to solution, it is still small compared to efficient donor-acceptor type emitters (where the DF/PF ratio is more than 4).²⁰

Table 4.3. Photophysical parameters of **DiKTa** and **Mes₃DiKTa** in solution and film.

	Toluene solution					3.5 wt% mCP film				
	Φ_{ISC}^a	k_{ISC}^b	Φ_{RISC}^c	k_{RISC}^d	$k_{nr}^{T e}$	Φ_{ISC}^a	k_{ISC}	Φ_{RISC}	k_{RISC}	$k_{nr}^{T e}$
		($\times 10^7$ s^{-1})		($\times 10^3$ s^{-1})	($\times 10^4$ s^{-1})		($\times 10^7$ s^{-1})		($\times 10^3$ s^{-1})	($\times 10^4$ s^{-1})
DiKTa	0.75	14.7	0.04	1.7	4.3	0.39	8.8	0.47	2.9	0.3
Mes₃DiKTa	0.64	9.6	0.05	1.4	3.0	0.27	4.6	0.33	0.9	0.2

^a Intersystem crossing yield; ^b rate constant of intersystem crossing; ^c reverse intersystem crossing yield; ^d rate constant of reverse intersystem crossing; ^e rate constant of non-radiative decay of the triplet state.

In general, the photophysical properties are comparable for both compounds, with a slightly higher RISC rate for **DiKTa**. Even though the photophysical properties are largely similar at a 3.5 wt% doping concentration, it is not clear how it would translate into the guest-host systems with a larger guest concentration. For this reason and with a view to application where normally higher doping concentrations are desired, both compounds were investigated as neat films. To compare the two molecules in terms of their tendency to aggregate, the neat film photoluminescence emission was compared with the doped film photoluminescence emission (Figure 4.5).

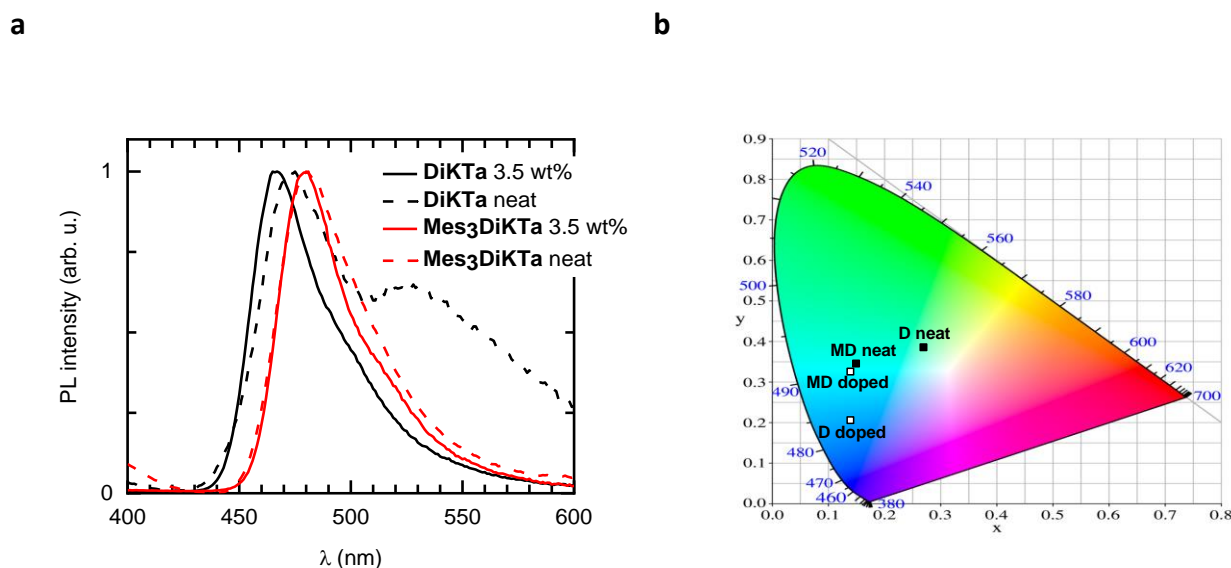


Figure 4.5. (a) Comparison between the PL emissions spectra of 3.5 wt% films and neat films, $\lambda_{exc} = 335$ nm; (b) the PL emission for **DiKTA** (**D**) and **Mes₃DiKTA** (**MD**) in CIE 1931 colour space.

Figure 4.5 demonstrates that for the neat film of **DiKTA**, the steady-state emission at 300 K shows an additional redshifted emission peak at around 540 nm, a new feature that is not present in solution and doped film. Based on the appearance of the feature at around 540 nm only in a highly-concentrated environment such as neat film, the feature can be ascribed to aggregation. A neat film of **Mes₃DiKTA**, however, preserves its narrow spectral shape (FWHM = 0.24 eV compared to 0.21 eV in 3.5 wt% mCP film) with no additional low energy feature, confirming that the additional mesityl groups reduce guest to guest interactions. To illustrate the colour change in the transition from doped to neat film, the CIE (International Commission on Illumination) emission coordinates can be calculated. For **DiKTA**, the transition from doped (3.5 wt%) to neat film shows a significant change in the CIE coordinate from (0.14, 0.21) to (0.27, 0.39). For **Mes₃DiKTA**, the change in the colour in the transition from doped to neat film is significantly suppressed, with a minimal change in the CIE coordinates from (0.14, 0.33) to (0.15, 0.35) for doped (3.5 wt%) and neat film, respectively. The emission colour is also compared visually by plotting the colour coordinates in the CIE 1931 colour space (Figure 4.5b). For **DiKTA**, there is a change in emission colour from blue to greenish in the transition from doped to neat film while for **Mes₃DiKTA** the sky-blue emission colour is preserved independent of emitter concentration. To better

understand how the doping concentration affects the PLQY, the photoluminescence quantum efficiency was studied as a function of doping concentration (Figure 4.6).

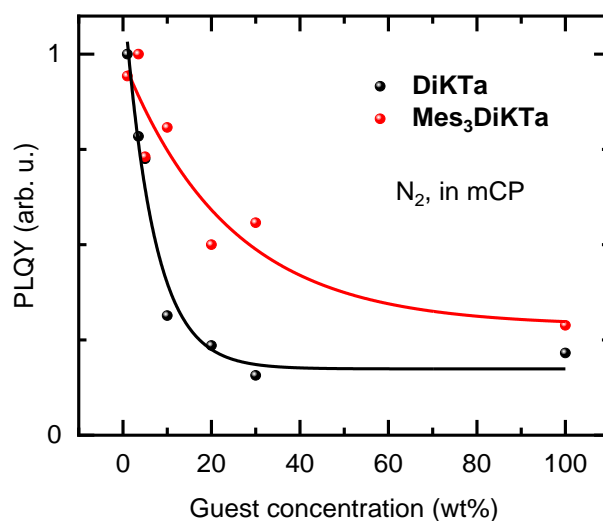


Figure 4.6. PLQY dependence on the guest concentration in mCP film. $\lambda_{\text{exc}} = 335 \text{ nm}$.

As can be seen from Figure 4.6, **DiKTa** shows a sharper drop in PLQY with increasing doping concentration compared to **Mes₃DiKTa**, indicating that only very low doping concentrations of **DiKTa** would be acceptable for application. The concentration quenching in **Mes₃DiKTa**, however, is strongly reduced.

To summarize the chapter, the investigated resonance TADF compounds indeed show high efficiency together with a narrow emission band (FWHM = 0.16 eV, in toluene), however, aggregation and strong concentration quenching due to a rigid and planar molecular structure are also present. The negative aggregation effects in resonance TADF emitters can be solved/minimized by introducing additional side groups, preventing guest to guest interactions. In this chapter, the effects of the addition of mesityl groups to prevent guest to guest interactions were studied on the photoluminescence emission colour, TADF-related parameters and efficiency. It is found that the photoluminescence quantum efficiencies are similar for both compounds, with **DiKTa** showing a slightly higher RISC rate compared to **Mes₃DiKTa**. However, as higher doping concentrations are employed, **DiKTa** also shows an additional redshifted emission peak and a severe drop in PLQY with increasing emitter concentration.

For **Mes₃DiK₂Ta**, where the additional mesityl groups are present to suppress guest to guest interactions, the decrease in PLQY with an increasing doping concentration is significantly reduced. Overall, the study demonstrates that **Mes₃DiK₂Ta** is a better candidate for application in terms of a pure monomolecular emission and suppressed concentration quenching, especially when higher doping concentrations are intended.

References of Chapter 4

1. Suresh, S. M.; Duda, E.; Hall, D.; Yao, Z.; Bagnich, S.; Slawin, A. M. Z.; Bässler, H.; Beljonne, D.; Buck, M.; Olivier, Y.; Köhler, A.; Zysman-Colman, E., A Deep Blue B,N-Doped Heptacene Emitter That Shows Both Thermally Activated Delayed Fluorescence and Delayed Fluorescence by Triplet–Triplet Annihilation. *Journal of the American Chemical Society* **2020**, *142*, 6588-6599.
2. Hall, D.; Suresh, S. M.; dos Santos, P. L.; Duda, E.; Bagnich, S.; Pershin, A.; Rajamalli, P.; Cordes, D. B.; Slawin, A. M. Z.; Beljonne, D.; Köhler, A.; Samuel, I. D. W.; Olivier, Y.; Zysman-Colman, E., Improving Processability and Efficiency of Resonant TADF Emitters: A Design Strategy. *Advanced Optical Materials* **2019**, *8*, 1901627.
3. Pershin, A.; Hall, D.; Lemaury, V.; Sancho-Garcia, J.-C.; Muccioli, L.; Zysman-Colman, E.; Beljonne, D.; Olivier, Y., Highly emissive excitons with reduced exchange energy in thermally activated delayed fluorescent molecules. *Nature Communications* **2019**, *10*, 597.
4. Hirai, H.; Nakajima, K.; Nakatsuka, S.; Shiren, K.; Ni, J.; Nomura, S.; Ikuta, T.; Hatakeyama, T., One-Step Borylation of 1,3-Diaryloxybenzenes Towards Efficient Materials for Organic Light-Emitting Diodes. *Angewandte Chemie International Edition* **2015**, *54*, 13581-13585.
5. Hatakeyama, T.; Shiren, K.; Nakajima, K.; Nomura, S.; Nakatsuka, S.; Kinoshita, K.; Ni, J.; Ono, Y.; Ikuta, T., Ultrapure Blue Thermally Activated Delayed Fluorescence Molecules: Efficient HOMO-LUMO Separation by the Multiple Resonance Effect. *Advanced Materials* **2016**, *28*, 2777-2781.
6. Nakatsuka, S.; Gotoh, H.; Kinoshita, K.; Yasuda, N.; Hatakeyama, T., Divergent Synthesis of Heteroatom-Centered 4,8,12-Triazatriangulenes. *Angewandte Chemie International Edition* **2017**, *56*, 5087-5090.
7. Matsui, K.; Oda, S.; Yoshiura, K.; Nakajima, K.; Yasuda, N.; Hatakeyama, T., One-Shot Multiple Borylation toward BN-Doped Nanographenes. *Journal of the American Chemical Society* **2017**, *140*, 1195-1198.
8. Liang, X.; Yan, Z.-P.; Han, H.-B.; Wu, Z.-G.; Zheng, Y.-X.; Meng, H.; Zuo, J.-L.; Huang, W., Peripheral Amplification of Multi-Resonance Induced Thermally Activated Delayed Fluorescence for Highly Efficient OLEDs. *Angewandte Chemie International Edition* **2018**, *57*, 11316-11320.
9. Han, S. H.; Jeong, J. H.; Yoo, J. W.; Lee, J. Y., Ideal blue thermally activated delayed fluorescence emission assisted by a thermally activated delayed fluorescence assistant dopant through a fast reverse intersystem crossing mediated cascade energy transfer process. *Journal of Materials Chemistry C* **2019**, *7*, 3082-3089.
10. Kondo, Y.; Yoshiura, K.; Kitera, S.; Nishi, H.; Oda, S.; Gotoh, H.; Sasada, Y.; Yanai, M.; Hatakeyama, T., Narrowband deep-blue organic light-emitting diode featuring an organoboron-based emitter. *Nature Photonics* **2019**, *13*, 678-682.
11. Yuan, Y.; Tang, X.; Du, X. Y.; Hu, Y.; Yu, Y. J.; Jiang, Z. Q.; Liao, L. S.; Lee, S. T., The Design of Fused Amine/Carbonyl System for Efficient Thermally Activated Delayed Fluorescence: Novel Multiple Resonance Core and Electron Acceptor. *Advanced Optical Materials* **2019**, *7*, 1801536.
12. Li, X.; Shi, Y.-Z.; Wang, K.; Zhang, M.; Zheng, C.-J.; Sun, D.-M.; Dai, G.-L.; Fan, X.-C.; Wang, D.-Q.; Liu, W.; Li, Y.-Q.; Yu, J.; Ou, X.-M.; Adachi, C.; Zhang, X.-H., Thermally Activated Delayed Fluorescence Carbonyl Derivatives for Organic Light-Emitting Diodes with Extremely Narrow Full Width at Half-Maximum. *ACS Applied Materials & Interfaces* **2019**, *11*, 13472-13480.
13. Mei, J.; Leung, N. L. C.; Kwok, R. T. K.; Lam, J. W. Y.; Tang, B. Z., Aggregation-Induced Emission: Together We Shine, United We Soar! *Chemical Reviews* **2015**, *115*, 11718-11940.
14. Dias, F. B.; Santos, J.; Graves, D. R.; Data, P.; Nobuyasu, R. S.; Fox, M. A.; Batsanov, A. S.; Palmeira, T.; Berberan-Santos, M. N.; Bryce, M. R.; Monkman, A. P., The Role of Local Triplet Excited States and D-A Relative Orientation in Thermally Activated Delayed Fluorescence: Photophysics and Devices. *Advanced Science* **2016**, *3*, 1600080.
15. Woo, S.-J.; Kim, J.-J., TD-DFT and Experimental Methods for Unraveling the Energy Distribution of Charge-Transfer Triplet/Singlet States of a TADF Molecule in a Frozen Matrix. *The Journal of Physical Chemistry A* **2021**, *125*, 1234-1242.

16. S. P. McGlynn, S. M. G., T. Azumi, M. Kinoshita, *Molecular Spectroscopy of the Triplet State*. 1969.
17. Kreiza, G.; Banevičius, D.; Jovaišaitė, J.; Maleckaitė, K.; Gudeika, D.; Volyniuk, D.; Gražulevičius, J. V.; Juršėnas, S.; Kazlauskas, K., Suppression of benzophenone-induced triplet quenching for enhanced TADF performance. *Journal of Materials Chemistry C* **2019**, *7*, 11522-11531.
18. Lee, J.; Shizu, K.; Tanaka, H.; Nakanotani, H.; Yasuda, T.; Kaji, H.; Adachi, C., Controlled emission colors and singlet–triplet energy gaps of dihydrophenazine-based thermally activated delayed fluorescence emitters. *Journal of Materials Chemistry C* **2015**, *3*, 2175-2181.
19. Wong, M. Y.; Krotkus, S.; Copley, G.; Li, W.; Murawski, C.; Hall, D.; Hedley, G. J.; Jaricot, M.; Cordes, D. B.; Slawin, A. M. Z.; Olivier, Y.; Beljonne, D.; Muccioli, L.; Moral, M.; Sancho-Garcia, J.-C.; Gather, M. C.; Samuel, I. D. W.; Zysman-Colman, E., Deep-Blue Oxadiazole-Containing Thermally Activated Delayed Fluorescence Emitters for Organic Light-Emitting Diodes. *ACS Applied Materials & Interfaces* **2018**, *10*, 33360-33372.
20. Dias, F. B.; Penfold, T. J.; Monkman, A. P., Photophysics of thermally activated delayed fluorescence molecules. *Methods and Applications in Fluorescence* **2017**, *5*, 012001.

5. Conclusions and outlook

In this work, I investigated several different factors controlling TADF-related properties in guest-host systems for OLEDs. In Chapter 1a, I demonstrated that TADF-related properties can be successfully fine-tuned by controlling the hole-electron wavefunction overlap using donor extensions of gradually increasing strength. I also demonstrated that a small ΔE_{ST} alone is not enough and that these donor extensions can lead to non-radiative losses, suppressing TADF. For an efficient emitter, such non-radiative channels should be minimized. In Chapter 1a, I also identified the carbazole-based donor extension to be the most promising in terms of ΔE_{ST} gap below 100 meV in mCP film and the increased TADF contribution in toluene compared to the reference compound.

In Chapter 1b, I investigated the effects of the linkage position of the donor unit to the acceptor core via a phenylene bridge on TADF-related properties. The compounds with donor groups owning the carbazole-based extensions were selected for the study. I demonstrated that a synergistic *meta*- and *para*-connection of the donor unit to the acceptor core leads not only to a small ΔE_{ST} gap but also to a high radiative decay rate. Furthermore, I discovered a very low concentration quenching in the compound with a synergistic *meta*- and *para*-connection. When comparing the compounds prepared as a 1 wt% doped film in PMMA and the neat film, the PLQY values of 90 and 86% were obtained, respectively. I demonstrated that such high PLQY is inherited from the *para*-connection while the minimal concentration quenching is the property of the donor-acceptor units linked in a *meta*-position. Overall, my photophysical study in Chapter 1b demonstrated that the ΔE_{ST} gap, TADF contribution to the total emission, PLQY and concentration quenching can be successfully controlled by the selection of the linkage position of the dendron donor unit to the acceptor core.

While Chapter 1 was focused on studying the changes to TADF-related properties when the donor group is extended or linked to the acceptor core via a phenylene bridge in a different position, Chapter 2 was dedicated to exploring the changes to TADF-related properties when the molecular structure is increased in length using repetitive donor-acceptor units. I found that increasing the oligomer size enhances TADF contribution to the total emission, the intersystem crossing and the

reverse intersystem crossing rates while still preserving the blue photoluminescence emission. I attributed the enhancement in TADF-related properties to the increasing number of intermediate triplet states along the series. Furthermore, I demonstrated that increasing the oligomer length also reduces the undesired low-energy emission band, which I assigned to aggregation. Overall, in Chapter 2, I showed that TADF-related properties can be successfully enhanced without redshifting the monomolecular photoluminescence emission wavelength.

While Chapter 1 and Chapter 2 focused on the effects on TADF-related properties in terms of modification of the emitter itself, it was not clear if and how the nature of the host molecule affects TADF of the guest-host system. To answer this question, I studied three different host materials in Chapter 3, consisting of TADF-active (ATRZ) and TADF-inactive hosts (DPEPO and mCP). I found that using a TADF-active host extends the TADF contribution to the total emission as well as increases the RISC rate of the guest-host system. The most pronounced difference between TADF-active and TADF-inactive hosts in terms of the magnitude of TADF was found at a lower emitter concentration (5 wt%). I attributed the enhancement of TADF-related properties using ATRZ as a host to a strong ISC channel in ATRZ, thus providing a larger triplet population in the guest-host system. In terms of electroluminescence, I found that devices with ATRZ as a host in the emissive layer outperform devices with TADF-inactive hosts at a lower doping concentration (5 wt%). I explained this considering two factors. First, as discovered from the photophysical study, TADF is more pronounced for the guest-host system with ATRZ as a host due to a strong ISC channel in ATRZ. Second, ATRZ is of bipolar electronic nature, leading to a better charge balance at a low emitter concentration in the device. In principle, TADF-active host ATRZ should be beneficial for emitters that show a strong concentration quenching, for example, resonance TADF emitters. Such resonance TADF emitters are often of rigid and planar nature, allowing them to be used only at a small emitter concentration. Therefore, such host materials, that allow achieving a higher efficiency of the device at a lower doping concentration, are necessary.

In Chapter 4, I focused on a new type of TADF emitters based on multi-resonant structures that are attracting attention in the TADF field due to their narrow emission spectra, allowing for a pure emission

Conclusions and outlook

colour, and high efficiency. Unfortunately, such advantages come at a cost of such emitters being very prone to concentration quenching and aggregation due to their rigid and planar structure. I demonstrated that adding mesityl groups on a rigid and planar structure can significantly suppress concentration quenching and preserve the emission colour due to suppressed aggregation even at higher emitter concentrations in the guest-host system. Importantly, I showed that smaller a concentration quenching and suppressed aggregation in the compound with additional mesityl groups can be achieved while still preserving TADF-related properties such as the ΔE_{ST} gap and the reverse intersystem crossing rate.

Overall, my results presented in this work show several tools to control TADF-related properties in the guest-host systems for OLEDs, starting from fine-tuning the emitter properties such as the ΔE_{ST} gap and TADF and finishing with a selection of a suitable host matrix. While my work successfully demonstrates that TADF can be successfully controlled in the investigated guest-host systems, with some of them achieving close to unity PLQY, the future studies should now involve more work on the final device performance, with a focus on efficiency roll-off and stability so that OLEDs based on TADF can successfully compete with the currently commercialized phosphorescent emitters for a wide user application, for example, the display market.

APPENDIX 1. List of publications

Publications with a major contribution:

1. **Duda, E.**; Hall, D.; Bagnich, S.; Carpenter-Warren, C.; Saxena, R.; Wong, M. Y.; Cordes, D. B.; Slawin, A. M. Z.; Beljonne, D.; Olivier, Y.; Zysman-Colman, E.; Köhler, A., Enhancing TADF Emission by Fine-Tuning the Dendron Donor Strength. *Accepted to the Journal of Physical Chemistry B*. → **Chapter 1a**
2. Sun, D.†; **Duda, E.†**; Fan, X.; Saxena, R.; Zhang, M.; Bagnich, S.; Zhang, X.; Köhler, A., Zysman-Colman, E., Thermally Activated Delayed Fluorescent Dendrimers that Underpin High-Efficiency Host-Free Solution-Processed Organic Light Emitting Diodes. *Prepared for submission*. → **Chapter 1b**
3. **Duda, E.**; Suresh, S. M.; Bagnich, S.; Hall, D.; Saxena, R.; Slawin, A. M. Z.; Beljonne, D.; Olivier, Y.; Zysman-Colman, E., Köhler, A., Controlling the RISC-related Parameters by Employing an Extendable Molecular Design for Blue TADF Emitters. *Under preparation*. → **Chapter 2**
4. **Duda, E.**; Saxena, R.; Kahle, J.; Bagnich, S.; Köhler, A., The Effects of TADF *versus* Non-TADF Host Materials on TADF Properties of Guest-Host Systems for OLEDs. *Under preparation*. → **Chapter 3**
5. Rodella, F.†; Bagnich, S.†; **Duda, E.**; Meier, T.; Kahle, J.; Athanasopoulos, S.; Köhler, A.; Strohriegl, P., High Triplet Energy Host Materials for Blue TADF OLEDs – A Tool Box Approach. *Frontiers in Chemistry* **2020**, *8*, 657.
6. Suresh, S. M.; **Duda, E.**; Hall, D.; Yao, Z.; Bagnich, S.; Slawin, A. M. Z.; Bäessler, H.; Beljonne, D.; Buck, M.; Olivier, Y.; Köhler, A.; Zysman-Colman, E., A Deep Blue B,N-Doped Heptacene Emitter That Shows Both Thermally Activated Delayed Fluorescence and Delayed Fluorescence by Triplet–Triplet Annihilation. *Journal of the American Chemical Society* **2020**, *142*, 6588-6599. → **partly presented in Chapter 4**

Publications with a minor contribution:

1. Hall, D.; Suresh, S. M.; dos Santos, P. L.; **Duda, E.**; Bagnich, S.; Pershin, A.; Rajamalli, P.; Cordes, D. B.; Slawin, A. M. Z.; Beljonne, D.; Köhler, A.; Samuel, I. D. W.; Olivier, Y.; Zysman-Colman, E., Improving Processability and Efficiency of Resonant TADF Emitters: A Design Strategy. *Advanced Optical Materials* **2019**, *8*, 1901627. → **I present the extended version of my part in Chapter 4**
2. Hall, D.; Rajamalli, P.; **Duda, E.**; Suresh, S. M.; Rodella, F.; Bagnich, S.; Carpenter-Warren, C.; Cordes, D. B.; Slawin, A. M. Z.; Strohriegl, P.; Beljonne, D.; Köhler, A.; Olivier, Y.; Zysman-Colman, E.; Substitution Effects on a New Pyridylbenzimidazole Acceptor for Thermally Activated Delayed Fluorescence. *Advanced Optical Materials* **2021**, *9*, 2100846.

APPENDIX 2. List of abbreviations

Abs	Absorption
Arb. u.	Arbitrary units
CT	Charge-transfer
DF	Delayed fluorescence
DFT	Density functional theory
DPEPO	Bis[2-(diphenylphosphino)phenyl] ether oxide
EL	Electroluminescence
EQE	External quantum efficiency
FI	Fluorescence
IC	Internal conversion
iCCD	Intensified charge-coupled device
ISC	Intersystem crossing
LE	Local-excitation
mCP	1,3-Di(9H-carbazol-9-yl)benzene
OLED	Organic light-emitting diode
PF	Prompt fluorescence
Ph	Phosphorescence
PL	Photoluminescence
PLQY	Photoluminescence quantum yield
PMMA	Poly(methyl 2-methylpropenoate)
RISC	Reverse intersystem crossing
SS	Steady-state
TADF	Thermally activated delayed fluorescence
TTA	Triplet-triplet annihilation

APPENDIX 3. Acknowledgements

First, I would like to mention that the funding which allowed me to work on research projects at the University of Bayreuth for three years was provided by the European Union's Horizon 2020 research and innovation programme under the Marie Skłodowska-Curie grant agreement No 812872 (*TADF*life**).

Second, I would like to say thank you to my supervisor Prof. Dr. Anna Köhler for providing the possibility to carry out research in her lab as well as feedback on my scientific work.

Third, I would like to thank Dr. habil. Sergey Bagnich for daily scientific discussions that helped me to understand many scientific phenomena as well as detailed and fast feedback on my work.

I would also like to thank my *TADF*life** colleagues at the University of Bayreuth, Rishabh Saxena and Francesco Rodella, for numerous discussions on thermally activated delayed fluorescence. And, of course, thank you to all the members of Soft Matter Optoelectronics, including our technical assistants, Irene Bauer and Frank Schirmer for helping out with the preparatory matters of the experimental work.

Many thanks to our collaborators in the TADF matters, including Prof. Dr. Peter Strohriegl (University of Bayreuth) and Prof. Dr. Eli Zysman-Colman (University of St Andrews, UK), for discussions and feedback on my work. I would also like to express my gratitude to the group members of Prof. Dr. Eli Zysman-Colman, including David Hall, Dr. Subeesh Suresh and Dr. Dianming Sun, for synthesizing TADF molecules that have led to numerous interesting projects and publications. A special thanks to David Hall for providing detailed DFT calculations for the compounds.

APPENDIX 4. Erklärung und eidesstattliche Versicherung

Einverständniserklärung

Hiermit erkläre ich mich einverstanden, dass die elektronische Fassung meiner Dissertation unter Wahrung meiner Urheberrechte und des Datenschutzes einer gesonderten Überprüfung unterzogen werden kann.

Des Weiteren erkläre ich mich einverstanden, dass bei Verdacht wissenschaftlichen Fehlverhaltens Ermittlungen durch universitätsinterne Organe der wissenschaftlichen Selbstkontrolle stattfinden können.

Eidesstattliche Versicherung

Hiermit versichere ich an Eides statt, dass ich die vorliegende Arbeit selbständig verfasst und keine anderen als die von mir angegebenen Quellen und Hilfsmittel verwendet habe.

Weiterhin erkläre ich, dass ich die Hilfe von gewerblichen Promotionsberatern bzw. -vermittlern oder ähnlichen Dienstleistern weder bisher in Anspruch genommen habe, noch künftig in Anspruch nehmen werde.

Zusätzlich erkläre ich hiermit, dass ich keinerlei frühere Promotionsversuche unternommen habe.

Bayreuth, den 05.07.2021

Eimantas Duda